UNIVERSITY OF CATANIA
International PhD Course in Chemical Science
XXIV Cycle

Dr. ZELICA MINNITI

Advanced characterization methods of organic materials of environmental and historical-artistic relevance through Micro-FTIR Mapping and Raman Microscopy

Tutor Prof. Vito Librando

Years 2008 - 2011

INDEX

Abstract

For many centuries paper was the main material for recording cultural achievements all over the world. Paper is mostly made from cellulose with small amounts of organic and inorganic additives which allow its identification and characterization and may also contribute to its degradation. Prior to 1850, paper was made entirely from rags, using hemp, flax and cotton fibres. After this period, due to the enormous increase in demand, wood pulp began to be commonly used as raw material, resulting in a rapid degradation of paper.

Spectroscopic techniques represent one of the most powerful tools to investigate the constituents of paper documents in order to establish its identification and its state of degradation. This work describes the application of Fourier-Transform Infrared spectroscopy and Raman techniques for the characterization of organic writing materials focusing the attention on the study of paper stained by the foxing process.

The spectroscopic techniques were also used for the characterization of the particulate matter (PM) collected in Catania using an high-volume cascade impactor. Assignment of PM vibrational bands has been studied and the distribution of functional groups in different size fraction stages were discussed. FTIR mapping was applied in order to better observe the particles distribution throughout the impactor stages.

INTRODUCTION

During my PhD course, I have dealt with application of FTIR and Raman spectroscopy on both cultural heritage and environmental samples.

One of the subject of my thesis is the application of FTIR and Raman spectroscopic techniques for the investigation of the degradation processes occurred on writing materials. The attention was focused in particular on cellulose paper samples coming from damaged or ancient books; some analysis were also carried on ancient parchment samples and inks used on them.

Infrared spectroscopy for its non-destructive approach represents a great potential for surface materials characterisation (Hon, 1986). Many authors have applied this spectroscopic technique to paper characterization. Calvini et al. (2006) studied the composition of old and modern Japanese papers. Hon (1986) demonstrated the effectiveness of FTIR in analyzing and determining acid impurities distributed on the surface of paper documents produced during the period 1790-1983. In one study (Mossini, 1990) , some naturally aged papers were subjected to FTIR analysis. In a study by Zotti et al. (2008) the main surface components of bio-deteriorated papers from the XVIII century were characterized by FTIR spectroscopy, the author also referred to the presence of gelatin, wood pulp, calcium carbonate, gypsum, hemicelluloses and glue in the paper composition, as well as to the corresponding bands in the FTIR spectra. The presence of fungi in these papers was also verified.

Raman spectroscopy has been applied to different types of artworks too. On paper artworks, the presence of fillers in the cellulose can be detected, a Raman analysis of a map from the XVII century (Castro, 2008) showed that gypsum ($CaSO_4 \cdot 2H_2O$) was used as a filler in the cellulose. Bicchieri et al. examined degraded papers with several non-destructive spectroscopic techniques, including Raman spectroscopy (Bicchieri, 2006). Cellulose undergoing accelerated hydrothermal ageing gives rise to a pattern of carbonyl groups; their vibrational modes were observed in Raman spectra by Lojewska et al. (2007).

The other subject of my thesis was the exploration of a non-destructive method for the study and the characterization of the particulate matter (PM) collected in Catania using an high-volume cascade impactor (which separates different sized particles into fractions) loaded with aluminium foil over which organic micro-pollutants are adsorbed.

A number of methods have been developed to determine the loadings of inorganic species in size segregated PM. Ion chromatography interfaced with impactors (John et al., 1989 a-b) proton induced x-ray emission (Cahill et al., 1989; Ouimette and Flagan, 1982) and x-ray fluorescence (Groblicki et al., 1981; Ondov et al., 1990) are just a few of the available methods. On the other hand, methods for analysis of organics in size segregated PM are limited, and most of the methods that are available rely on organic and elemental carbon analysis (McMurry and Zhang, 1989; Turpin et al., 1989a, b), or on extraction followed by mass spectroscopic analysis, which requires large sample mass (Mazurek et al., 1989; Rogge et al., 1993).
In my work a method for the analysis of size segregated PM based on infrared spectroscopy was developed. This method has a number of advantages

compared to more traditional methods of PM analysis. First, it is a non-destructive analytical method, requiring no solvent extractions. Second, this method is suitable for the characterization of a large fraction of the inorganic and organic PM mass. Third, due to the high sensitivity of the method, short sampling runs are possible. Balancing these advantages is the fact that individual organic species are not identified, only compound classes are. Overall, however, the chemical insight provided by infrared spectroscopy represents a significant advance in the analysis of size segregated PM. The use of infrared spectroscopy in PM analysis was used extensively in the 1970s and early 1980s to investigate the composition of atmospheric PM (Blanco and McIntyre, 1975; Cunningham et al., 1974, 1976; Kellner, 1978; Bogard et al., 1982); however, these methods were largely abandoned because of the difficult sample collection and the lack of sensitivity. Recent advances in infrared optics and detectors have now overcome the problem of the samples preparation (Kellner and Malissa, 1989). A complete review of recent advances in PM analysis by infrared spectroscopy has been presented by Allen and Palen (1989).

During my work, some of the pros and cons of different FTIR methods of spectral-data acquisition were studied. The main spectra features were analyzed in order to get useful information for the characterization of PM functional groups distribution on different sized particles. Determining the composition of atmospheric PM, as a function of the PM size, is a challenging problem. The challenge is due partly to the complex nature of atmospheric PM, which are a mixtures of inorganic salts, metals, organic compounds and water. Despite these difficulties, sample collection and spectral interpretation of infrared absorbance bands was discussed.

Fourier-Transform Infrared spectroscopy

Infrared spectroscopy is one of the most important methods for the identification and characterization of chemical structures (Hon, 1986), is a versatile experimental technique and it can be used to obtain important information about everything from delicate biological samples to though minerals. One of the great advantages of infrared spectroscopy is that virtually any sample in virtually any state may be studied. Liquids, solutions, pastes, powders, film, fibres, gases and surfaces can all be examined with a judicious choice of sampling technique.

Infrared spectroscopy is of major importance in paper characterization (Workman, 2001), it covers several different fields of application in paper analysis. Mainly, it allows the identification of the origin of the fibres and the determination of the chemical composition of the additives used in the papermaking.

Moreover, infrared spectroscopy plays an important role in the study of paper deterioration processes (Bitossi et al., 2005). In museums, archives and libraries, the application of analytical techniques free of chemicals or solvents is mandatory. Furthermore, considering the huge number of items surveyed to establish the state of preservation of a collection, the time of analysis must be short. Sampling of historical artefacts for analysis is rarely permitted. More and more, only non-destructive or at best micro-destructive analytical techniques are allowed. Infrared spectroscopy is suitable for all these

demands and shows great potential for conservation and restoration of surface materials studies (Hon, 1986).

Infrared spectrometers have been commercially available since the 1940s. At this time the instruments relied on prisms to act as dispersive elements, but in the mid of 1950s, diffraction gratings had been introduced into dispersive machines. The most significant advances in infrared spectroscopy, however, have come about as a result of the introduction of Fourier-transform spectrometers. This type of instrument employs an interferometer and exploits the well-established mathematical process of Fourier-transformation. Fourier-transform infrared (FTIR) spectroscopy has dramatically improved the quality of infrared spectra and minimized the time required to obtain data. In addiction with constant improvements to computers, infrared spectroscopy has made further great strides.

Infrared theory

Infrared spectroscopy is a technique based on the vibrations of the atoms of a molecule. An infrared spectrum is commonly obtained by passing infrared radiation through a sample and determining what fraction of the incident radiation is absorbed at a particular energy. The energy at which any peak in an absorption spectrum appears corresponds to the frequency of a vibration of a part of a sample molecule.

In order to show infrared absorptions, a molecule must possess a specific feature, i.e. an electric dipole moment of the molecule must change during the vibration. This is a selection rule for infrared spectroscopy.

The dipole moment of such a molecule changes as the bond expands and contracts. An example of an ‘infrared-active’ molecule is an heteronuclear diatomic molecule. By comparison, an example of an ‘infrared-inactive’

molecule is a homonuclear diatomic molecule because its dipole moment remains zero no matter how long the bond.

So, the interactions of infrared radiation with molecules may be figured out in terms of changes in molecular dipoles associated with vibrations and rotations.

Figure 1 shows stretching and bending movements that are collectively referred to as vibration. Vibrations can involve either a change in bond length (stretching) or bond angle (bending). In the bending vibrations the atoms can move in-plane or out-of-plan.

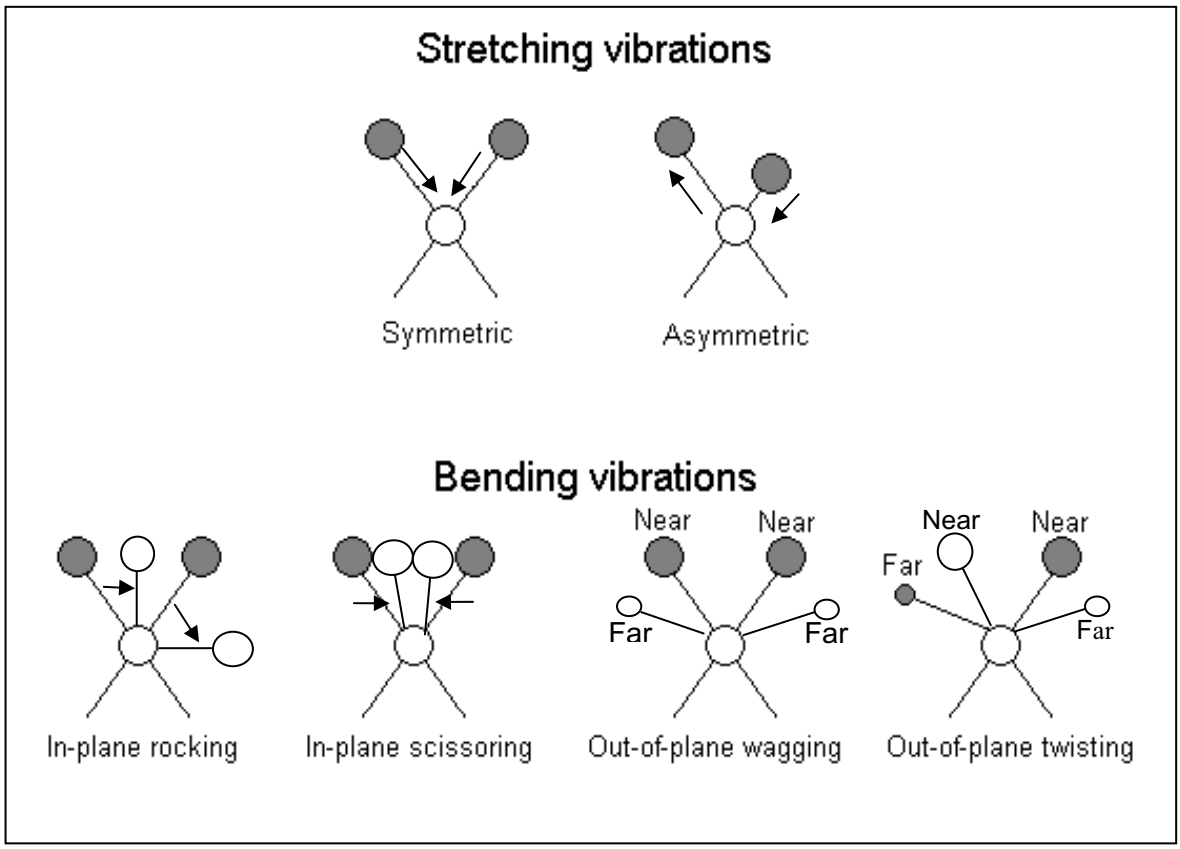

Fig.1: Molecule Vibrational Modes

Symmetrical molecules will have fewer 'infrared-active' vibrations than asymmetrical molecules. This leads to the conclusion that symmetric

vibrations will generally be weaker than asymmetric vibrations, since the former will not lead to a change in dipole moment. It follows that the bending or stretching of bonds involving atoms in widely separated groups of the periodic table will lead to intense bands. Vibrations of bonds such as C-C or N=H will give weak bands. This again is because of the small change in dipole moment associated with their vibrations.

There will be many different vibrations for even fairly simple molecules. The complexity of an infrared spectrum arises from the coupling of vibrations over a large part of or over the complete molecule (Stuart, 2004). Such vibrations are called skeletal vibrations. Bands associated with skeletal vibrations are likely to conform to a pattern or *fingerprint* of a molecule as a whole, rather than a specific group within the molecule (fig.2).

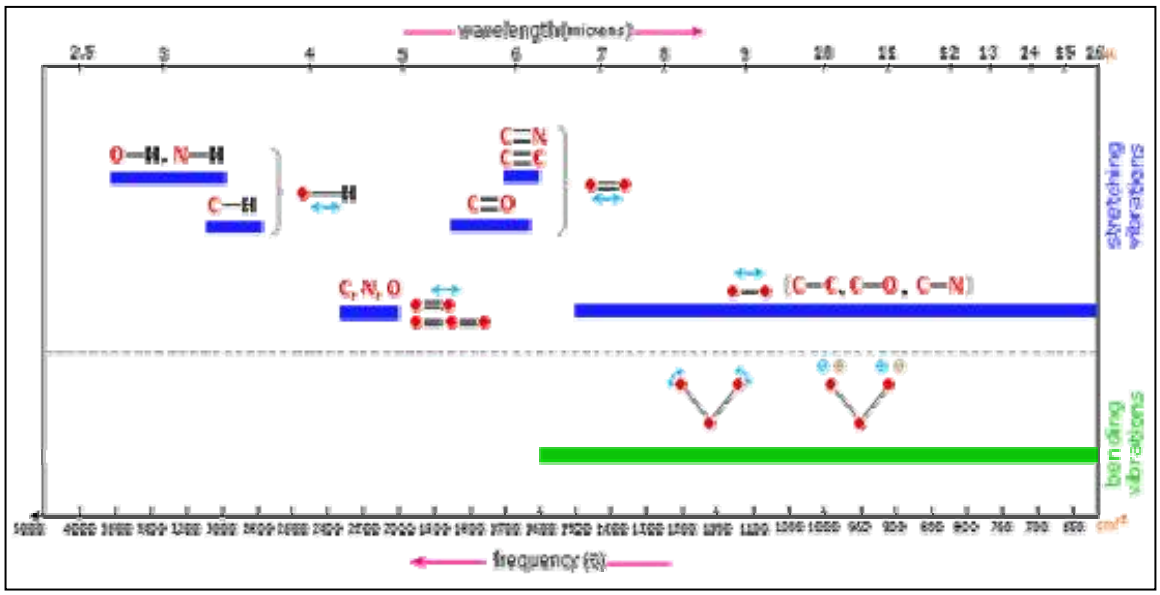

Fig. 2: Group frequencies

(3650 – 2500 cm^{-1}) → stretching single bond X–H
(2300 – 2100 cm^{-1}) → stretching triple bond
(1800 – 1500 cm^{-1}) → stretching double bond
(1650 – 1300 cm^{-1}) → bending in-plane X–H
(1300 – 900 cm^{-1}) → stretching single bond X–Y; fingerprint region
(< 1000 cm^{-1}) → bending out-of-plane H – X

Fourier-Transform Infrared Spectrometer

FTIR spectroscopy is based on the idea of interference of radiation between two beams to yield an interferogram (Griffiths and de Haseth, 1986). The latter is a signal produced as a function of the change of pathlenght between the two beams. The two domains of distance and frequency are interconvertible by the mathematical method of Fourier-transformation.

The basic components of an FTIR spectrometer are shown schematically in figure 3. The radiation emerging from the source is passed through an interferometer to the sample before reaching a detector. The data are transferred to the computer for Fourier-transformation.

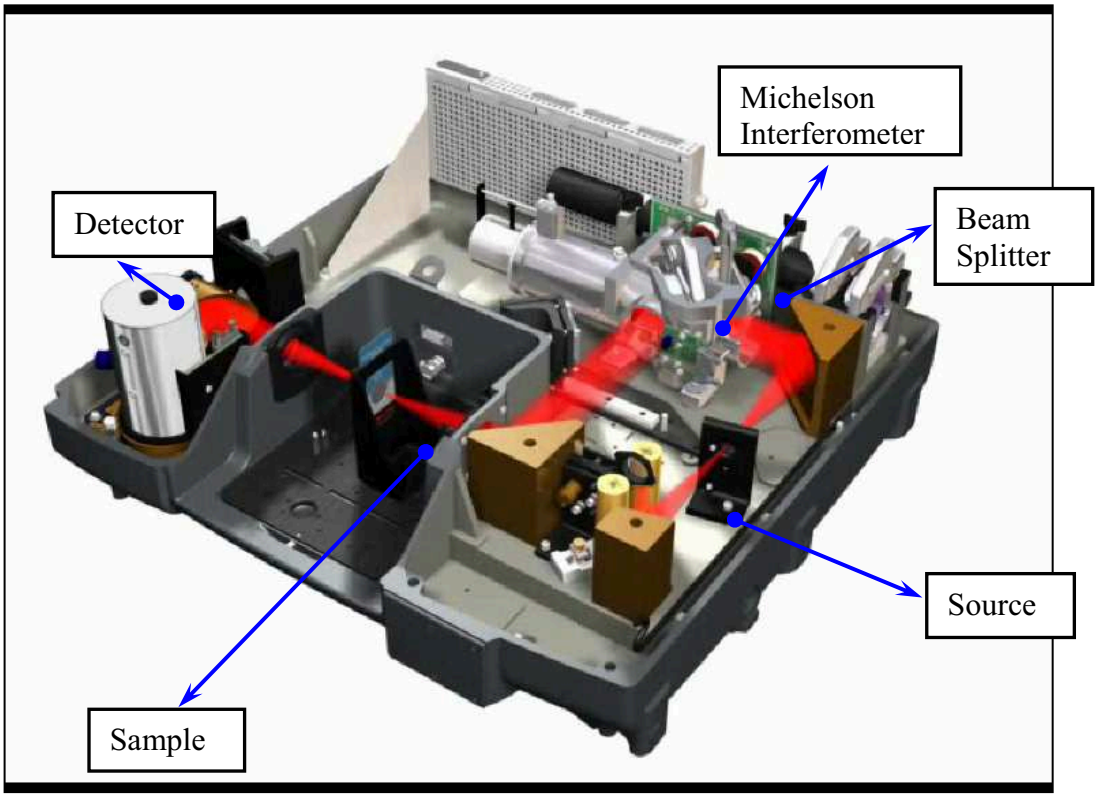

Fig.3: Basic components of an FTIR spectrometer

Michelson Interferometer

The most common interferometer used in FTIR spectroscopy is a Michelson interferometer, which consist of two perpendicularly plane mirrors, one of which can travel in a direction perpendicular to the plane (fig. 4) A semi-reflecting film, the beamsplitter, bisect the plane of these two mirrors. So 50% of the incident radiation will be reflected to one of the mirrors while 50% will be transmitted to the other mirror. The two beams are reflected from these mirrors, returning to the beamsplitter where they recombine and interfere.

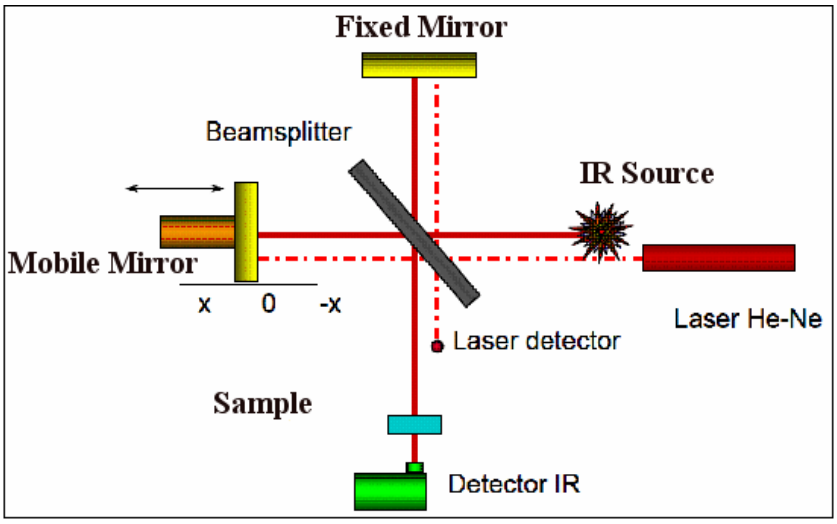

Fig.4: Michelson interferometer

The moving mirror produces an optical path difference between the two arms of the interferometer. The result interference pattern is shown in figure 5.

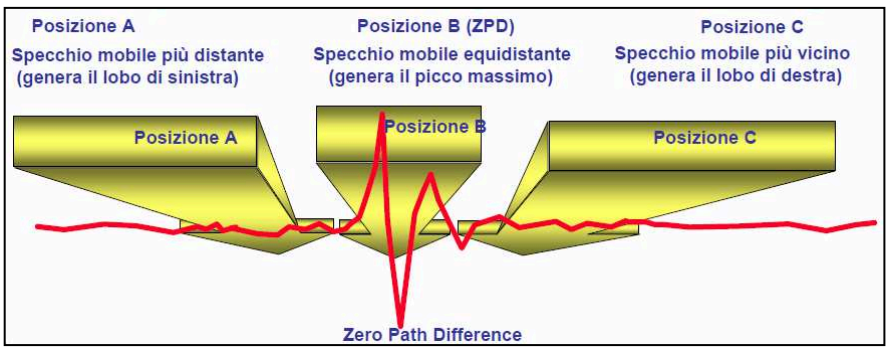

Fig.5: Interferogram

Advantages

FTIR instruments have several advantages over older dispersive instruments: improvement in SNR (signal to noise ratio) per time unit and the total source output can be passed through the sample continuously. This results in a substantial gain in the energy at the detector, hence translating to higher signals and improved SNRs.

Spectra

Early infrared instruments recorded percentage of transmittance or absorbance on the wavenumber scale.

The infrared spectrum can be divided in to three regions: the far-infrared (<400 cm^{-1}), the mid-infrared (4000-400 cm^{-1}) and the near-infrared (13000-4000 cm^{-1}) (fig.6). Many infrared applications employ the mid-infrared region, but the near- and far-infrared region also provide important information about certain materials (Gunzler and Gremlich, 2002).

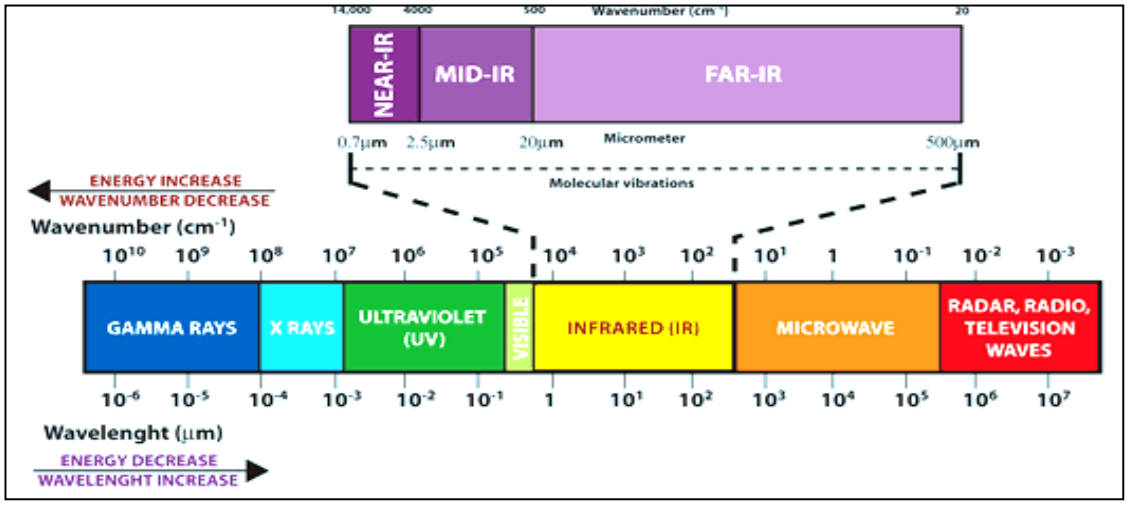

Fig.6: Spectra Regions

Transmission Method

Transmission spectroscopy is the oldest and most straightforward method. This technique is based upon the absorption of infrared radiation at specific wave-lengths as it passed through a sample. It is possible to analyse sample in liquid, solid or gaseous forms when using this approach (Sommer, 2002).

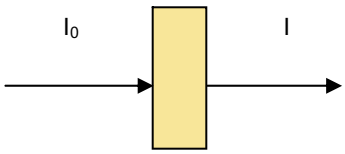

The amount of radiation absorbed may be measured in a number of ways

Transmittance: $T = I / I_0$
Absorbance: $A = \log 1 / T$

Reflectance Method

Reflectance technique may be used for samples that are difficult to analyse by the conventional transmittance methods. Reflectance methods can be divided into two categories: external and internal..

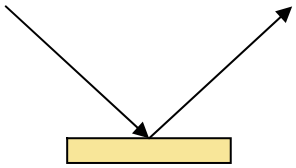

External reflectance measurements involve an infrared beam reflected directly from the sample surface

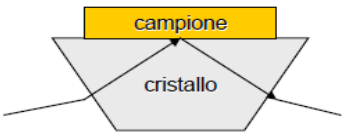

Internal reflectance measurement can be made by using an attenuated total reflectance (ATR) cell in contact with the sample.

ATR Method

Attenuated total reflectance (ATR) is a sampling technique used in conjunction with infrared spectroscopy which enables samples to be examined directly in the solid or liquid state without further preparation.

ATR uses a property of total internal reflection called the evanescent wave. A beam of infrared light is passed through the ATR crystal in such a way that it reflects at least once off the internal surface in contact with the sample. This reflection forms the evanescent wave which extends into the sample, typically by a few micrometres. The beam is then collected by a detector as it exits the crystal.

This evanescent effect works best if the crystal is made of an optical material with a higher refractive index than the sample being studied.

Typical materials for ATR crystals include i.e. germanium, zinc selenide, but the excellent mechanical properties of diamond make it an ideal material for ATR.

Micro-sampling Method

It is possible to combine an infrared spectrometer with a microscope in order to study very small samples (Humecki, 1999). It is possible to work in reflection, transmission and also with micro-ATR accessory.

Fig.7: μATR accessory.

The sample is placed in direct contact with the crystal mounted on the accessory in the picture. The principle of analysis is the same one used by ATR.

Infrared Mapping (FTIR equipped with a single element mercury-cadmium-telluride MCT detector) and infrared imaging (FTIR equipped with focal plane array FPA detector) using FTIR micro-spectroscopic techniques has emerged as an effective approach for studying complex or heterogeneous specimens (Kidder et al., 2002). The technique can be used to produce a two- or three-dimensional 'picture' of the properties of a sample. In particular Imaging, due to the development of FPA detectors, allows thousands of interferograms to be collected simultaneously and then transformed into infrared spectra.

FTIR application field

Applications of FTIR spectrometer to the different fields of investigation are considerably large and related to different types of analysis. Here are the most significant.

Cultural Heritage

The most interest applications concern the field of cultural heritage. They can be schematized as follows:

- Characterization of materials and colours of binders
- Identification of degradation products
- Monitoring of degradation processes
- Characterization of protective materials
- Dating works of art and accuracy of the findings
- Analysis of glass inclusions

Analysis of pharmaceuticals

Most of the classic pharmaceutical products have a specific chemical structure, and a specific molecular target on receptor. FTIR spectrometer can serve as an excellent analytical tool for the analysis of natural medicines, with

advantages in sensitivity, selectivity, speed and regulatory compliance through validation protocols.

Biology and Biochemistry:

- Bacteria classification
- Identification of biomolecules such as aminoacids, proteins, DNA / RNA.

Environmental

Analysis of biodiesel, exhausts, hazardous air pollutants, greenhouse gases and other emissions from wide-ranging products such as derivatives from coal mines, agricultural plants and industrial sites.

Geological

- Analysis of diamonds, emeralds, rubies and wedges
- Identification of mineral species

Forensic science

- Analysis and identification of illegal substances (cocaine identification, etc..)
- Analysis and characterization of trace organic and inorganic explosive materials, flammable compounds, fiber, etc..
- Analysis of different types of ink and tracking of paper materials.
- Identification of drugs

Raman spectroscopy

In 1928, Sir C.V. Raman documented the phenomenon of inelastic light scattering. Radiation, scattered by molecules, contains photons with the same frequency as those of the incident radiation, but may also contain a very small number of photons with a changed or shifted frequency. The spectroscopic process of measuring these shifted photons was later named after Sir Raman, with the shifting of frequency referred to as the Raman effect. By the end of

the 1930s, Raman spectroscopy had become the principle method of non-destructive chemical analysis. Infrared spectroscopy replaced Raman as the preferred method after World War II, when the development of sensitive infrared detectors and advances in electronics made infrared easier to use. Infrared spectroscopic measurements became routine, whereas Raman spectroscopy still required complex instrumentation, skilled operators and darkroom facilities.

Later developments, such as the availability of less expensive and more sensitive Charge Coupled Devices (CCDs), the availability of holographic notch filters and the advent of Fourier transform Raman (FT-Raman), launched a renaissance of Raman as a routine laboratory technique. Today, the most advanced modern Raman instruments are completely integrated into a single unit and computer controlled, are interlocked for laser safety, have automated protocols for calibration and offer large spectral libraries. These advances make the collection and utilization of Raman spectra a routine exercise.

Raman theory

In Raman spectroscopy, a sample is irradiated with a strong monochromatic light source (usually a laser). Most of the radiation will scatter “off” the sample at the same wavelength as that of the incoming laser radiation, a process known as Rayleigh scattering. However, a small amount – approximately one photon out of a million (0.0001%) – will scatter from that sample at a wavelength shifted from the original laser wavelength (fig. 8).

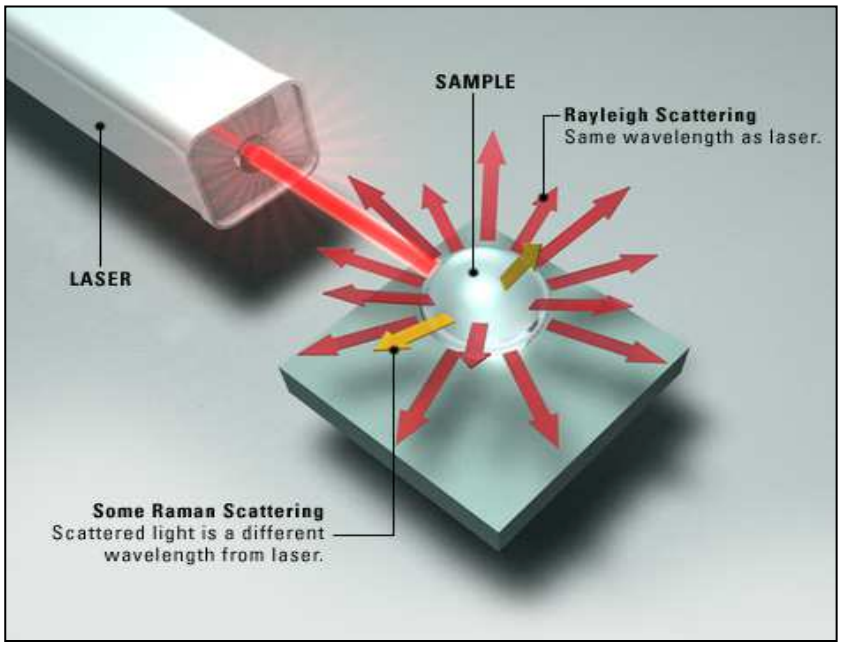

Fig.8. Raman scattering

As illustrated in the following simplified energy level diagram (fig. 9), a molecule at rest resides in the ground vibrational and electronic states. The electric field of the laser raises the energy of the system for an instant by inducing a polarization in the chemical species. The polarized condition is not a true energy state and is widely referred to as a "virtual state". Relaxation from the virtual state occurs almost instantaneously and predominately returns to the initial ground state. This process results in Rayleigh scatter. Relaxation to the first excited vibrational level results in a Stokes-Raman shift. Stokes-Raman shift scatter is of lower energy (longer wavelength) than that of the laser light.

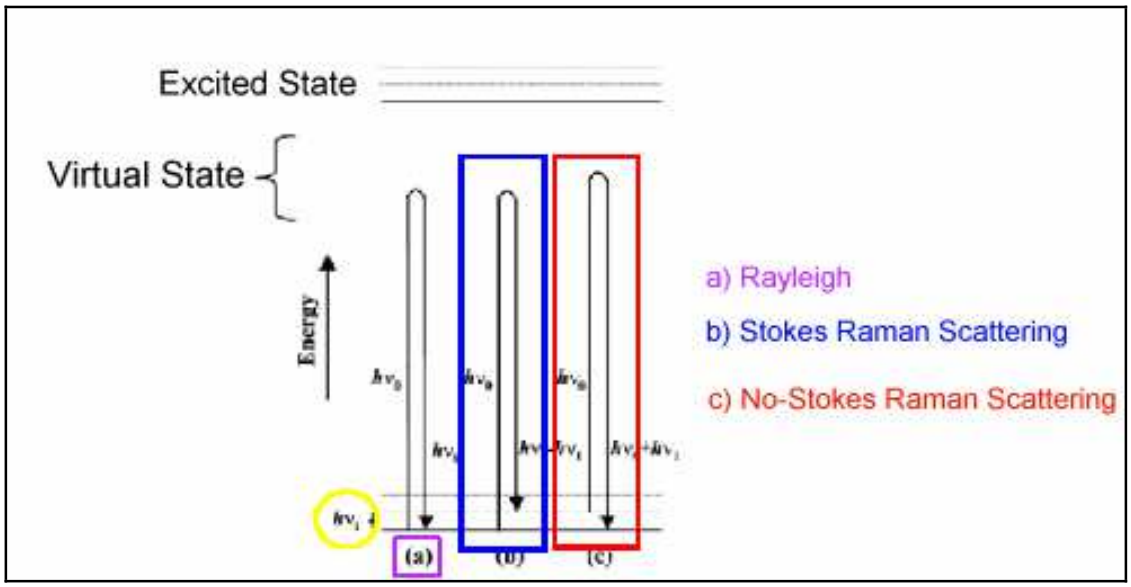

Fig.9: Raman scattering

Most systems have at least a small population initially in an excited vibrational state. When the Raman process initiates from the exited vibrational level, relaxation to the ground state is possible, producing scatter of higher energy (shorter wavelength) than that of the laser light. This type of scatter is called anti-Stokes- Raman scatter (not illustrated).

Dispersive Raman Spectroscopy

To observe the Raman spectrum, it is necessary to separate the collected Raman scattered light into individual wavelengths. In dispersive Raman instruments, this is accomplished by focusing the Raman signal on a grating, which spatially separates the different wavelengths (fig. 10). This spatially dispersed beam is directed to a CCD. Dispersive Raman usually employs visible laser radiation. Typical laser wavelengths are 780 nm, 633 nm, 532 nm, and 473 nm although others are common.

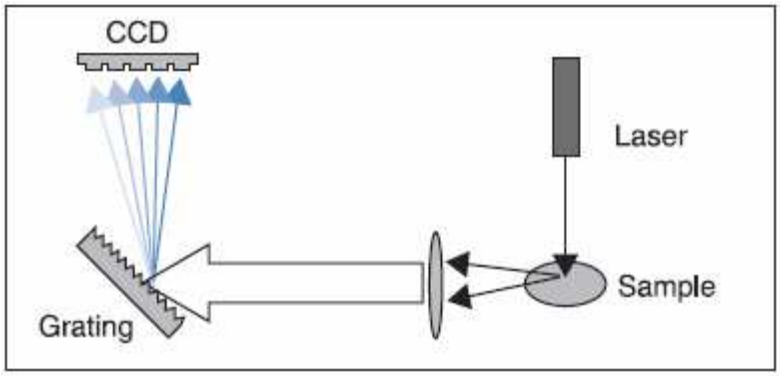

Fig.10: Basic components of a dispersive Raman spectrometer

The efficiency of Raman scatter is proportional to $1/\lambda^4$, so there is a strong enhancement as the excitation laser wavelength becomes shorter. This would suggest that all Raman should be done with the shortest wavelength lasers available. However, one factor hindering the practice of Raman as a routine tool is the unpredictable fluorescence that often occurs. Fluorescence is a very efficient emission several orders of magnitude stronger than the Raman signal, so minor fluorescence can overwhelm the desired Raman measurement.

Fluorescence occurs when the virtual energy level overlaps an upper Electronic level, so as the energy of the laser gets higher (shorter wavelength), the likelihood of fluorescence increases. The phenomenon is excitation wavelength dependent, so a sample that fluoresces at one wavelength may not at another. Thus, when selecting an instrument, it is important to look for rapid and effortless exchanges between two difficult excitation lasers. The grating has a strong influence on spectral resolution and instrument throughput. Gratings have many lines or grooves “blazed” into the surface, which disperse the incoming light. The higher the number of grooves on the grating, the wider the dispersion angle of the exiting rays.

Ideally, gratings should be specifically matched to the laser and experimental conditions of the experiment.

The CCDs commonly used for dispersive Raman are silicon devices with very high sensitivity. The detecting surface of the CCD is a two-dimensional array of light-sensitive elements, called pixels (usually each pixel is <30 μm). Each pixel acts as an individual detector, so each dispersed wavelength is detected by a different pixel (or closely spaced group of pixels).

It is advantageous to couple the strength and flexibility of Raman spectroscopy with a microscope that allows analysis of very small samples. The goal of microscopy is to analyze the smallest samples possible and to distinguish the substance of interest from its surroundings. This is known as spatial resolution, and in microscopy, the highest spatial resolution is attained using small pinholes or “apertures” somewhere in the microscope.

Dispersive Raman Key Applications

Dispersive Raman spectroscopy has been applied to many types of samples. Shorter laser wavelengths and more sensitive CCDs make the technique ideal for minor component analysis, offering low detection limits for such applications as impurity analysis in solutions, polymers or environmental sampling. Major applications for visible Raman are in the semiconductor and microelectronics industries where silicon and various coatings are routinely analyzed. Dispersive Raman is often very powerful for analyzing very dark samples, such as carbon black loaded or highly coloured samples. Many other techniques suffer from total absorbance or sample heating, which is often not present when using the dispersive Raman technique, owing to lower laser powers that can be used.

Inorganic analysis and identification in areas such as geology and gemmology are more commonly done using dispersive Raman because it is often free of the metal oxide fluorescence background that may be seen in FT-Raman. The confocal approach has also been used to probe inclusions in gems and stones by focusing on the region within the body of the material.

FTIR *vs* Raman

The vibrational states probed by Raman spectroscopy are the same as those involved in infrared spectroscopy. As such, Raman spectroscopy is very similar to the more frequently used Fourier transform infrared (FTIR) spectroscopic technique. The two vibrational spectroscopy techniques are, in fact, complementary. Vibrations that are strong in an infrared spectrum (those involving strong dipole moments) are usually weak in a Raman spectrum. Likewise, non-polar functional group vibrations that give very strong Raman bands usually result in weak infrared signals (Thermo Electron, 2008).

ABOUT PAPER

Papermaking History

Papermaking is considered to have originated in China. In AD 105 the court Tsai Lun presented to the emperor a process for papermaking with specific reference to its use for writing and record keeping. They produced the first usable writing material from tree bark and plant fibres, as well as from old rags and fishing nets. Since that time, paper has been in general use all over China (Winter, 2008) and has been playing a major role in the development of cultures all over the world. Papermaking technology has undergone extensive development in the past 200 years. Prior to 1850 paper was made essentially from cellulose and water in almost equimolar amounts. Antique paper was made entirely from rags, i.e., from linear long cellulose fibres, only with the addition of sizing compounds (Erhardt and Tumosa, 2005), whilst contemporary paper can be manufactured from short fibres, hemicelluloses and lignin, and may contain non-fibrous components including various colouring agents, fillers, coatings and other additives used to improve paper properties.

Originally, animal glue was used for sizing. It was substituted in the XIX century by rosin and alum, and more recently by other synthetic products (Blumich et al.,2003; Capitani et al., 2002; Viola et al., 2004). The change of fibre resource from cotton and linen rags to wood fibres and the use of alum rosin sizes had significant adverse effects on the permanence and durability of paper materials (Hon, 1986).

Additives:
- *Rosin+ Sodium carbonate+ S tarch+ Alum*
- *Gelatin+ Alum*
- *ADK (alkylketene dimes)*
- *ASA (alkenylsuccinic anhydride)*

Additives for sizing purposes may be mixed into the pulp and/or applied to the paper web later in the manufacturing process. The purpose of sizing is to establish the correct level of surface absorbency to suit the ink or paint.

Internal sizing is applied to almost all papers while surface sizing is added for the highest grade bond, ledger, and writing papers.

Surface sizing solutions consists of mainly modified starches or sometime other hydrocolloid as gelatin and a surface sizing agent such as AKD or acrylic co-polymers. Surface sizing agents are amphipathic molecules, having both hydrophilic (water-loving) and hydrophobic (water-repelling) ends. The sizing agent covers the cellulose and forms a film, with the hydrophilic tail facing the fibre and the hydrophobic tail facing outwards. This creates a water-repellent situation. Sizing improve the surface strength, printability and water resistances of the paper surface. In the sizing solution also optical brightening agents are added to improve the opacity and whiteness of the paper surface.

Internal sizing chemicals used in papermaking at the wet end are ASA, AKD and rosin. By making the paper web more hydrophobic, the sizing agents influence dewatering and retention of fillers and fibres in the paper sheet. Internal sizing agents main effect is on runability of the paper machine next to paper quality.

Modern paper from wood pulp can be divided into chemical and mechanical pulp.

Chemical pulping

The purpose of a chemical pulping process is to break down the chemical structure of lignin and render it soluble in the cooking liquor, so that it may be washed from the cellulose fibers. Because lignin holds the plant cells together, chemical pulping frees the fibres and makes pulp. The pulp can also be bleached to produce white paper for printing, painting and writing. Chemical pulps tend to cost more than mechanical pulps, largely due to the low yield, 40–50% of the original wood. Since the process preserves fibre length, however, chemical pulps tend to make stronger paper. Another advantage of chemical pulping is that the majority of the heat and electricity needed to run the process is produced by burning the lignin removed during pulping.

Papers made from chemical wood-based pulps are also known as woodfree papers.

The Kraft process is the most commonly practiced strategy for pulp manufacturing and produces especially strong, unbleached papers that can be used directly for bags and boxes but are often processed further, e.g. to make corrugated cardboard.

The main process to obtein paper are: kraft process, sulfite process, and soda pulping.

Chemical pulp content:

- *Calcium bisulphite*
- *Sodium bisulphite*
- *Soda sulphate*
- *Lime*

Mechanical pulping

There are two major mechanical pulps, thermomechanical pulp (TMP) and mechanical pulp. In the TMP process, wood is chipped and then fed into large steam-heated refiners where the chips are squeezed and fibreized between two steel discs. In the groundwood process, debarked logs are fed into grinders where they are pressed against rotating stones and fibreized. Mechanical pulping does not remove the lignin, so the yield is very high, >95%, but also causes paper made from this pulp to yellow and become brittle over time. Mechanical pulps have rather short fibre lengths and produce weak paper. Although large amounts of electrical energy are required to produce mechanical pulp, it costs less than chemical pulp.

Mechanical pulp content:

- *Hemicellulose*
- *Lignin*
- *Tannins*
- *Resins*
- *Rubber*

Coating and paper fillers

Coated paper has a thin layer of material such as calcium carbonate or china clay applied to one or both sides in order to create a surface more suitable for high-resolution halftone screens. Coated papers are divided into matte, semi-matte or silk, and gloss. Gloss papers give the highest optical density in the printed image.

Coating and paper fillers are inorganic substance natural or artificial powder which give the paper a high degree of whiteness, opacity and printability (Copedè, 2003).

Coating and Fillers:

- *Kaolin $Al_2Si_2O_5(OH)_4$*
- *Calcium carbonate $CaCO_3$*
- *Talc $Mg_3Si_4O_{10}(OH)_2$*
- *Barium sulfate $BaSO_4$*
- *Gypsum $CaSO_4$*
- *Kieselguhr (diatom powder)*
- *Titanium dioxide TiO_2*

Paper structures

Paper consists of mostly bonded cellulose fibres that are linear polymers of glucose (β-D-glucopyranose) monomers linked by β-1,4-gycosidic bonds (fig.11). Cellulose from native wood exhibit degree of polymerization (number of linked monomers) up to 10 000, while the one from native cotton can reach up to 15 000.

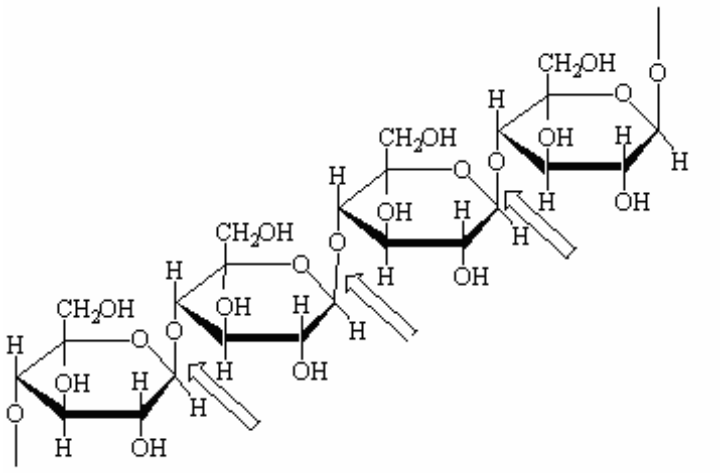

Fig.11: cellulose chain (β-1,4-gycosidic bonds)

All chemical reactions occur at hemiacetal bond (the glycosidic linkage) and/or hydroxyl groups. These two determine chemical properties of cellulose. Cellulose chains are held together by strong intramolecular hydrogen bonds that promote aggregation of single chains into highly

oriented structure. Also water molecules, since cellulose is naturally hydrophilic, that are embedded into cellulose matrix play a very important role in hydrogen bond formation. This aggregates are ordered up to even 80% (crystalline forms). The rest, that is unordered, is called ‘amorphous’ form (Fengel et al., 1989). In addition to cellulose fibres, paper contains hemicellulose (wood polyoses), lignin and certain amount of additives, e.g. fillers, pigments, metal ions. Paper is a relatively stable material but undergoes natural aging process that causes the degradation of cellulose. This process is related to the presence of acid substances, moisture, oxidative agents or microrganisms. Especially, the presence of acidic substances results in the hydrolysis of cellulose that appears in shortening of its chain along with changes in content of crystalline form (Browing, 1977; Wilson, 1979).

Hydrolysis

Hydrolysis causes the depolymerization of cellulose by attacking the β-glycosidic bond. Strong mineral acids dissolve cellulose completely up to the formation of glucose. Weak mineral acids and organic acids cause partial hydrolysis (Bicchieri and Brusa, 1997).

The mechanism of hydrolysis is the protonation of oxygen and the cleavage of glycosidic bond with formation of new reducing terminal units (fig. 12).

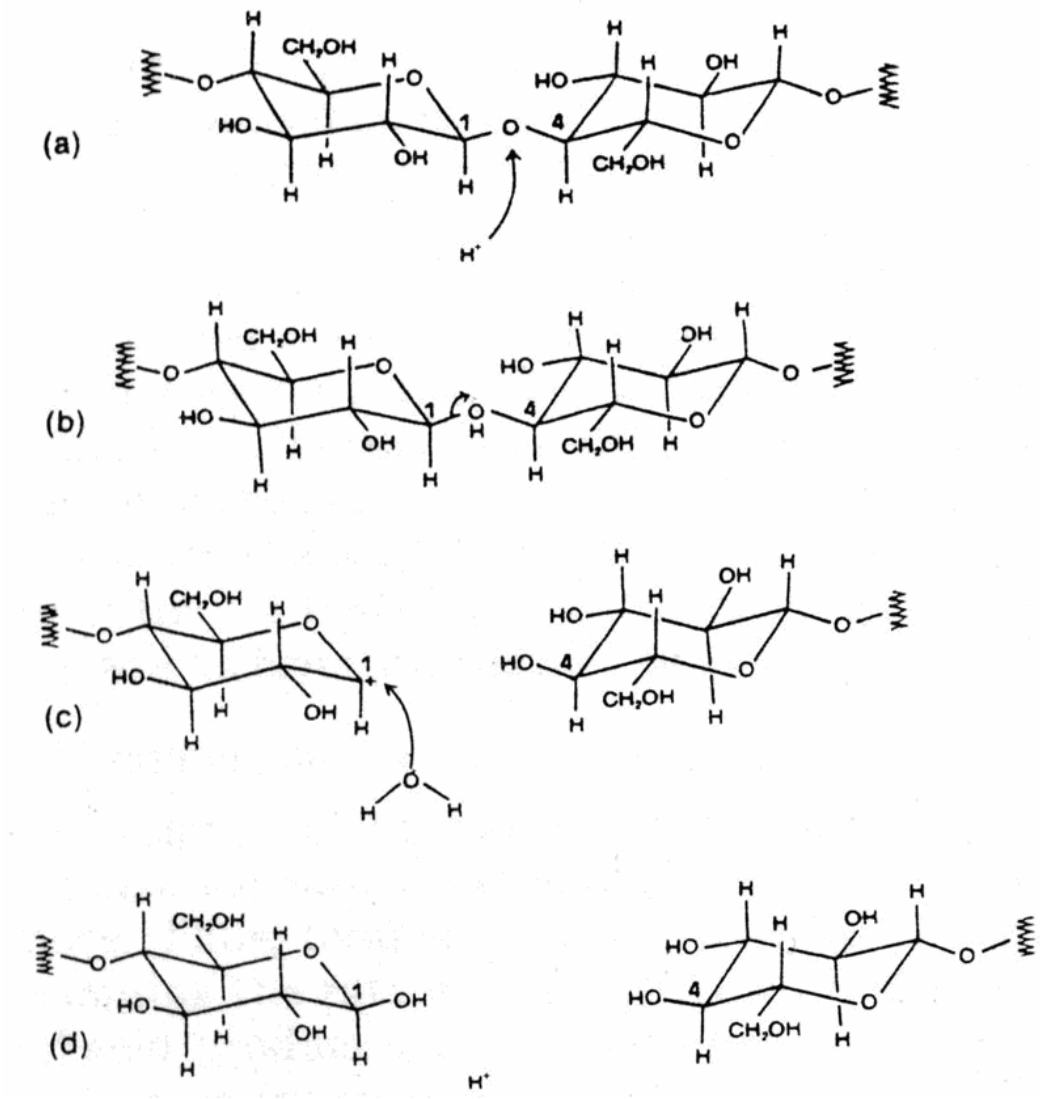

Fig.12: Cellulose Hydrolysis

Step a) *The proton H^+ binds to oxygen*

Step b) *The charge is transferred on carbon 1*

Step c) *The link between oxygen and carbon is broken and a water molecule is fixed on carbon 1, positively charged*

Step d) *A proton is detached from the molecule of water and continue the action of hydrolysis.*

The result is the breaking of the bond and the formation of two OH (on the C1 and C4).

The progressive fragmentation of the chains makes the paper brittle, leading to increased oxidation also causes yellowing.

Oxidation

The oxidative degradation occurs both in acidic and in alkaline environment. This process may involve primary and secondary alcohol groups (fig. 13), but it is also possible the formation of double and triple carbon-carbon bonds in the ring. The primary alcohol group at C6 can be oxidized to aldehyde and then to carboxyl; the secondary alcohol group in C2 and C3 can be oxidized to ketones. The reducing end groups of each chain are oxidized to carboxyl.

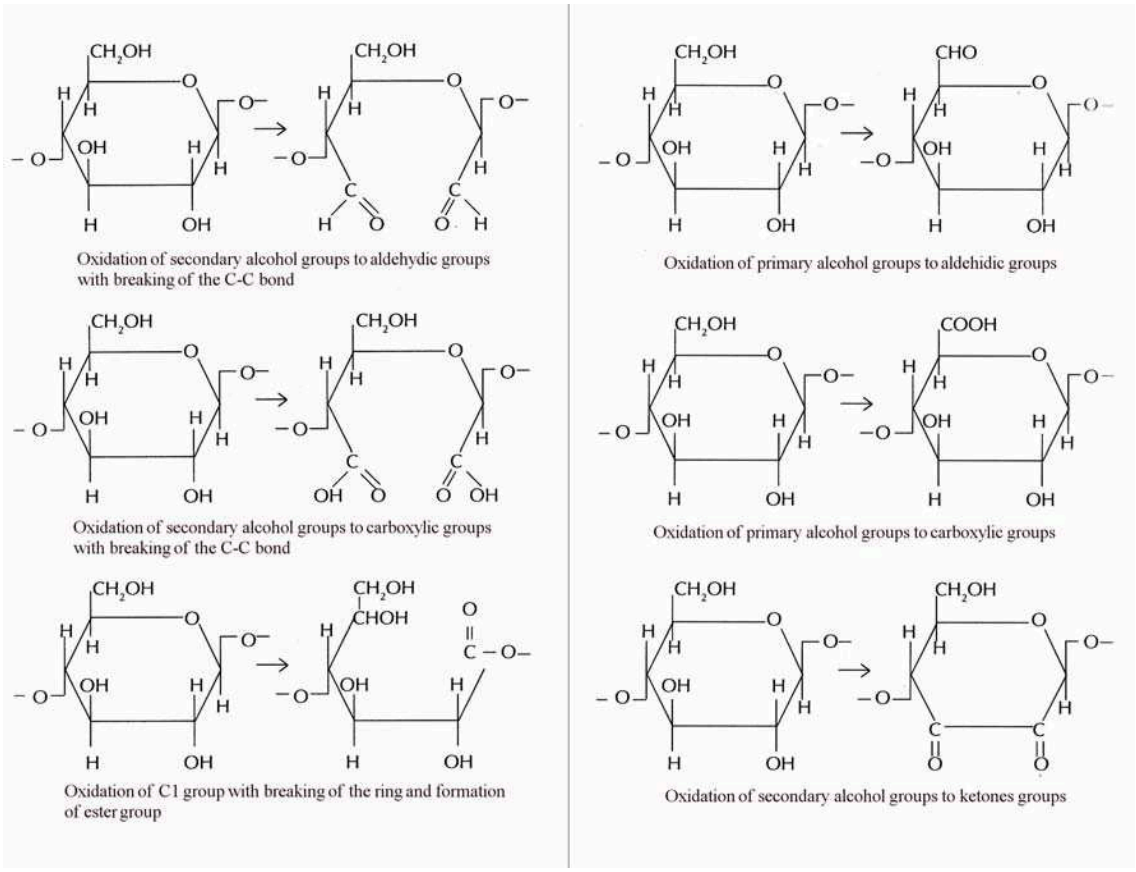

Fig. 13: Oxidation of primary and secondary alcohol groups in cellulose chain

There is synergy between hydrolysis and oxidation, for this reason the study of the alterations is very difficult. Indeed, the presence of oxidants groups accelerates the reactions of hydrolysis.

Foxing

Foxing is the term that describes the stains, spots, and blotches on old papers or documents which doesn't affect the integrity of the paper (fig. 14). The name "Foxing" is believed to come from the fox-like reddish-brown colour of the stains. The foxing stain may be due to metals (iron or copper), fungi or microganisms.

However in correspondence of the spots there is a strong oxidation of the cellulose chain, characterized by a high content of carbonyl groups and the presence of double and triple carbon-carbon bonds.

Fig. 14: Foxed paper

The main reason for the destruction of old paper lies in the oxidation of the cellulose fibers, which leads to paper yellowing and gives rise to foxing stains

(yellowish or dark brown spots). The nature of foxing stains is still debated in spite of extensive studies in this field (Brandt et al. 2009).

Some authors observed a biological attack, others the presence of chemical salts, others again both fungal spores and chemicals. It is then difficult to state whether biological attack caused the degradation or whether it simply happened on the surface of an already degraded paper substrate. Nevertheless, it is known that foxing is characterised by a three-dimensional structure, since it can penetrate into the paper, and even migrate through successive pages (Buzio et al. 2004).

At present, the nature of foxing is still under discussion. The complexity of the problem is related to a variety of chemical reactions and physical processes that take place during the ageing of paper. Moreover, these processes can vary depending on external conditions and the original composition of the paper.

The problem of the foxing diagnostics at early stages is also very important. At present, several methods have been developed to prevent oxidative damage. They are based on the application of chemicals that neutralize the paper's acidity and of antioxidants, in particular, molecules that form complexes with metal ions with variable valence (Brandt et al. 2009).

Several spectra from foxed paper are characterized by the presence of conjugated (C=C, C=O, or C=N) bonds. More accurate identification of the bonds is unavailable. It is not clear whether different types of foxing correspond to different processes of their evolution or different stages of a single degradation process.

FTIR-ATR analysis of foxed stains appears very promising (Choisy et al. 1997; Manso et al. 2009) as this technique has been used for the analysis of paper composition and degradation (Calvini and Gorassini 2002; Calvini and Vassallo 2007; Zotti et al. 2007, Zotti et al. 2008), as well as for the analysis

of fungal strains in mycological research (Gordon et al. 1997; Irudayaraj et al. 2002; Erukhimovitch et al. 2005; Fischer et al. 2006; Szeghalmi et al. 2007). However, the interpretation of FTIR spectra is severely hampered by the similarity between the organic compounds present in fungi (e.g., polysaccharides, lipids, and proteins) and sizing compounds or surface coatings of paper documents. Since FTIR-ATR spectroscopy is sensitive to several organic chemical groups that are in common with both fungi and gelatin-sized ancient paper, FTIR analysis was performed both on the spots and on the neighbouring unstained paper surface. Zotti el al. applied FTIR spectroscopy to still living fungi isolated from the surface of a wood pulp cardboard (fig. 18). In particular, in order to prove the biological nature of the foxing stains, it was showed the presence of the main absorption bands observed for living fungi: amide I at about 1635 and amide II at about 1540 cm^{-1} and the presence of the broad plateau between 1500 and 1200 cm^{-1} typical of fungal agents.

Others degradation processes

The nature of paper manufacturing can also affects its degradation. The use of wood pulp rather than rags, causes an increase in lignin content which is easier to hydrolyze. The products of the lignin hydrolysis catalyze acid reactions and cause paper browning. Also additives, bleaching substances, glues and colours significantly accelerate the degradation.

Many additives in modern paper cause degradation: the calcium carbonate (which stabilizes the acid reaction) if used in large quantities change the mechanical properties of paper.

Environmental factors can influence the cellulose physical condition. Among these: the climate, lighting, air pollution and dust. Infact, both the absorption of water and the temperature increase catalyze the hydrolysis reactions and promote microbial attack. Moreover wrong lighting (artificial or natural) can cause photo-degradation phenomena.

The pollutants in the atmosphere catalyze many reactions of degradation, especially in association with water. The most harmful substances are sulphurs compounds which cause oxidation.

Dust increases chemical and physical damage absorbing water vapour, pollutants and microrganisms (Copedè, 2003).

ABOUT PARCHMENT

Throughout the entire Middle Ages, parchment, alongside papyrus, was the predominant writing material in Europe and in the Near and Middle East. Only after the invention of paper and the diffusion of bookmaking, the parchment was not used anymore for ordinary documents.

According to the reports of various Classical authors, parchment was 'invented' by Eumenes II of Pergamon (197–159 BC). To perpetuate his memory and fame, he wanted to establish a library in Pergamon that would rival the most famous library of the time, the Alexandria library (Fuchs, 2004).

However, writings on treated animal skin are even older: some Egyptian Fourth Dynasty texts were written on parchment. Though the Assyrians and the Babylonians impressed their cuneiform on clay tablets, they also wrote on parchment from the 6th century BC onward. Rabbinic culture equated a "book" with a parchment scroll. Early Islamic texts are also found on parchment.

In the Middle Ages calfskin and split sheepskin were the most common materials for making parchment in England and France, while goatskin was more common in Italy.

There was a short period during the introduction of printing when both parchment and paper were used.

In the later Middle Ages, parchment was largely replaced by paper. New techniques in paper milling allowed it to be cheaper and easer to manufacture than parchment.

Fig. 15: A) In the early Middle Ages, even parchment with holes was used for manuscripts; B) Old stitched repair in a manuscript in the Berlin Staatsarchiv.

After the invention of printing in the later fifteenth century, the demands of printers far exceeded the supply of animal skins for parchment.

The shortage of raw materials led to the reuse of early medieval damaged manuscripts whose texts were erased in order to be written on again.

There were different qualities of parchment, more or less thick, rough or clear. Depending on the use one product might be preferred over another. So, while the parchment for bookbinding (from the sixteenth century onwards) was thinner, parchment for documents of relevant importance (for example, the papal brief) resulting from pieces of young or dead animal skin was bright white and very thin. Although in Europe since the thirteenth century the use of parchment in books had greatly reduced, there were areas in which this did not happen. In fact the vast majority of public documents issued by kings, emperors and popes continued to be written on this support beyond the end of the nineteenth century and, although rarely, the same parchment was also used for printing, at least until the end of the nineteenth century (Fuchs, 2004).

Fig. 16: Folchart psalter, 9th century AD (Stiftsbibliothek, St. Gallen). The parchment maker and his client. 1255 Hamburg Bible (Royal Library, Copenhagen).

The parchment production

The parchment preparation methods was quite similar both in ancient times and in the Middle Ages, and indeed remained fairly unchanged right into modern times (fig. 17).

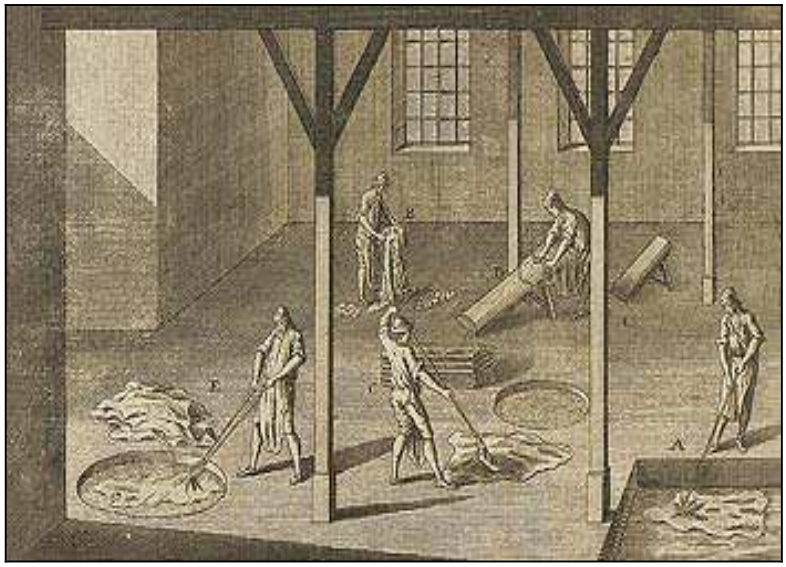

Fig. 17:The manufacture of parchment. From J.H.G. von Justi, Die Kunst Pergament zu machen, Berlin, 1763.

Only after the introduction of industrial technology and modern chemistry the process has changed significantly. The ancient preparation methods was the following: soaking the fresh animal skin for 2–6 weeks in a 5–10% solution of slaked lime (Calcium hydroxide - $Ca(OH)_2$), a process called liming. The different layers of the skin swell at different rates and gradually begin to break up (fig. 18).

Fig. 18: A skin being removed after 3 weeks from the lime bath for dehairing.

The epidermis reacts most quickly. Because the hairs have their roots here, after the soaking process, the hairs along with the roots are easily removed by draping the skin over a beam and shaving with a dull blade (fig. 19).

Fig. 19: After liming, the hairs and fat layers are removed with a blunt blade from the skin draped over a beam.

The skin is then reversed and the remains of fat, muscle and loose flesh are likewise removed from the flesh side. After washing, the transparent skin is stretched and dried on a frame. These physical and chemical processes orient the fibers in sheets and open up the inner structure of the collagen so that air penetrates between the layers causing the parchment to become opaque, and thus suitable for writing or decoration on both sides. To enhance the properties of the surface for writing, both sides of the dried parchment are carefully polished so that they are neither too rough nor too smooth. Polishing (also known as pouncing) is done while the skin is still stretched on the frame, either with a crescent-moon-shaped (semi-lunar) knife (Latin *lunelarium*) (fig. 20), with pumice or with a specially prepared sanding bread.

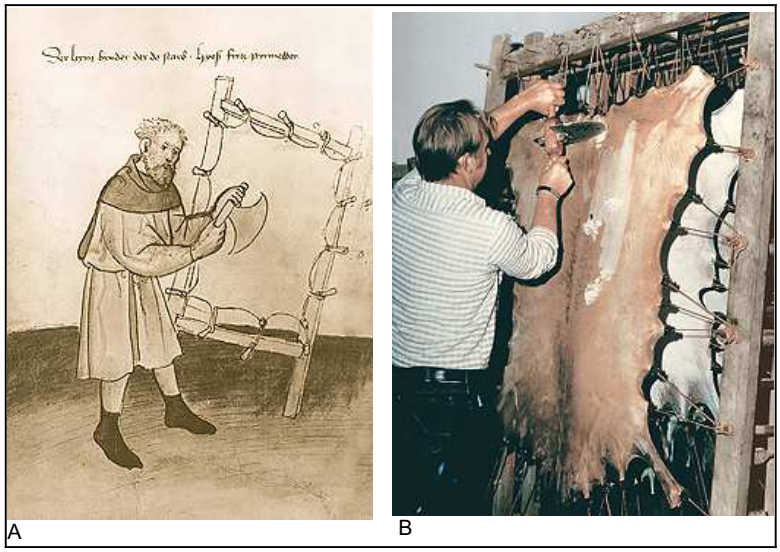

Fig. 20: Pouncing of stretched parchment with the lunelarium. A) Yesterday: Fritz Pyrmenter, 73rd brother of the Nuremberg 'Mendelschen Zwölfbrüderstiftung', 1425. B) Today.

For the latter, bread dough is mixed with glass splinters, formed into small rolls and baked. The parchment surface can be treated far more sensitively with such sanding bread than with pumice or a knife. With inattentive use of the knife, the skin can be damaged quite quickly; pumices are not completely homogenous and contain hard stone-like nodules which leave scratches on the

parchment surface. Cuts and tears that occur before the stretching procedure are usually sewn before the skin is put into the frame, so that they don't stretch or expand during drying. They can be cut out after drying, but often they are left in the parchment and can be seen today in the old manuscripts. In the modern manufacture of parchment, sodium sulphide and enzymes are used for dehairing. The result is a product differing significantly in durability and quality from historic parchment, which can cause problems if modern material is used in parchment restoration (Fuchs, 2004).

The parchment biochemical structure

The essential components of parchment from animal skins are the fibers of the connective tissue. This extracellular matrix in the skin is composed of bundles of long-chained fibrils of the scleroproteins collagen and elastin.

The basic unit of collagen is tropocollagen (MW 300 kD), a right-handed helix of three polypeptide chains. A single tropocollagen molecule is a microfibril that, packed together by hydrogen bonds, salt bridges and covalent intermolecular bonding, form fibrils with a diameter of approximately 250–500 nm. Adjacent intertwining molecules in the fibrils are displaced relative to one another by a quarter of their length, giving rise to a periodicity of about 70 nm visible as dark bands in the electron microscope (fig. 21).

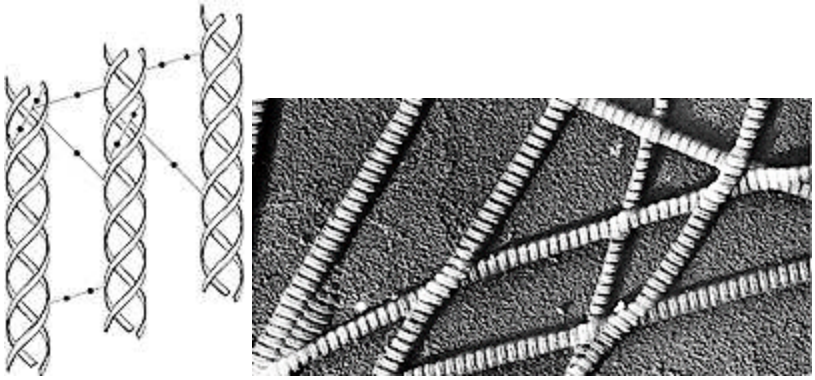

a b

Fig. 21: a) Intermolecular bonds between the triple helices of collagen fibers. b) Scanning electron micrograph of collagen.

In contrast to the relative stiffness of collagen, elastin stretches and recoils. It is assembled from tropoelastin monomers, and hydrophobic domains alternate with intramolecular cross-linking (at lysine residues) domains which confer the elasticity on the randomly coiled molecules (Fuchs, 2004).

The parchment conservation

The biochemical structure of parchment influences its response to the environment. The collagen fibers are heat sensitive. Above 70°C, they begin to shrink irreversibly and denaturation sets in. The fibers also respond to changes in humidity by continuous shrinking and stretching. This can only be prevented by keeping the parchment in a constant environment. This is one of the most important basic conditions for the preservation of painted parchment manuscripts. The pigment layers have a tendency to peel off if heat and humidity keep changing. In addition, high humidity or water are hostile to all parchments: they cause the parchment to become transparent and to decompose.

Parchment is a material of outstanding stability that can survive for many centuries; if correctly archived, it can theoretically be preserved, in an unchanging state, indefinitely. Nevertheless, it has certain peculiar properties requiring a restorer special skills and a feeling for the skin (Fuchs, 2004).

The importance of fragments: Maculature

'Maculature' is a word used to describe a recycled fragment of parchment.

Fragments of manuscripts and printed books were used, especially in XV-XVII century, to reinforce the worn pages, the books binding and cover. Those pieces of parchment, therefore, are in poor condition and unreadable. During the Middle Ages, the reuse of manuscripts was a common practice in monastic libraries, where the old manuscripts were dismantled and the parchment was re-used. Obviously these parchment fragments quote a printed text which has no relationship with the body of the volume and therefore, identification work, is problematic. A thorough investigation of the fragments (procurement, inventory, description, allocation, etc..) has became important nowadays .The pioneers of this type of investigation are Wolfenbùttel Librarians, that in the twentieth century inspected the bindings of stored books, finding more than thirty fragments of the same manuscript "*Historia Francorum*" by Gregorio of Tour (IX century) (Butz-Mann, 1966).

In the current century, notable is the work of Ker on the Oxford books bindings (XVII - XXIII century) that revealed more than 2,000 manuscript fragments used as sheets guard (Ripley Ker, 1954). Is also very important the survey made by Lehmann and Glauning on the bindings stored in two libraries in Monaco.

In Italy the first survey of parchment fragments, unfortunately unpublished, was made by Filippo Di Benedetto, who has streamlined the fragments cataloging method (Innocenti, 1994).

Fig. 22: The fragments of Codex Gregorianus (III century AD) an ancient text on Roman law, considered a lost book, were found between the "parchment recycled" used to bind together the pages of other books of later times.

The inks

Usually inks can be described as liquid, semi-liquid or solid preparations, which can be used to draw graphic signs on a support. Ink recipes have been modified over the ages: the Chinese were the first to use ink, usually mixing lake colours and a black pulverized stone, but the birth of real ink occurred in the Third century B.C. Two centuries later Vitruvius wrote the first true ink recipe in his book De Architectura: he mixed lamp black (a pigment from burnt wood) with camphor and gelatine. Between 2500 and 3000 B.C. a mixture of lamp black ink and oil was used in Egypt while the Arab world only knew of the existence of metal–gall inks. Later Pliny and Cicero described inks based on lamp black, water and Arabic gum. In several Medieval and Renaissance recipe collections the first iron–gall inks were described: for example, in *Schedula diversarum artium Theophylus* described its steps production from vegetable extract maceration to ferrous sulphate addition (Gambaro et al., 2009).

Fig. 23: Carbon black powder and inked papers

From the 17th century on detailed recipes were written and marketed inks were produced using scientific methods. In 1663 Boyle attempted to discover the reaction between vitriol and oak galls; in 1666 Tachen created an ink by mixing oak galls with silver, copper or mercury. In 1748 Lewis listed a series

of products to be used in order to prepare long-lasting ink. In 1785 Schule synthesized gallic acid, while ten years later Dejeux and Seguin artificially produced tannins.

Fig. 24: Ingredient to make iron-gall ink: vitriol, oak galls, Arabic gum, iron-gall inks.

By the 19th century innovative synthetic colorants were employed in ink formulations. The aging of inks is one of the most important causes of corrosion of paper, the mechanism of which depends on the nature of the components and their interactions with paper. Different ink types age differently: the literature pays particular attention to iron–gall inks, which have been shown to be the principal cause of paper penetration. This is due to the acid hydrolysis of cellulose (caused by an excess of sulphuric acid in the recipe) or to iron (II) ion oxidation reactions (caused by an excess of Fe ions) (Calvini, 2001; Reißland et al. 2001).
Conversely carbon black inks are stable due to their chemical inactivity, they just become duller with age. Synthetic inks do not cause paper corrosion but they are very photosensitive (Maraval and Flieder, 1993).

FTIR techniques may provide further information on different types of paper and/or on the writing itself. Some preliminary tests have been carried on original drawings, in order to identify the type of ink used (Burandt, 1994).

The identification of metal-gallic or organic ink via FTIR spectroscopy appears rather difficult, since the main signal is due to the cellulose absorption: indeed, the cellulose remains the major component of the sample even in inked and damaged paper and only small discrepancies are observed between inked or damaged paper spectra and pure cellulose spectra. The interpretation of discrepancies measured on original samples remains difficult since the ink and the paper degradation processes.

Particulate matter

Particulates are dust-size pollutants dispersed in the atmosphere. They can originate from numerous sources such as automobiles, power plants and mines. Research on the effects of particulate matter on human health was initiated in the 1970s (Larsen, 1970; Holland et al., 1979) and have been strongly developed since then.

There is a growing body of clinical evidence indicating that adverse public health effects are caused by the presence of respirable or inhalable particulate matter (PM) in the ambient air (Neukirch et al., 1998). Particles with diameters smaller than 10 μm (denoted PM10) are problematic. The deleterious effects increase with decreasing size. The most signifcant dangers occur for particles smaller than 2.5 μm (PM2.5) (Monn et al., 1997; Wilson and Suh, 1997) because these penetrate deeply into the lungs, from where they cannot be removed by respiration. Of course, particles are not dangerous simply because they are small, but rather because of the material on and in them, which they carry into the lungs.

The mechanisms by which particulate organic matter affects the human body remain controversial. Some researchers hypothesize that ‘ultrafine’ particles (one hundredth of a micrometer in diameter) are the major cause of the deleterious effects (Environment Protection Agency, 1994). They suggest that these very fine particles reach lungs in abundance and, when bound to alveoli, may induce oxidant production and lung inflammation. Other hypotheses point to the hazardous effects of the reaction between organic matter with

attached transitional metals and cell membranes, protein and cell receptors (Mastalerza et al., 1998).

Because of these public health dangers, it is important to have accurate and sensitive analytical methods for the detection and analysis of carbonaceous particles. Chemical speciation of these particles, however, is difficult due to their complexity.

The atmospheric PM particles are composed of a mixtures of water soluble inorganic salts, insoluble mineral dust and carbonaceous material. This carbonaceous fraction includes organic compounds plus elemental carbon.

The organic fraction of atmospheric PM contains hundreds to thousands of chemical components (Schuetzle et al., 1975). Identifying and determining the concentration of individual compounds in mixtures of this complexity is extremely difficult. Most methods for speciation require large quantities of sample, analysis times are long and only a small fraction of the organics can be identified. Due to these constraints, some recent work on analyzing PM organics has focused on functional group and compound class characterization (Gordon et al., 1988). Most functional group characterizations of PM have focused on material extracted from hi-volume quartz and glass filters. The organics are extracted, separated chromatographically, and the separated fractions are examined using infrared spectroscopy (Gordon et al., 1988). This allows a much larger fraction of the PM organics to be characterized but still involves long analysis times and large sample sizes. The large mass required for analysis makes size segregated sampling particularly difficult. Methods for size segregated sampling interfaced with compound class characterization have been reported by Kellner and Malissa (1987) and Dangler et al. (1987). Size segregated samples are collected using impactors and the size fractions are analyzed directly using infrared spectroscopy. The advantage of this approach is the

information it provides about the size distribution of compound classes. A further advantage is that the spectroscopy is done directly, with no extraction. The disadvantage of this approach is that no individual organic molecules, only compound classes, can be identified in ambient PM. A complete discussion of methods for compound class characterization of atmospheric PM is given by Allen and Palen (1989).

EXPERIMENTAL SECTION

Scope of the work on writing materials

The main objectives of this work were the use of the FTIR and Raman spectroscopy to:

- characterize cellulose paper samples and their degradation products;
- characterize cellulose paper samples from great historical and artistic value books;
- characterize the main components detected on parchment samples;
- identify inks on paper and parchment samples;
- characterize stained cellulose paper samples from great historical and artistic value books;

Scope of the work on PM samples

The main objectives of this work were the use of the FTIR and Raman spectroscopy to:

- increase the knowledge about the atmospheric particulate matter composition, using different FTIR analytical techniques;
- using the spectroscopic analysis for the determination of the loadings of organic and inorganic functional groups in size segregated ambient PM.

Methods

The infrared analysis was carried out at room temperature and humidity, spectra were acquired on a Thermo-Nicolet 6700 FTIR spectrometer with Attenuated Total Reflectance (ATR) sampling accessory (Diamond Crystal window).

Raman spectra were recorded on a Thermo Dispersive Raman DXR equipped with a 780 nm excitation laser and full range grating coupled to a micro-probe (CCD detector). The head of micro-probe implements a 10x, 50x and 100x magnifying lenses. Neutral density filters implemented in the system were used to attenuate the laser power on the samples (between 1 and 14 mW).
All the configurations and sampling data are reported on spectra figures.

Paper samples

In order to characterize new and aged paper two analytical methods were performed on paper using strips sampled from no-printed page area of 14 books (age ranging from 1934 to 2009) (fig. 25). Spectra from different aged paper samples were compared to each other and to modern paper in order to point out the differences among the new and old samples and the increase of the degradation process in older samples ones.

Fig. 25: Some of the 14 sampled books (age ranging from 1934 to 2009).

To characterize the cellulose in ancient paper samples, the spectroscopic analysis were carried out on samples from ancient books of high artistic and historical interest. Spectra from ancient paper samples were compared to each other and to modern paper in order to point out the different degradation pattern among the samples.

These samples, provided by the Siracusa Public Library, come from the following books: "*Histoire Naturelle generale et particulaire*" volume 13th written by Georges Louis Leclerc de Buffon[1] and published in Paris in 1789 (fig.26);

Fig. 26: "Histoire Naturelle generale et particulaire".

[1] Georges Louis Leclerc de Buffon (1707–1788) was an eighteenth-century French naturalist.
Buffon developed his interest in natural history after being appointed by Louis XV in 1739 as director of the Jardin du Roi (Royal Gardens and Natural History Collections) in Paris. He was ambitious and produced a collection of books about natural history (animals, plants, and minerals). In 1749 he published (along with a set of co-workers) the first three volumes of his famous *Histoire Naturelle, générale et particulière* that ultimately comprised thirty-six volumes published over a period of fifty years. The *Histoire naturelle* was an enormous success and became one of the most widely read books of the century.
Buffon also included a number of theoretical essays in his *Histoire Naturelle* that were historically important for the theory about the evolution of life and on the concept of species.

"*Tractatus in Quinque Ecclesiae Praecepta*", written by Tommaso Tamburino[2] and published in Lyon in 1626 (fig. 27).

Fig. 27: "Tractatus in Quinque Ecclesiae Praecepta".

In order to characterize cellulose and parchment some fragments belonging to two prestigious books were analyzed: "*Augustini*" (1533) and "*Officia Propria Sanctorum*" (1794). These samples, although not datable, have proved important about the main constituents of such media and its inks. These samples, also provided by the superintendence of BBCCAA Siracusa, include:

[2] The Jesuit, " Tommaso Tamburino " (Caltanissetta, March 6, 1591 - Palermo, October 10, 1675) is the dominant figure of Italian casuistry production, which had developed in Sicily in the seventeenth century following the Spanish one (School of Salamanca). Tamburino works, thanks to the efforts of the Jesuits, were widespread throughout Europe since the mid-seventeenth century. Tamburino's writings of moral theology collected in "Opera Omnia", were published several times in Italy and abroad, and were used as reference books in Europe for a century even after his death.

- six cellulose fragments glued to the board of the back plate of the Restoration Project n. 22/07 "*Augustini*" published in Lugduni (Lyon) in 1533, belonging to the Gubernale Fund, samples were glued on a non-acid paper (Canson gr. 8/10) neck with an adhesive compound based on methyl cellulose MH300p diluted to 4% (fig. 28)

Fig. 28: “Augustini”: restored book and fragments.

- three parchment fragments from Restoration Project n. 20/07 "*Officia Propria Sanctorum*" published in 1794, belonging to the Gubernale Found (fig. 29).

Fig. 29: "*Officia Propria Sanctorum*": restored book and its fragments.

In order to better figure out the foxing process and to verify the biotic nature of foxing, spectroscopic analysis were performed on paper from strongly stained books: "I cavalieri della tavola rotonda" published in 1924; "Francesco Petrarca – Rime scelte" published in 1945. The paper from those two books shows many yellow-brown spots, so although they have little historical-artistic interest they were chosen for the characterization of foxed paper (fig. 30).

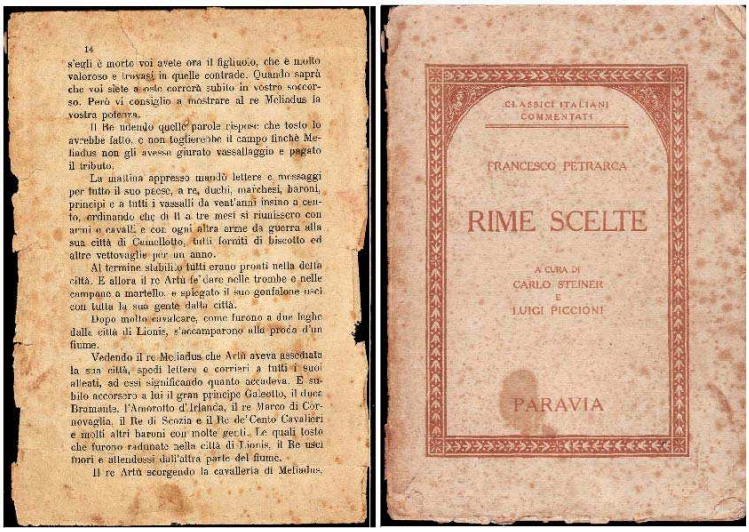

Fig. 30: *Left:"I cavalieri della tavola rotonda"* ; Right:"*Francesco Petrarca - Rime Scelte"* .

Two ancient books of high artistic and historical interest were studied too: "*La Sacra Bibbia*" translated by Giovanni Diodati[3] and printed in London in 1859 (fig. 31);

"La Divina Commedia"[4] a book probably published in the 19th century (fig. 32). This book, although not datable, gave important information about the conservation state of ancient paper and about the characterization of foxed paper.

[3] Giovanni Diodati was the first person to translate the Bible into Italian from Hebrew and Greek sources. Diodati's Bible is "THE" Bible translation, it was edited in Geneve in 1607 using the original books. His Bible version is stylistically speaking one of the Italian language masterpieces of the 17th century. Diodati's credit was to write, all by himself, one of the major Bibles of the European Protestantism, it could be considered peer to Luther's German Bible and to the English Bible authorized by King James.

[4] The "La Divina Commedia" book is not be datable. It has been stored in the Siracusa Noble Society Library until the beginning of the 2nd world war. It survived the Noble Society site bombing but its cover was lost, hence the loss of the book publication date. Later on, the book was found out by a private book collector that replaced the cover with a new one.

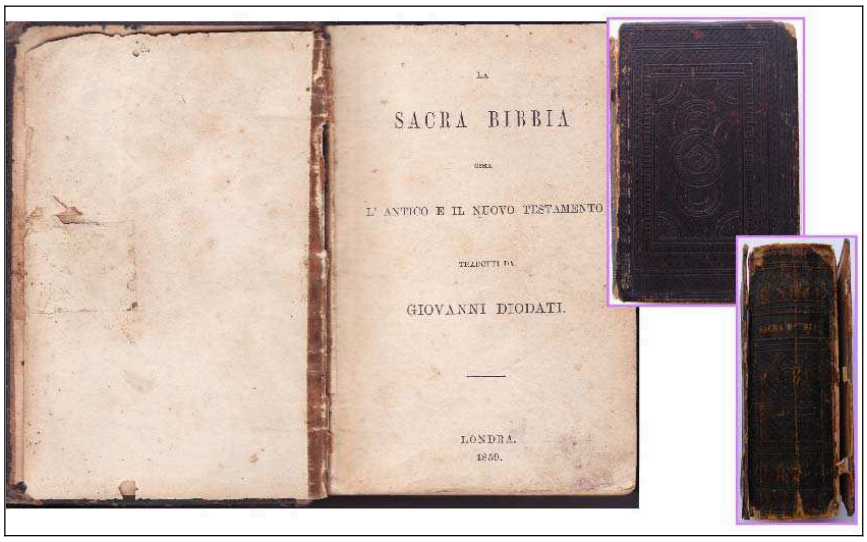

Fig. 31: “La sacra Bibbia”.

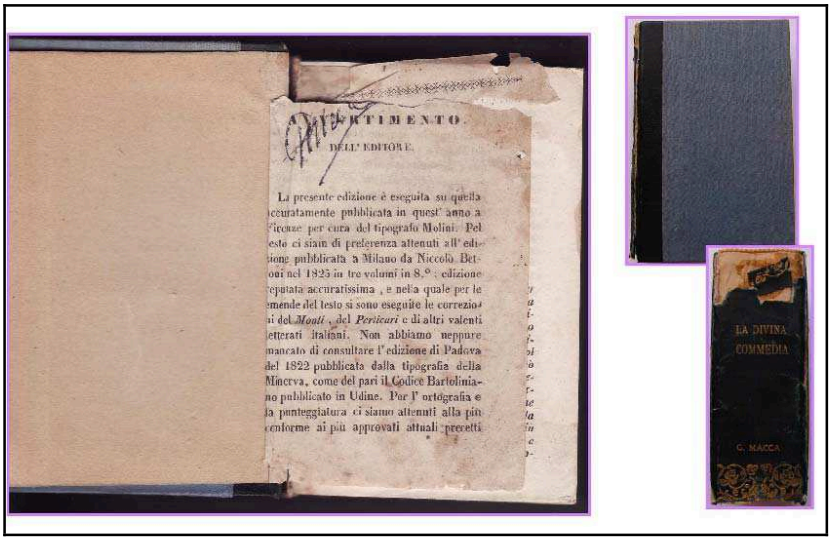

Fig. 32: “La Divina Commedia”

Results

Figure 33 shows the FTIR spectrum of modern paper, sample *A yr. 2009*. It is possible to note the typical bands due to cellulose molecular vibration; table 1 lists wavenumbers and vibrational assignments for some of those bands.

Tab. 1: FTIR/ATR paper vibrational mode assignment

Wavenumber cm^{-1}	Vibrational mode
3200-3400	OH stretching
2890	CH stretching
1600-1650	H_2O bending
1420	CH_2; COH bending
1370; 1335; 1316	CCH; COH bending
1150	COC stretching

The modification of the bands intensity can be used for the interpretation of paper structural changes. Some bands can be exactly assigned to paper components, i.e. band at 1024 cm^{-1} is characteristic of cellulose, the increase of 998 and 984 cm^{-1} bands suggests the presence of starch.

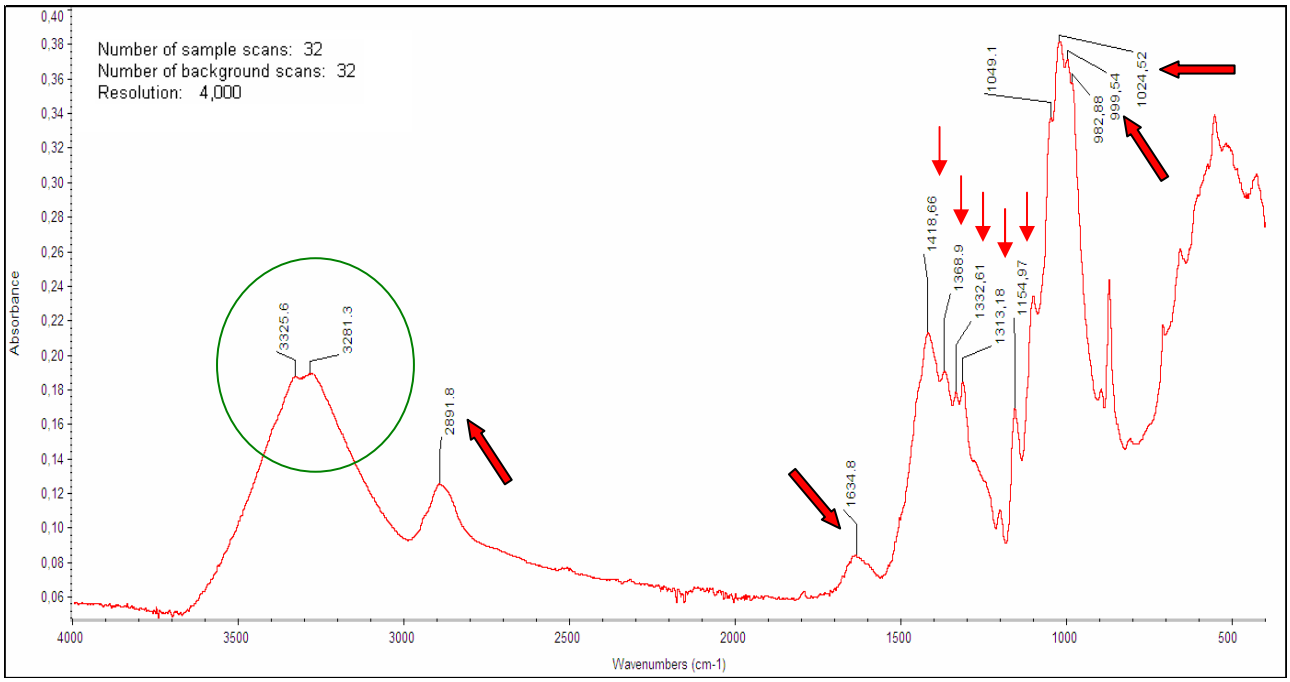

Fig. 33: FTIR spectrum of modern paper sample *A yr. 2009*.

The examination of other spectral features indicates that sample *B yr. 1989* and *C yr. 1940* are gelatine sized paper characterized by the amide I and II bands at approximately 1650 and 1545 cm^{-1}. The slight asymmetry of amide I band suggests the presence of another component, the small band at 1620 cm^{-1} typical of gypsum. Sample *C yr. 1940* contains more gypsum, as shown by the shoulders at 3519 and 3394 cm^{-1} and by the increased small peaks at 1620, 661 and 595 cm^{-1} (fig. 34).

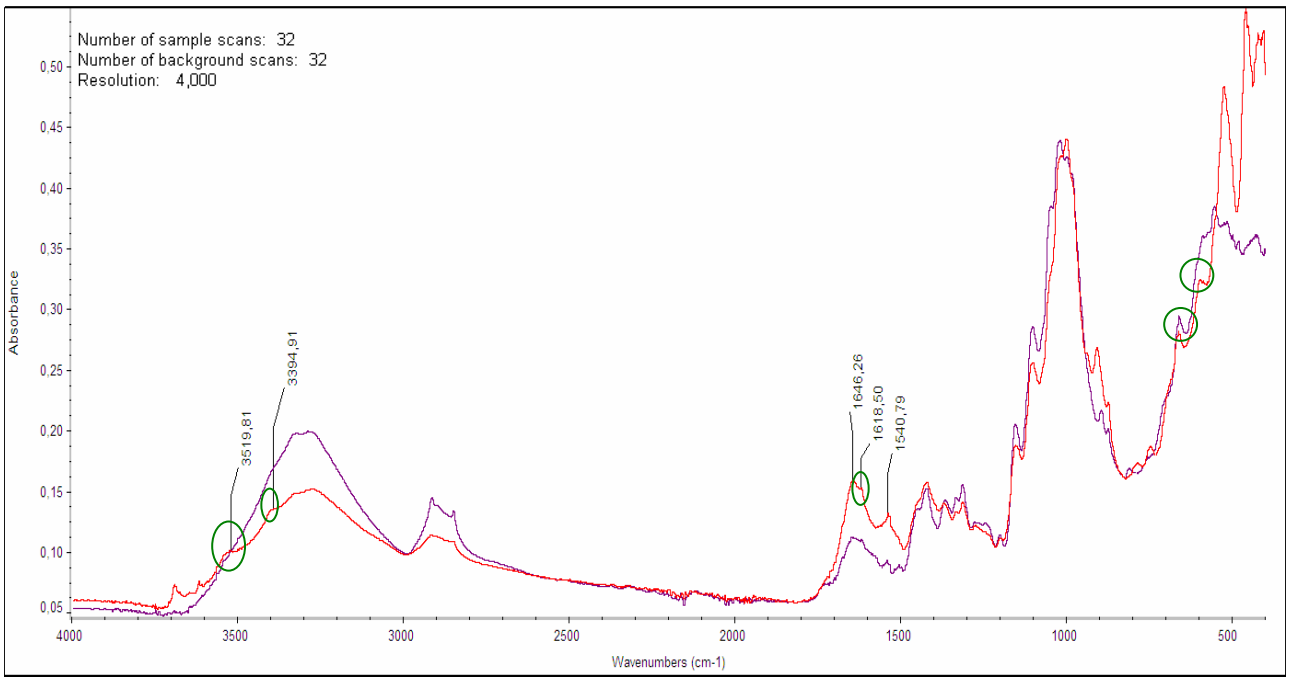

Fig. 34: FTIR spectra of gelatine sizing samples *B yr. 1989* (violet), *C yr. 1940* (red). The green circle underline the gypsum peaks.

Sample *D yr. 1955* contains calcium carbonate (broad absorbance at about 1422 cm^{-1} and peak at 869 cm^{-1}) (fig. 35), while some other features in sample *C yr. 1940* (fig. 36) (small peaks at 2851 and 1541 cm^{-1}) are probably due to calcium stearate (Gilbert et al., 2000). Also in sample *C yr. 1940* there are the shoulders of gypsum at 3519 and 3394 cm^{-1}. The increase of 1000 and 984 cm^{-1} bands in the fingerprints region suggests the presence of starch.

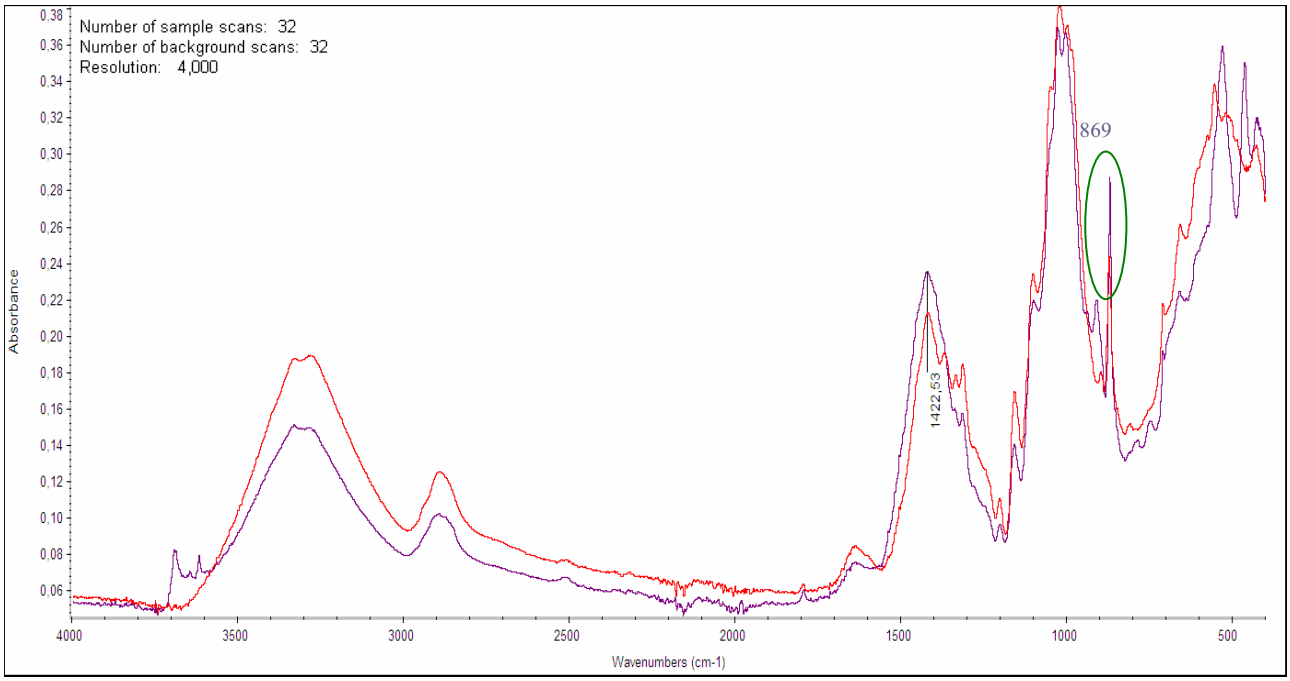

Fig. 35: FTIR spectrum of modern paper sample *A yr.2009* (red) compared to the spectrum of sample *D yr.1955* (violet) contains calcium carbonate: peak at 1422 cm-1 and peak at 869 cm-1 (green circle).

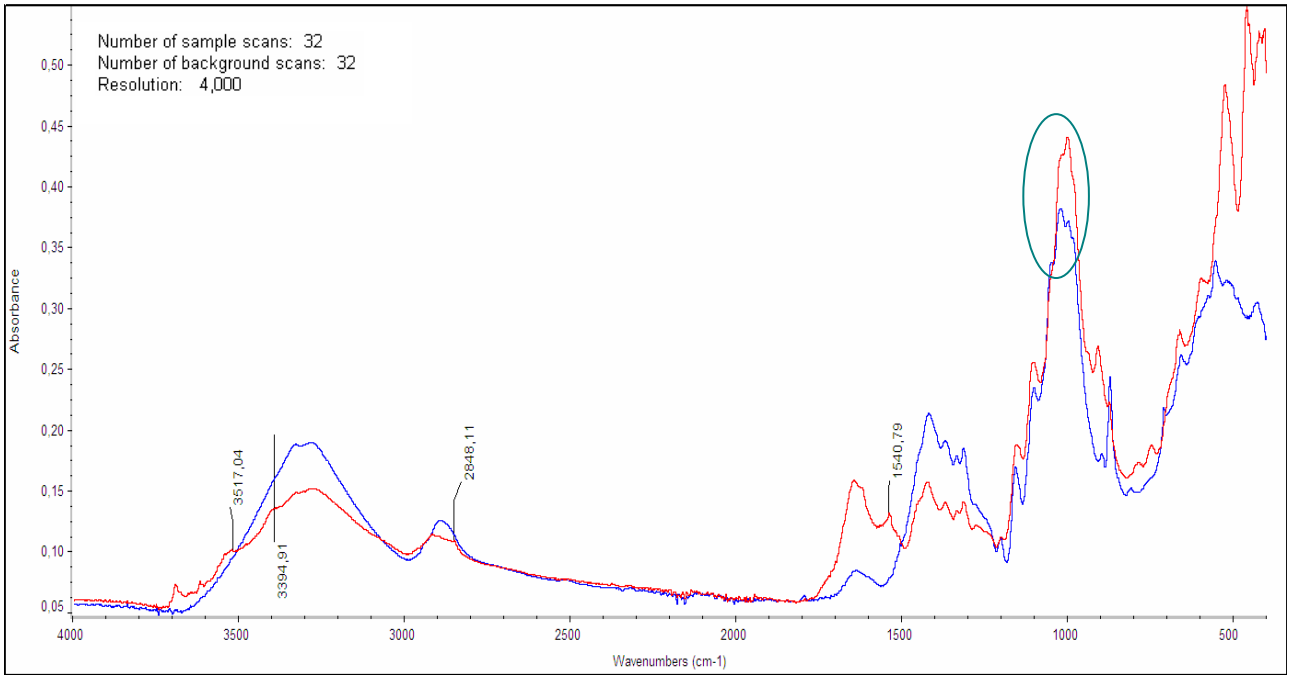

Fig. 36: FTIR spectrum of modern paper sample *A yr.2009* (blue) compared to the spectrum of sample *C yr.1940* (red). Small peaks at 2851 and 1541 cm^{-1} are probably due to calcium stearate; shoulders of gypsum at 3519 and 3394 cm^{-1}; increase of 1000 and 984 cm^{-1} bands in the fingerprints region suggests the presence of starch.

All IR active vibration are also Raman active, so cellulose Raman bands (from modern paper sample) have their counterparts in proper FTIR spectrum, except the 1600-1650 cm^{-1} range where bending vibrations of water molecules cover in IR spectra the lignin peak at 1600 cm^{-1} that appears strongly in Raman spectrum (fig. 37). Additional changes are observed in the 1000-1500 cm^{-1} region.

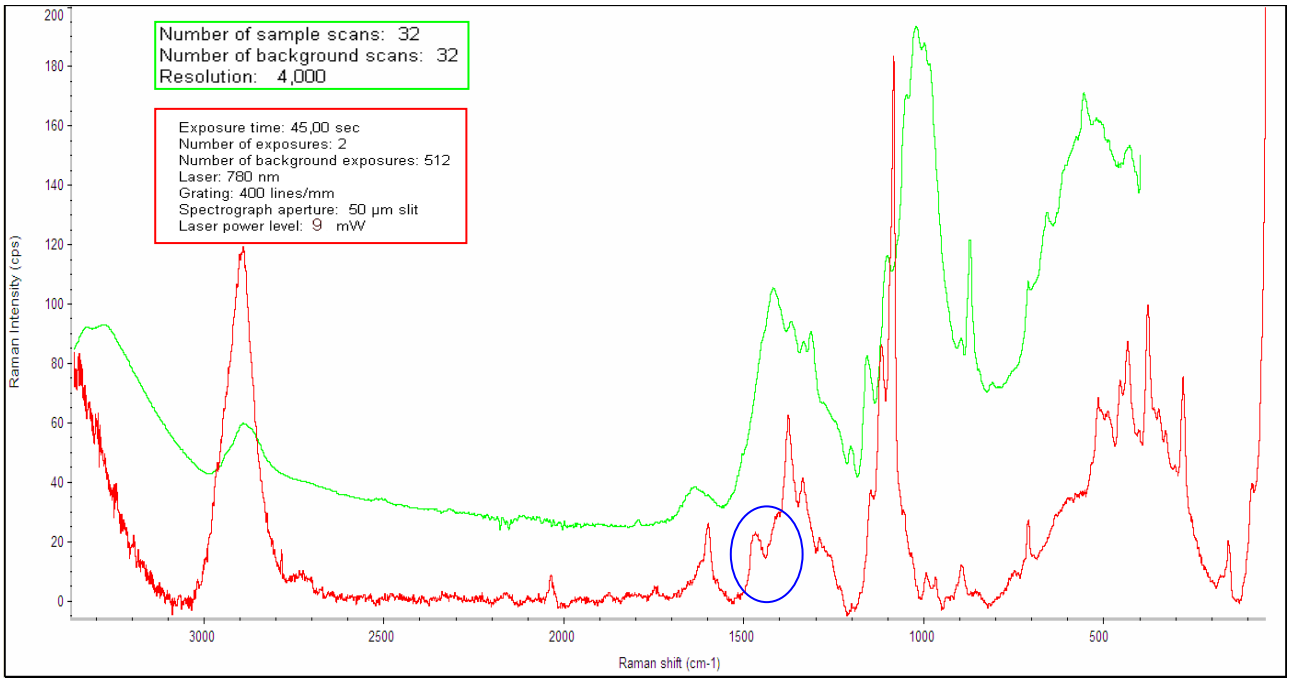

Fig. 37: Comparison between FTIR (green) and Raman (red) spectra of modern paper sample *A yr.2009*. Lignin peak at 1600 cm-1 (blue circle).

Non-polar functional group vibrations that usually result in weak infrared signals give very strong Raman bands.

The most intense Raman bands were located at 1377 and 1336 cm^{-1} due to CH_2, 1118 cm^{-1} (COC of α-glycosidic bond of hemicellulose) and 1085 cm^{-1} (COC of β-glycosidic bond of cellulose and hemicellulose). Besides, there are other less intense bands that can be assigned to CH_2 at 1469, 1414, 1292, 1003 and 967 cm^{-1}, to CO at 1056 cm^{-1} (secondary alcohol) and 1035 cm^{-1}

(primary alcohol) and 1145 cm^{-1} due to CC (asymmetric ring stretching) (fig. 38) (Liu et al. 1998). All this Raman vibrational mode assignment are listed in table 2.

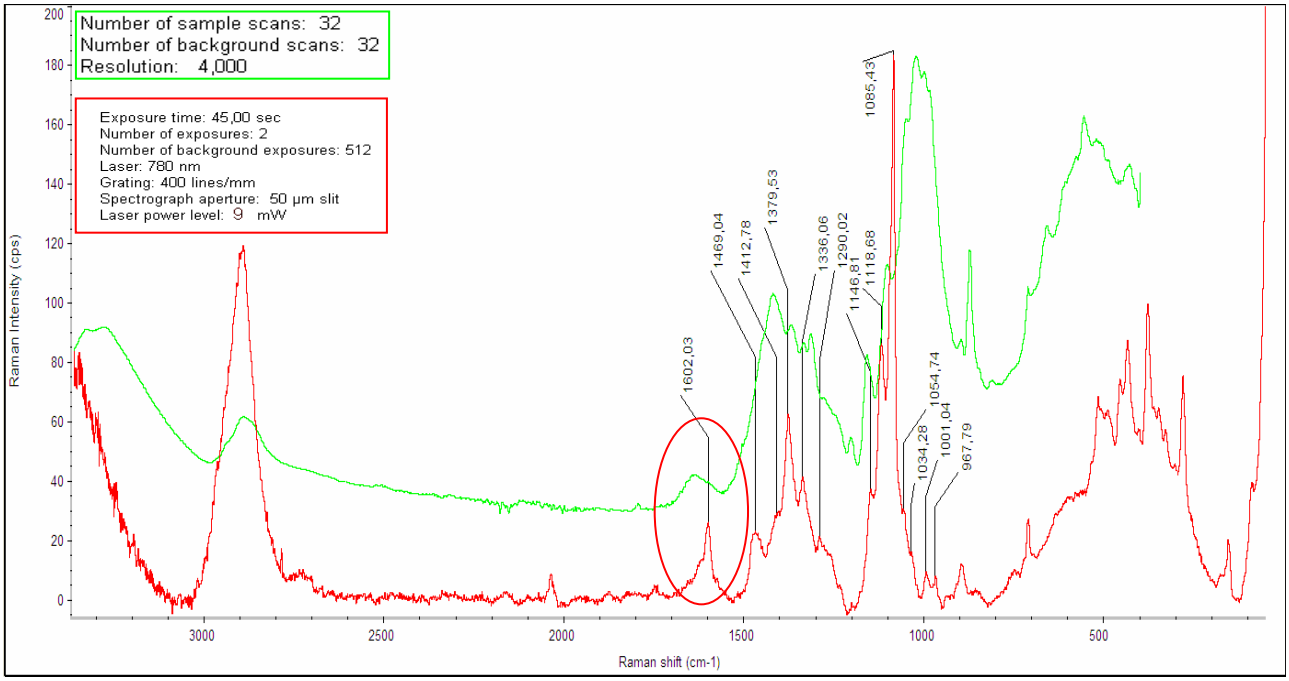

Fig. 38: FTIR (green) and Raman (red) spectra of modern paper sample *A yr.2009*: bands assignment in 1000-1500 cm^{-1} region.

Tab. 2 : Raman paper vibrational mode assignment

Raman Shift cm^{-1}	**Vibrational mode**
1469; 1414; 1377; 1336	CH_2 bending
1118	COC α-glyc. Hemicellulose.
1085	COC β-glyc. Hemicellulose
1292; 1003; 967	CH_2 bending
1056	CO secondary alcohol stretching
1035	CO primary alcohol stretching

FTIR spectrum of modern paper is compared to some ageing paper samples in order to identify the bands due to paper degradation processes.

The intensity of the 900 cm^{-1} bands is very sensitive to the amount of disordered cellulose structure: broadening of this bands reflects an higher amount of disordered structure (fig. 39).

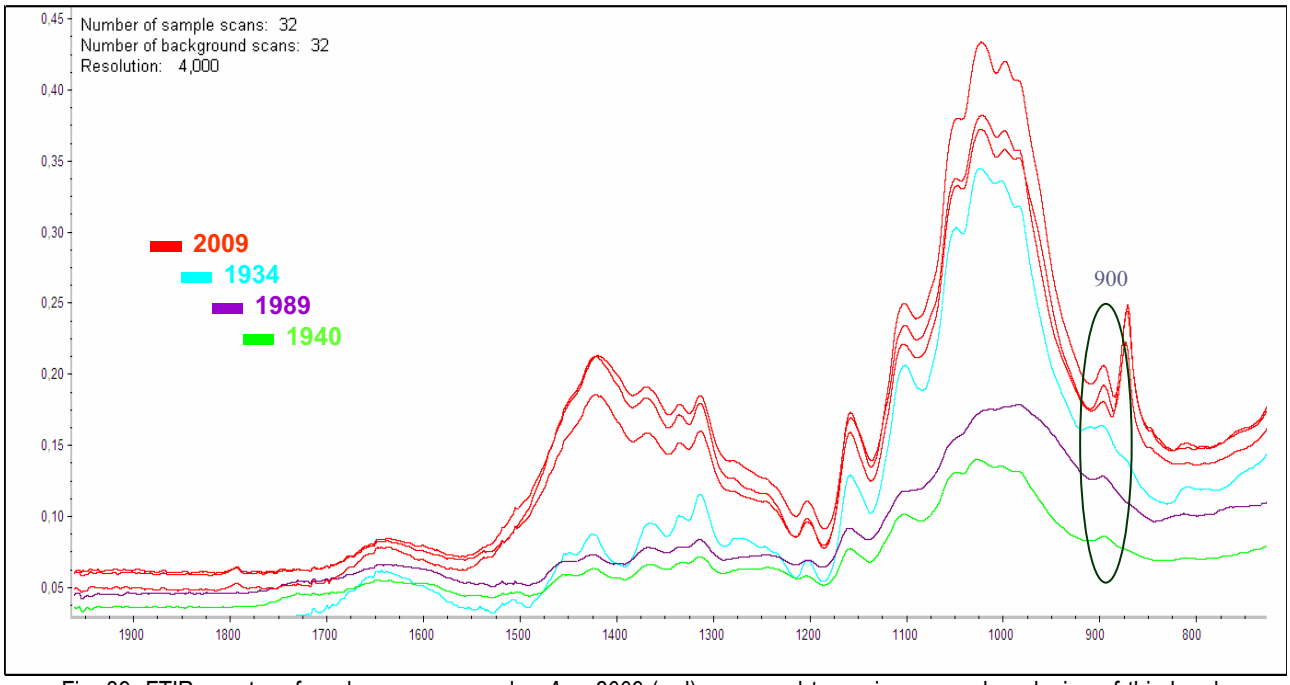

Fig. 39: FTIR spectra of modern paper samples *A yr.2009* (red) compared to ageing paper: broadening of this bands reflects higher amount of amorphous cellulose structures.

Since disorder is expected by the difference arrangement caused by changes in the angles around β–glycosidic linkages and in hydrogen bond rearrangement thus, this band is assigned to the deformation modes of COC, CCO, CCH and stretching vibration in which motions of C5 and C6 are strongly involved (Vasco et al., 1972), (Lin-Vien et al., 1991), (Zhbankov et al., 1995), (Zhbankov et al., 1995), (Wiley and Atalla, 1979).

The oxidation of OH groups causes the formation of ketons, aldehydic and carboxylic groups with a tic absorption band at 1730 cm^{-1} as shown in figure 40.

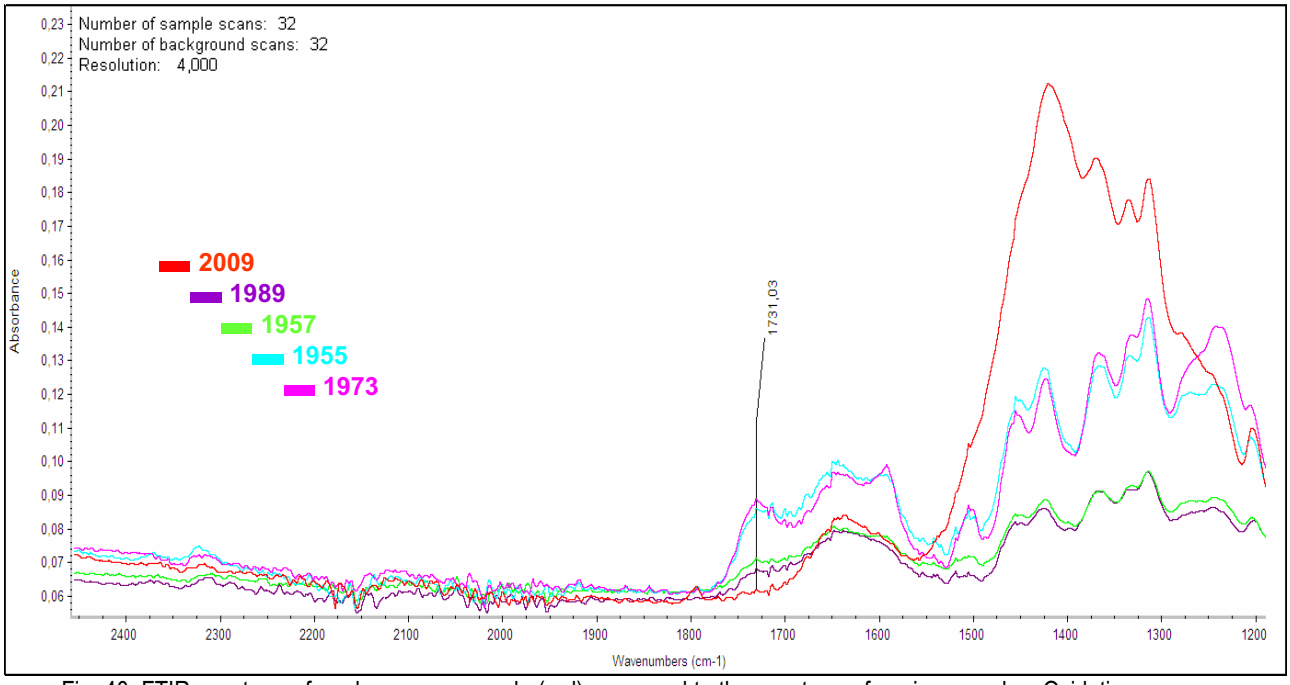

Fig. 40: FTIR spectrum of modern paper sample (red) compared to the spectrum of ageing samples. Oxidation causes a tic absorption band at 1730 cm^{-1}.

The most pronounced changes in intensities are observed for two bands at 1425 and 1316 cm^{-1} with smaller changes at the 1335 and 1370 cm^{-1} frequencies (fig. 41). The 1425 cm^{-1} band which is mainly due to H-C-H and O-H-C in plane bending vibrations gains intensity with accelerated aging of cellulose, while the 1316 cm^{-1} band that is due to C-O-H and H-C-C bending vibrations is losing its intensity. Smaller changes in intensity are observed for the 1335 and 1370 cm^{-1} band that are, similarly to the 1316 cm^{-1} band, assigned to C-O-H and H-C-C bending vibrations (Vasco et al., 1972), (Lin-Vien et al., 1991), (Zhbankov et al., 1995), (Zhbankov et al., 1995), (Wiley and Atalla, 1979), (Tu et al., 1979), (Gilbert et al., 1993).

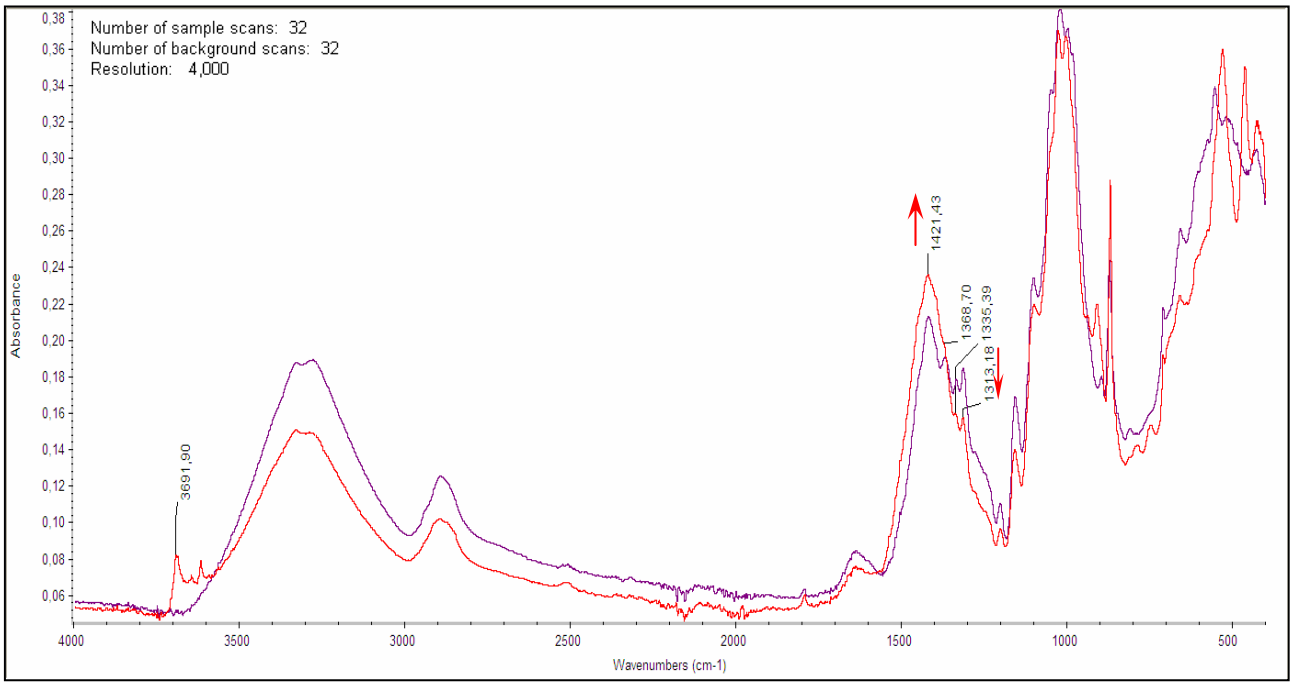

Fig. 41: FTIR spectrum of modern paper sample *A yr. 2009* (violet) compared to the spectrum of ageing sample *D yr.1955* (red): 1425 cm^{-1} band gains intensity with accelerated aging of cellulose, while the 1316 cm^{-1} band loses its intensity. Smaller changes in intensity are observed for the 1335 and 1370 cm^{-1} bands.

It is very difficult at this point to clearly interpret the data. However, it seems likely that hydrolysis of glycoside bonds at this level of "destruction" has to cause changes in the polymeric structure mainly by forcing rearrangement in hydrogen bonding (changing from a crystalline to an amorphous form) that in turn changes the vibrational pattern of CCH, COH, OCH and HCH bending vibrations. Rearrangement in hydrogen bonding is further supported by the observation of a band due to the O-H bending from water molecules shifting towards higher frequency (from 1635 to 1650 cm^{-1}) (fig. 42).

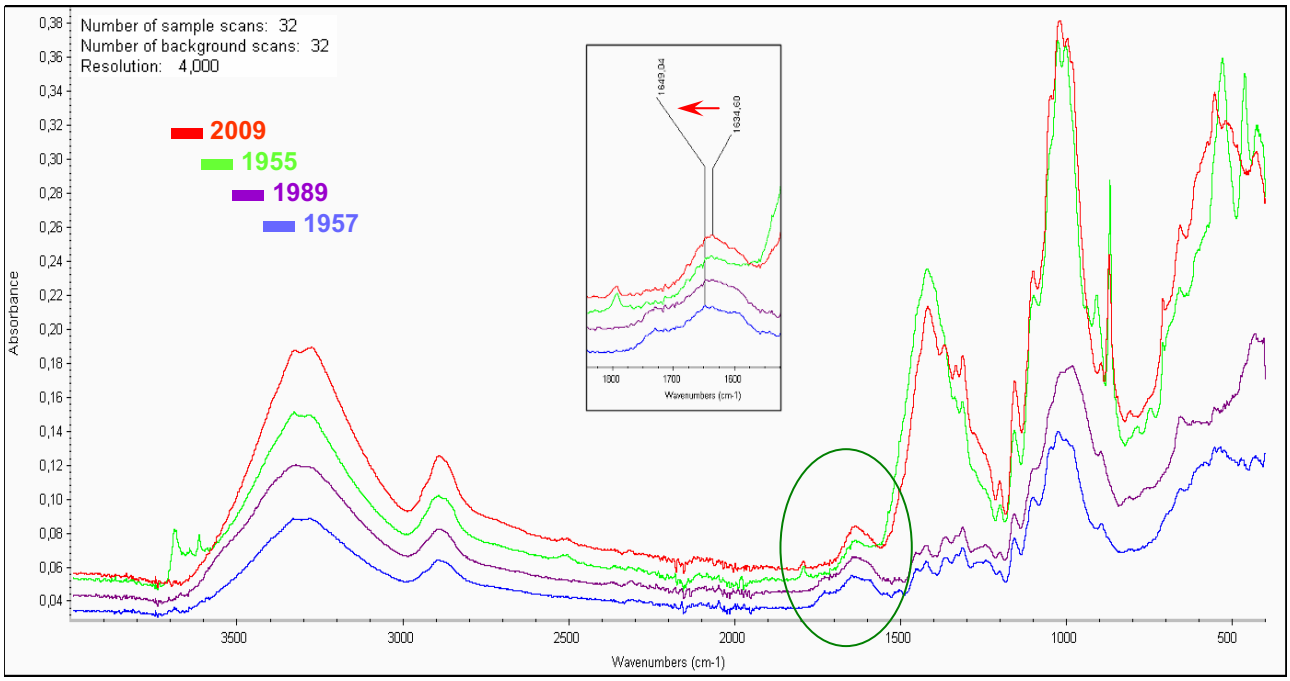

Fig. 42: FTIR spectrum of modern paper (red) compared to the spectrum of ageing samples. Rearrangement in hydrogen bonding causes a shift of O-H bending band of water molecules towards an higher frequency (from 1635 to 1650 cm^{-1}).

Characterization of ancient books

Table 3 lists wavenumbers and vibrational assignments reported in the previous section, these assignments have been used for the interpretation of data obtained from ancient books analysis.

Tab. 3 : FTIR/ATR paper vibrational mode assignment

Wavenumbers cm^{-1}	**Vibrational mode**
3690	Kaolin
3200-3400	OH stretching
3519; 3394	Gypsum
2890	CH stretching
2851; 1541	Calcium stearate
1600-1625	HO bending
1650	Primary NH_2 bending
1620	Gypsum
1545	Secondary NH_2 bending
1422; 869	Calcium carbonate
1420	CH_2 ; COH bending
1370; 1335; 1316	CCH ; COH bending
1150	COC stretching
1024	Cellulose
1000; 984	Starch
661; 595	Gypsum

The FTIR analysis on ancient books were carried out on samples from books listed in table 4.

Tab. 4 : Description of samples from ancient books

Books information	Samples description	Books code
Histoire Naturelle generale et particulaire volume 13th published in Paris in 1789	Cellulose paper samples	*E yr. 1789*
Tractatus in Quinque Ecclesiae Praecepta, published in Lyon in 1626	Cellulose paper samples	*F yr. 1626*
Augustini, published in Lyon in 1533	Cellulose paper fragments glued to the board of the back plate of the book. Not datable paper samples.	*G yr. 1533*
Officia Propria Sanctorum, published in 1794.	Parchment fragments reinforcing the back of the book cover. Not datable parchment samples.	*H yr. 1794*

Paper samples from books *E (yr. 1789)*, *F (yr. 1626)* and *G (yr. 1533)* show typical absorption bands of calcium stearate (shoulders at 2835 and 1541 cm^{-1}) and the presence of gypsum (peaks at 661 and 595 cm^{-1}).

The most marked changes in intensities are observed for two bands at 1425 and 1316 cm^{-1} with smaller changes at the 1335 and 1370 cm^{-1} frequencies. Infact, the rearrangement in hydrogen bonds due to oxidative reactions causes changes on the vibrational pattern of those bands (fig. 43).

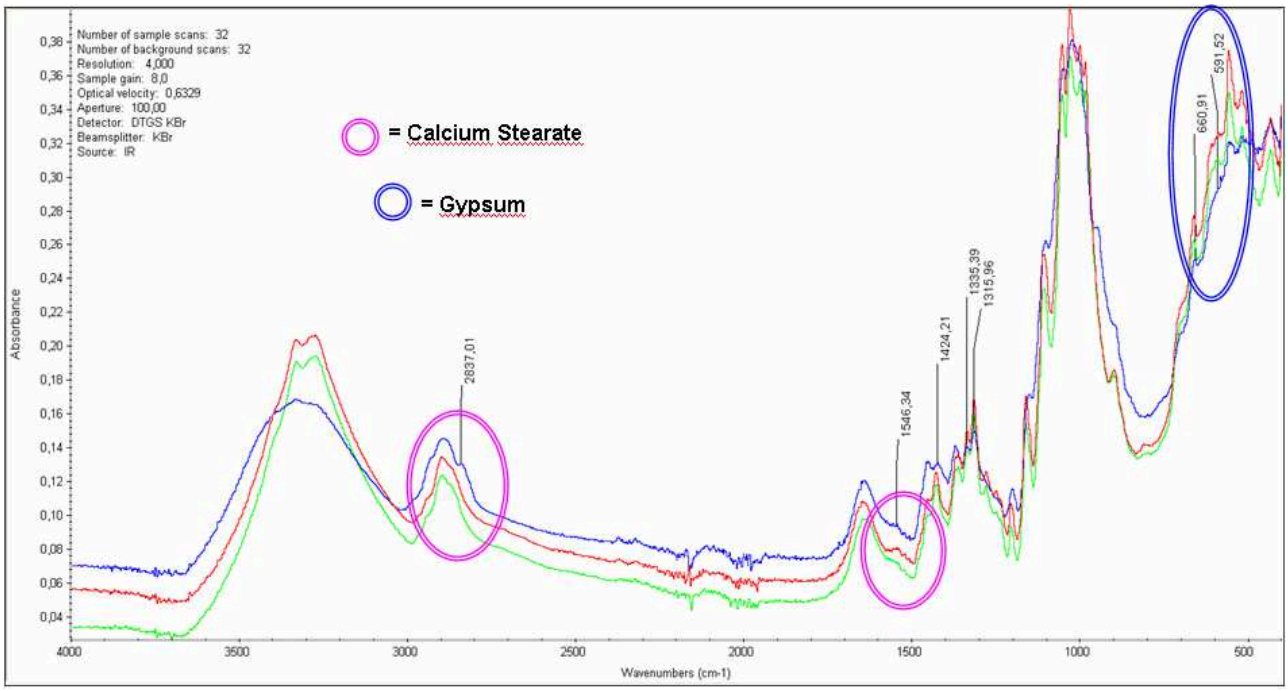

Fig. 43. FTIR spectra of paper samples from ancient books: *E yr. 1789* (green), *F yr. 1626* (red) and *G yr. 1533* (blue). The bands at 1425, 1316, 1335 and 1370 cm^{-1} are very sensitive to paper ageing process.

The 1425 cm^{-1} band which is mainly due to H-C-H and O-H-C in plane bending vibrations gains intensity with the accelerated aging of cellulose, while the 1316 cm^{-1} band that is due to C-O-H and H-C-C bending vibrations is losing its intensity. Smaller changes in intensity are observed for the 1335 and 1370 cm^{-1} band that are, similar to the 1316 cm^{-1} band, assigned to C-O-H and H-C-C bending vibrations (Vasco et al., 1972), (Lin-Vien et al., 1991), (Zhbankov et al., 1995), (Zhbankov et al., 1995), (Wiley and Atalla, 1979), (Tu et al., 1979), (Gilbert et al., 1993).

Comparing the spectra of the ancient samples to those of modern paper or at least with last century samples, the oldest samples show a much less marked degree of oxidation (fig. 44). This better samples conservation state is due to higher quality of raw materials used to manufacture paper in the seventeenth

and eighteenth centuries and the use of a smaller variety of additives which promote the paper degradation processes.

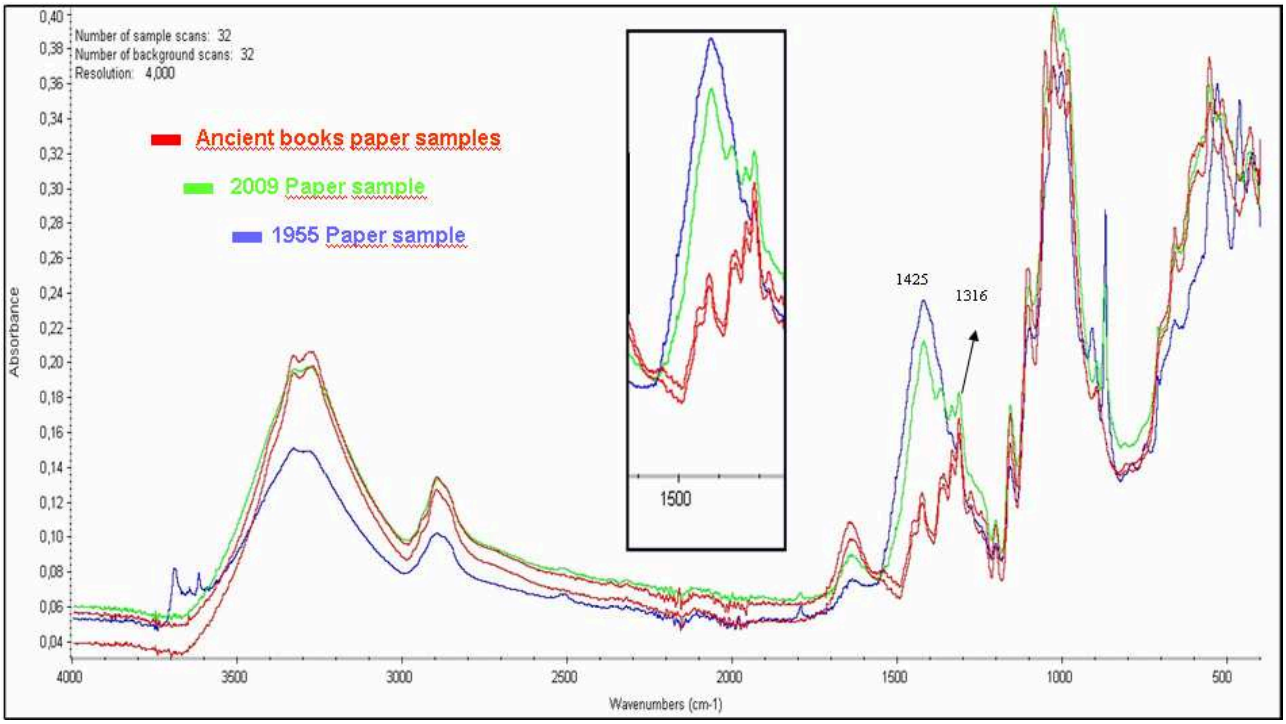

Fig. 44. FTIR spectra of paper samples from ancient books (*E yr. 1769* and *F yr. 1626*, red spectra) compared to recently produced paper from 2009 (*A yr. 2009*, green) and to the last century paper (*D yr. 1955*, blue): the band at 1425 cm^{-1} gains intensity with the accelerated aging of cellulose, while the 1316 cm-1 band lowers its intensity.

Parchment characterization

Even though parchment has been used as a library and archive substrate for centuries, the structure of this material and degradation patterns are less investigated than paper ones. In this preliminary work vibrational studies highlighting a distinction between parchment components are presented. Advances in conservation methods can be achieved by an improved knowledge of the microscopic and spectroscopic features of the parchment components. Unlike paper, however, no industrial of semi-industrial process for parchment production has ever been developed, nowadays parchment is still hand-made and, therefore, every specimen is unique. The lack of reproducibility is why research on parchment at a structural level is still ongoing (Bicchieri et al., 2008).

The aim of this study on parchment samples has provided an insight about the main structural aspects of this material and the most effective non-destructive techniques in its characterization through the spectroscopic analysis. I also focused on the identification of historical inks and pigments.

Figure 45 shows the FTIR average spectrum of parchment samples from book *H yr. 1794*. Some characteristic collagen absorption bands were assigned. The peak at 1030 cm^{-1} is typically due to the amino acids component and can be interpreted as a stretching of the C-N groups.

The peak at 1028 cm^{-1} is interpretable as C-N stretching of amino acids. Peaks at approximately 1075 cm^{-1} are found in L-proline, trans-4-hydroxy-proline and gelatine: it can be interpreted as a C-O stretching or skeletal stretching (Arney and Jacobs,1978).

Eventually, the peak at 1155 cm^{-1} is only found in L-proline and probably belongs to the range of the NH_3^+ vibrational modes (Kowalik, 1980).

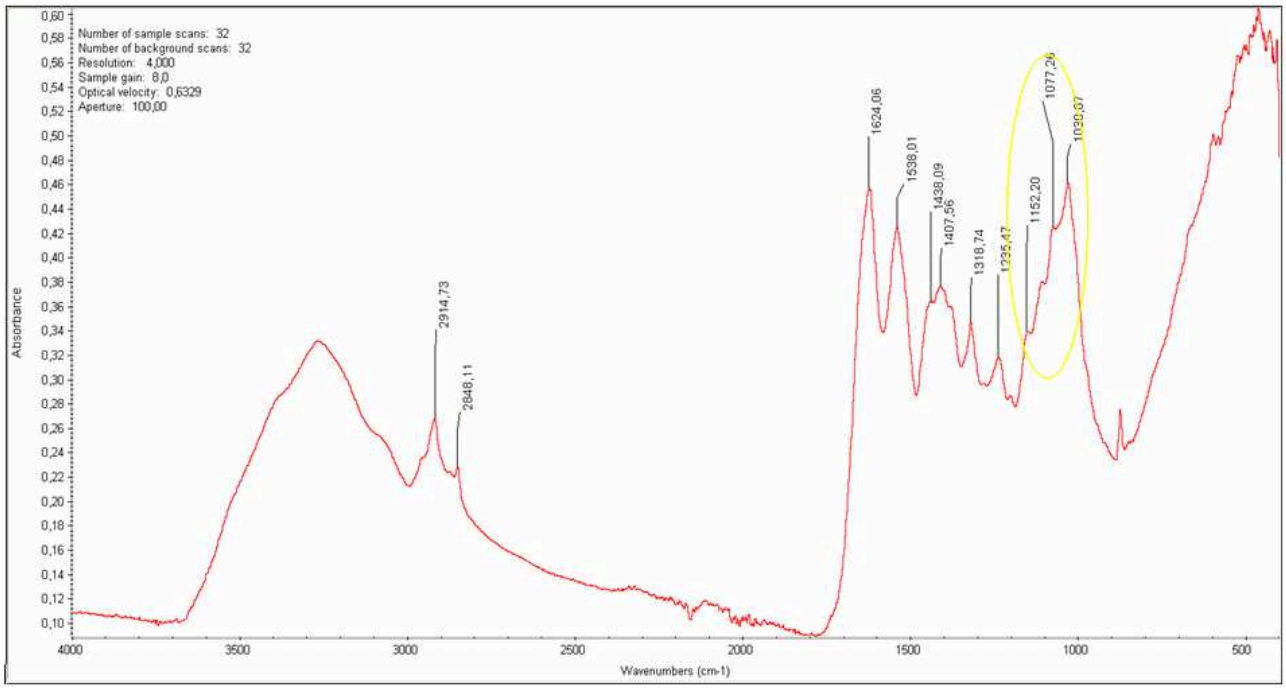

Fig. 45: FTIR average spectrum of parchment fragments samples from book *H yr.1974:*Into the yellow circle the peaks due to collagen aminoacids *(*L-proline, trans-4-hydroxyproline), gelatine components and NH_3^+ groups. The other peaks are typical of parchment.

Some characteristic parchment absorption bands are listed in table 5 where the wavelengths and corresponding vibrational mode are listed (Bicchieri et al., 2008) (Edwards et al., 2001).

Tab. 5 : FTIR/ATR paper vibrational mode assignment

Wavenumbers cm^{-1}	**Vibrational mode**
1235	NH bending
1320	CH_2 wagging
1408	CH_2 wagging
1435	CH_2 bending
1535	Amide II
1625	Amide I
2850	CH_2 stretching
2915	CH_2 stretching

Inks characterization

Spectroscopic analysis revealed important information about the type of ink used in the samples from *E (yr. 1789)* and *F (yr. 1626)*. Both samples shows the typical oxalates absorption bands at 1637 and 1315 cm^{-1} but, without more specific analyses, it is difficult to state whether these signals come from the degradation of ink or are typical of an iron-tannin complex. The weak peak at 821 cm^{-1} in both samples suggests the presence of Iron(II) oxalate (Ferrer and Sistach, 2005) (fig. 46).

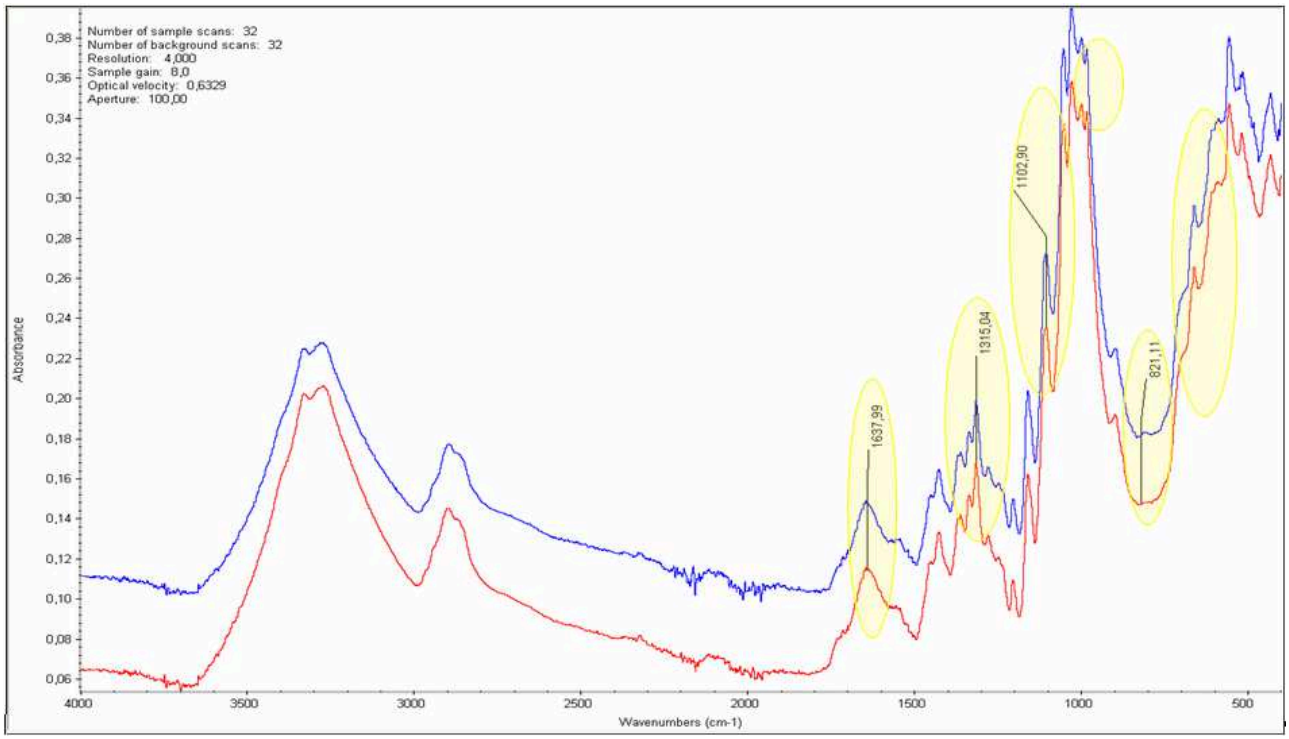

Fig. 46: FTIR ink spectra from the following books: *E yr.1789* (blue) and *F yr.1626* (red): the yellow regions are very sensitive to the presence of oxalate, sulfate and carboxylic groups.

One of the main problems of the FTIR analysis is the presence of hidden bands, due to other components (e.g., calcium oxalate, iron-oxycellulose complexes, copper oxalate, aluminium oxalate) that absorb at about the same frequencies of iron oxalates and change both the shape and the relative

heights of the main peaks. The signal at about 1100 cm^{-1} indicates the presence of sulphates, but the uncertainty about the nature of sulphates (i.e., calcium, iron or sodium sulphate) makes a careful analysis of degraded iron-gall inks difficult (Calvini, 2006) (Calvini et al., 2006).

Comparing the ink spectrum to the respective paper one, it is possible to notice the increase in intensity of the characteristic absorption bands due to the stretching vibrations in SO_4^{2-} (strong in the ranges 1120-1040 cm^{-1} and 645-570 cm^{-1}, and weak at 976 cm^{-1}) and in CO-OH (strong between 1700-1650 cm^{-1} and 1350-1340 cm^{-1} and medium between 950 and 825 cm^{-1}) (Senvaitienė et al., 2006) (figs. 47, 48).

It is not certain whether they are iron gall inks or not, it is likely that a part of them is metal-gallic.

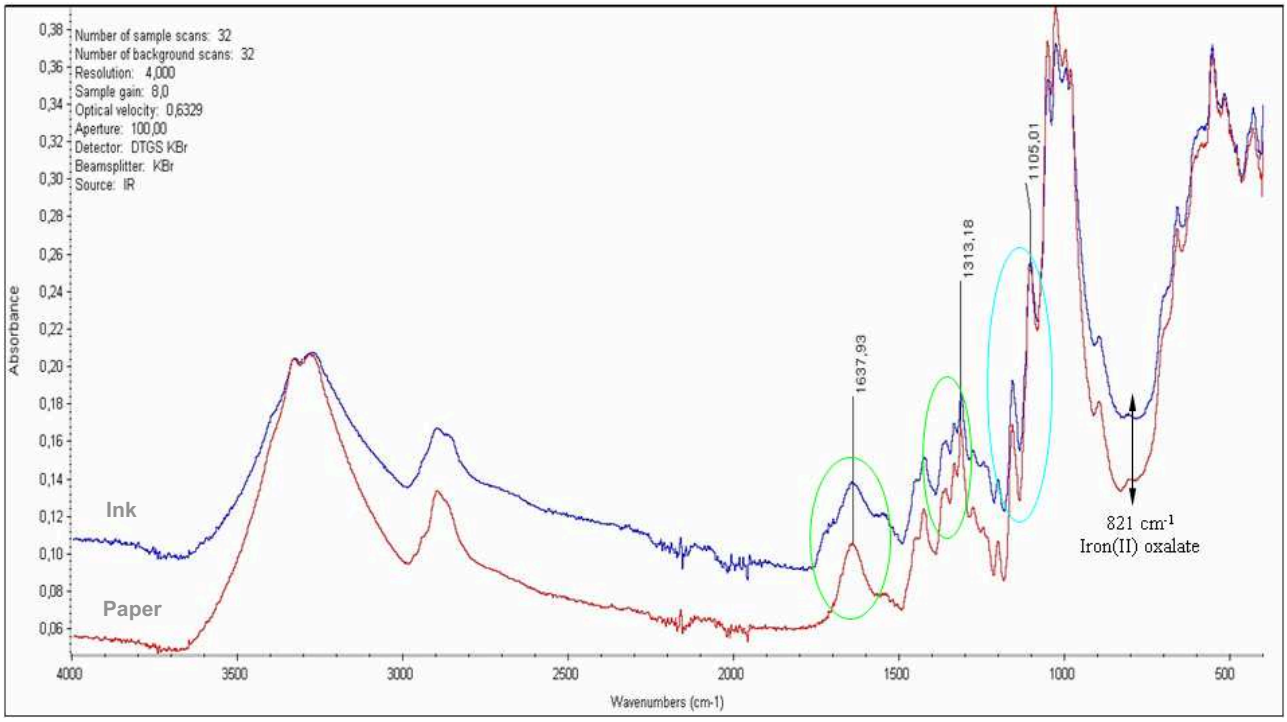

Fig. 47: Ink sample from book *E yr.1789*:comparison between the ink FTIR spectrum (top curve) and the respective paper one (bottom curve) It is possible to notice the increase in intensity of the characteristic SO_4^{2-}-absorption bands (in the 1120-1040 and 645-570 cm^{-1} ranges); into the circles the typical oxalate and carboxylic groups bands (in the 1700-1650 and 1350-1340 cm^{-1} regions) of metal-gall inks.

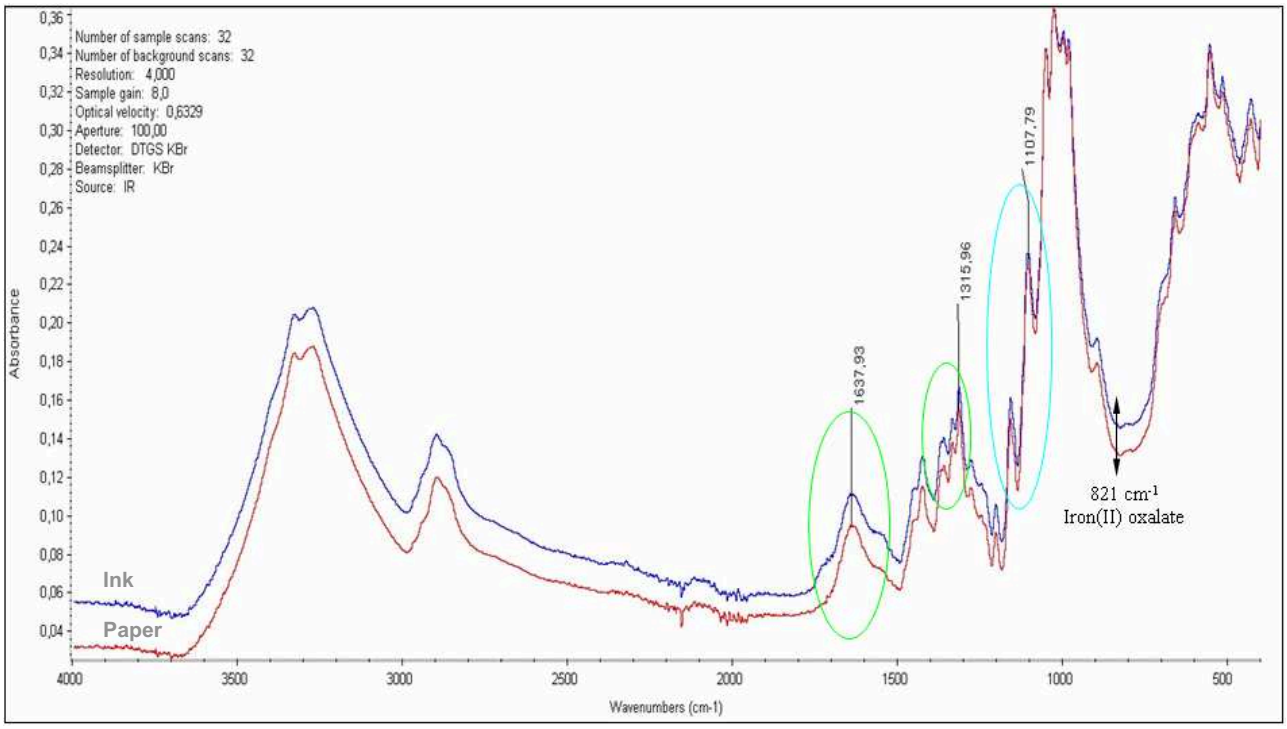

Fig. 48: Ink sample from book *F yr.1626*: comparison between the ink FTIR spectrum (top curve) and the respective paper one (bottom curve), it is possible to notice the increase in intensity of the characteristic SO_4^{2-}-absorption bands (in the 1120-1040 and 645-570 cm^{-1} ranges); into the circles the typical oxalate and carboxilc groups bands (in the 1700-1650 and 1350-1340 cm^{-1} regions) of metal-gall inks.

Through Raman analysis it was possible to characterize red and black inks found on very degradated samples from book *G yr.1533* as shown in figures 35 and 36. In particular the stronger peak in the red ink Raman spectrum at 244 cm^{-1} (fig. 49) is typical of vermilion (mercury sulfide HgS of a natural mineral) (Edwards et al., 2001).

Raman absorption bands of black ink in the 1350-1380 and 1580-1600 cm^{-1} range, are typical of amorphous carbon, the so-called “Lamp black” or carbon black, used since ancient times. In the spectrum of ink sample from book *F yr.1626* the two bands are located at 1365 and 1578 cm^{-1} (fig. 50) (Bugio et al., 1997), (Bell et al., 1997).

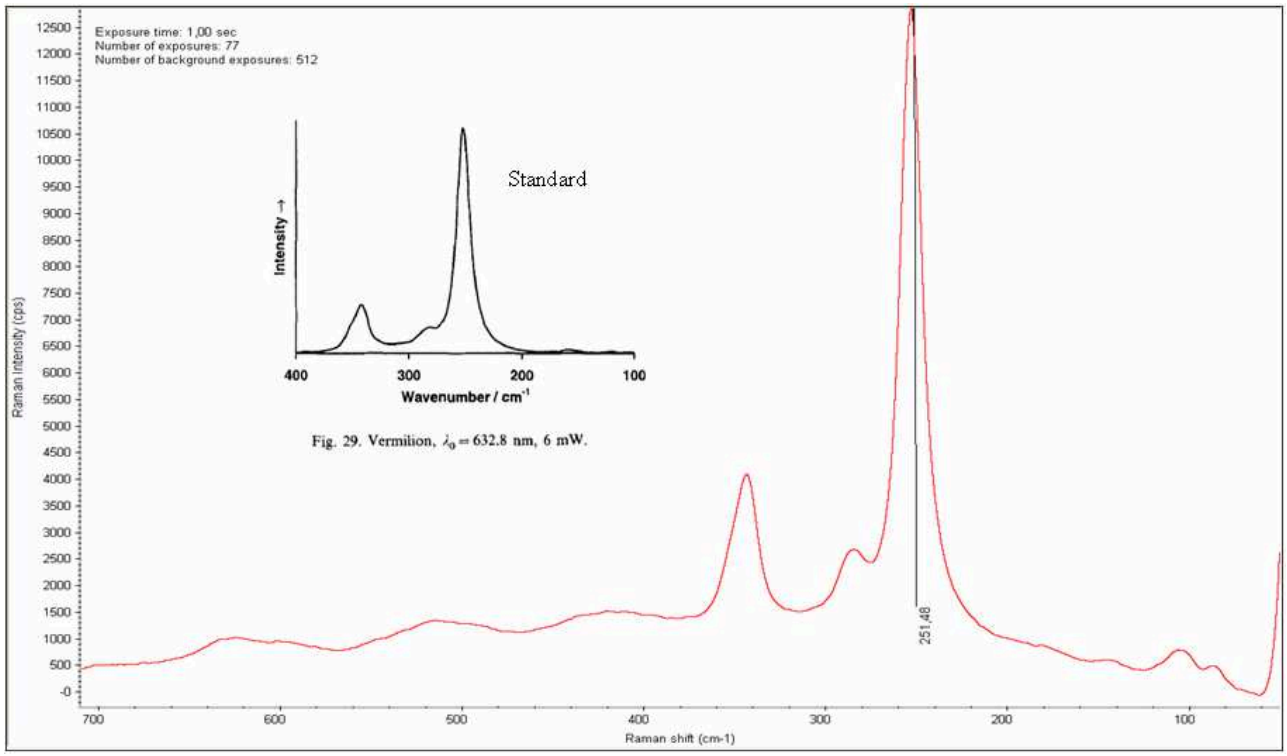

Fig. 49: Red ink on paper fragments from book *G yr.1533* and characteristic Raman spectrum of *vermilion* (251 cm^{-1} absorption band of mercury sulphide HgS).

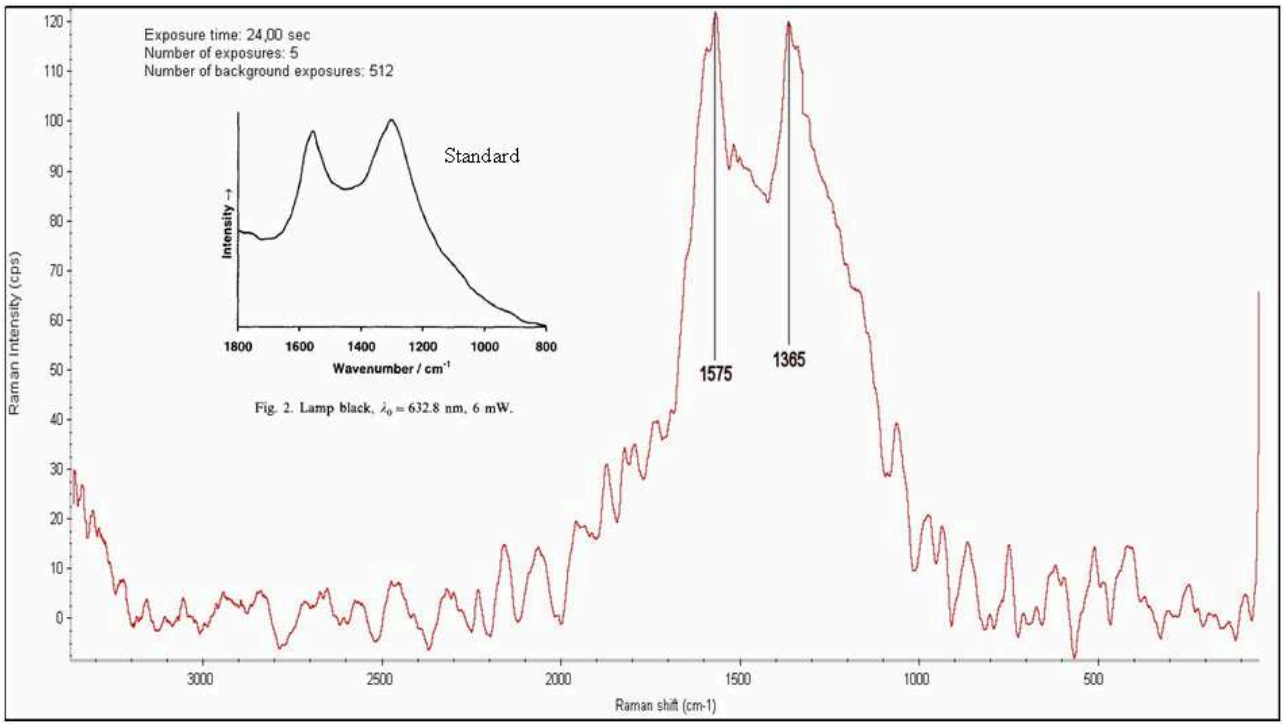

Fig. 50: Black ink on paper fragments from book *G yr. 1533* and characteristic Raman spectrum of *Lamp black* (1575 and 1365 cm^{-1} absorption bands of amorphous carbon)

Through Raman analysis it was also possible to characterize the ink found on parchment fragments samples from book *H yr. 1794*, as shown in figure 51. In particular the very strong band at 1474 cm^{-1} is typical of iron-gall ink and the broad band at about 580 cm^{-1} may be related to the presence of metal salts. The absorption bands around 1334 and 1588 cm^{-1} are probably due to the presence of a certain amount of amorphous carbon in the ink mixture. Sometimes they used to add the amorphous carbon (carbon black) to the metal-gallic ink (which was transparent immediately after preparation) in order to make the ink immediately usable.

The other absorption bands are probably independent of the ink composition and may be related to organic iron complexes (Edwards et al., 2001).

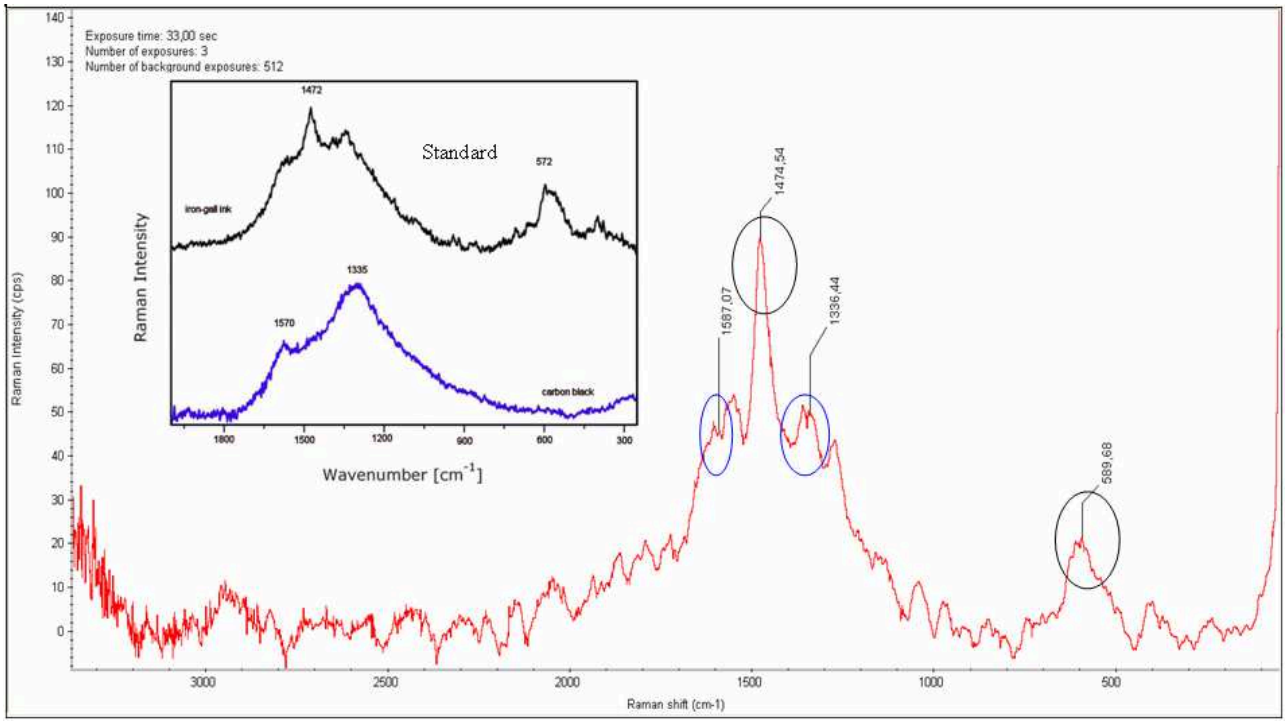

Fig. 51: Black ink on parchment fragments from book *H yr.1794:* into the black circles the typical absorption bands of iron-gall inks; into the blue circles absorption bands probably due to the presence oh amorphous carbon in the ink mixture. Into the box the standard spectra iron-gall and lamp-black inks.

Interpretation of spectra from foxed paper

In this section the biotic nature of foxing stains on selected paper samples was verified by finding the typical spectral features of fungi attack.

The identification of some paper components was done by comparing the main features of the obtained spectra with those discussed in the previous sections, in their absence, with published spectra.

The identification of biotic attack on stained paper was done by comparing the main spectra features of my samples to those obtained by Zotti et. al. in FTIR analysis of fungi isolated from the surface of wood pulp cardboard (fig. 52). All the fungi examined by Zotti et. al. show the characteristic infrared absorbance of OH groups and absorbed water (3700 e 3000 and approximately 1635 cm^{-1}), CH groups (approximately 2900 cm^{-1}), polypeptide bonds (amide I at approximately 1635 and amide II at approximately 1540 cm^{-1}), and polysaccharide groups (approximately 1035 cm^{-1}). The broad plateau between 1500 and 1200 cm^{-1} composed of several overlapping bands is extremely interesting. This broad plateau is typical of fungal agents and helps to differentiate the FTIR spectra of paper subjected to biotic attack from those of gelatin-sized paper samples.

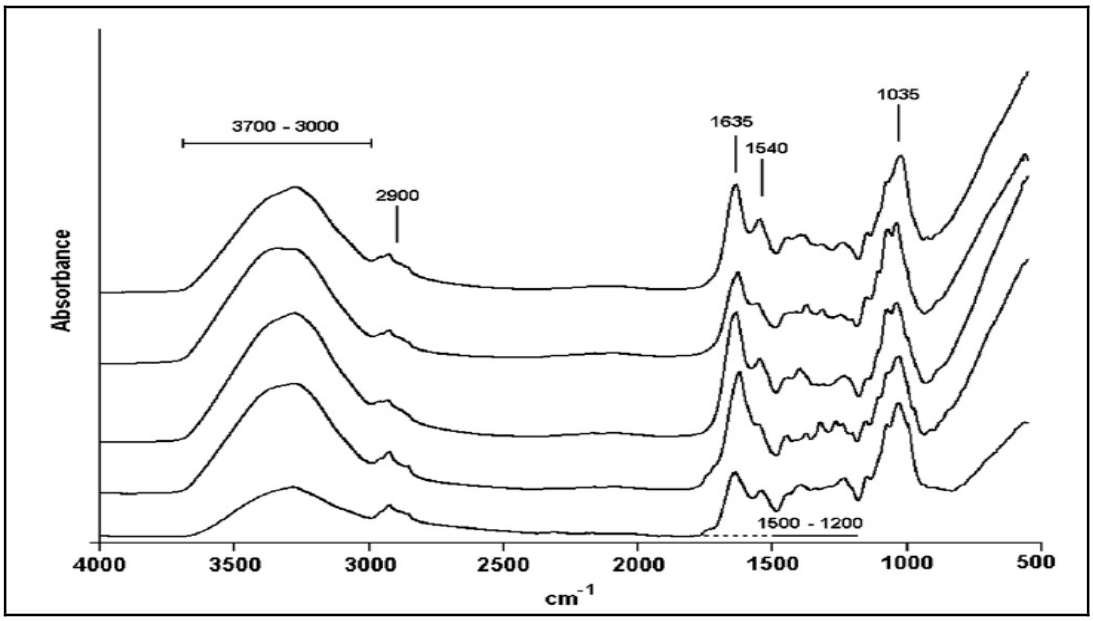

Fig. 52: FTIR spectra of live fungi. Bottom to top: *Cladosporium sphaerospermum, Penicillium pupurogenum, Aspergillus melleus, Pithomyces chartarum, Aspergillus sclerotiorum.*

FTIR characterization of stained paper samples

The FTIR analysis was performed both on the spots and on the neighbouring unstained paper surface.

Table 6 shows the main characteristics of paper samples, as detected by the FTIR-ATR analysis of their unstained surfaces.

Tab. 6 : FTIR analysis of unstained region of selected books

Books code	Books information	Book description and main FTIR bands (cm^{-1}) other than cellulose bands	Figure
I yr. 1924	*I cavalieri della tavola rotonda* published in 1924	Strongly stained book, paper coated by clay 3690 and 3620 (small doublet), 1000, 910, 790, 750, and 670; 1740 small, 1590 shoulder, adhesive on surface(likely carboxymathyl cellulose)	20 bottom
J yr. 1945	*Rime scelte* published in 1945	Strongly stained book. Peaks: 3690 small; 1740 small; 1590 shoulder some clay and adhesive on surface (likely carboxymethyl cellulose)	22 bottom
K yr. 1859	*La Sacra Bibbia* printed in London in 1859	Ancient books, good conservation state. Peaks: 3519 and 3394 shoulders; 1110, 665, and 600 typical of gypsum; increase of 1000 and 984 cm^{-1} typical of starch	24 bottom
L yr.?	*La Divina Commedia* probably published in the 19th century	Ancient books, good conservation state. Good-quality cellulose fibres with some gypsum, band at 1110, 665, and 600	26 bottom

The FTIR graphs were shifted onto the vertical axis to allow convenient comparisons, so that no absorbance scale is given in the figures.

The sample *I yr. 1924* showed a great number of brown stains (fig.53). Figure 54, the bottom curve, shows the FTIR analysis of the unstained surface that appears coated by clay as shown by the strong bands at approximately 3690, 3620, 1000, 910, 790, 750, and 670 cm^{-1}.

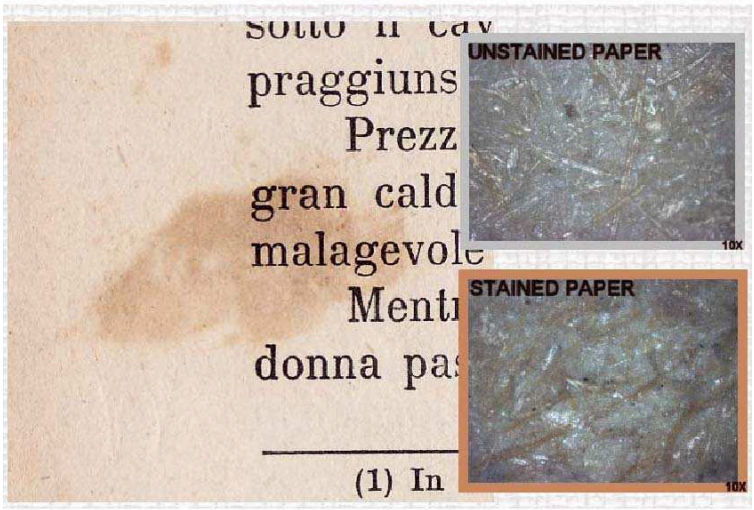

Fig. 53: Stained surface from book *I yr.1924* acquired by an optical scanner at 1200 dpi. The insets show a microscopic magnification (10X) of the unstained paper (top) and of the brown stain (bottom)

The small band at approximately 1740 cm^{-1} and the shoulder at approximately 1590 cm^{-1} are typical of carboxyl and carboxylate groups, respectively, and suggest the presence of a synthetic adhesive on the surface (probably carboxymethyl cellulose: Gilli et al. 2009). Figure 54, the top curve, shows the FTIR spectrum of a brown stain, where the amide bands (at approximately 1635 and 1540 cm^{-1}) and the plateau between 1500 and 1200 cm^{-1} of fungal agents are clearly visible.

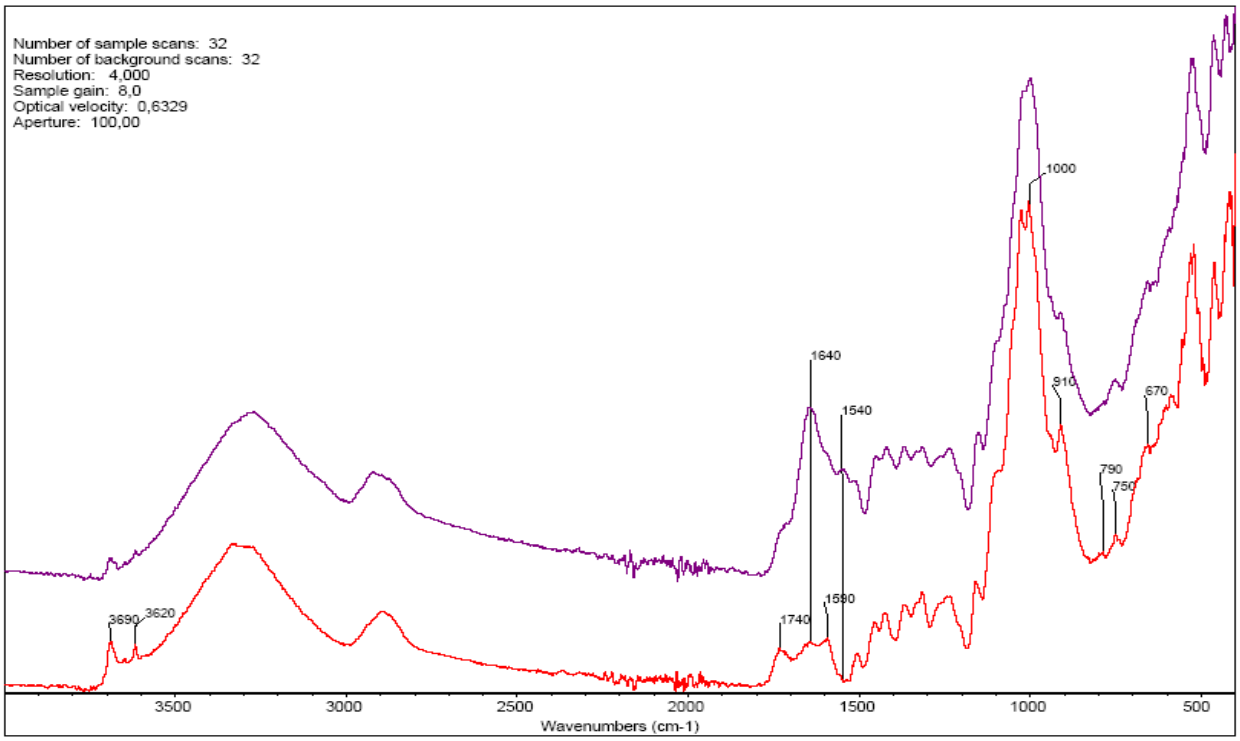

Fig. 54: FTIR spectra of book *I yr. 1924*. Unstained surface (bottom curve) and brown stains (top curve)

The analyzed foxed area of the sample *J yr. 1945* is showed in fig 55. The FTIR spectrum of the unstained paper of sample *J yr. 1945* is shown in figure 56 (bottom curve).

Paper spectrum present a small band at approximately 1740 cm^{-1} and a shoulder at approximately 1590 cm^{-1} (typical of carboxyl and carboxylate groups respectively) that suggests the presence of a synthetic adhesive

Fig. 55: Stained surface from book *J yr.1945* acquired by an optical scanner at 1200 dpi. The insets show a microscopic magnification (10X) of the unstained paper (top) and of the brown yellowish stain (bottom)

on the surface. The small band at 3690 cm^{-1} is due to a small amount of kaolin.

Figure 56 (top curve) shows the FTIR spectrum of a brown yellowish stain on the cover book *J yr. 1945*. The FTIR spectrum is characterised by an increased absorbance at approximately 1635 cm^{-1}. However, the overall shape of the spectrum (a shoulder rather than a distinct amide II band at approximately 1540 cm^{-1}), rules out the presence of active fungi on paper.

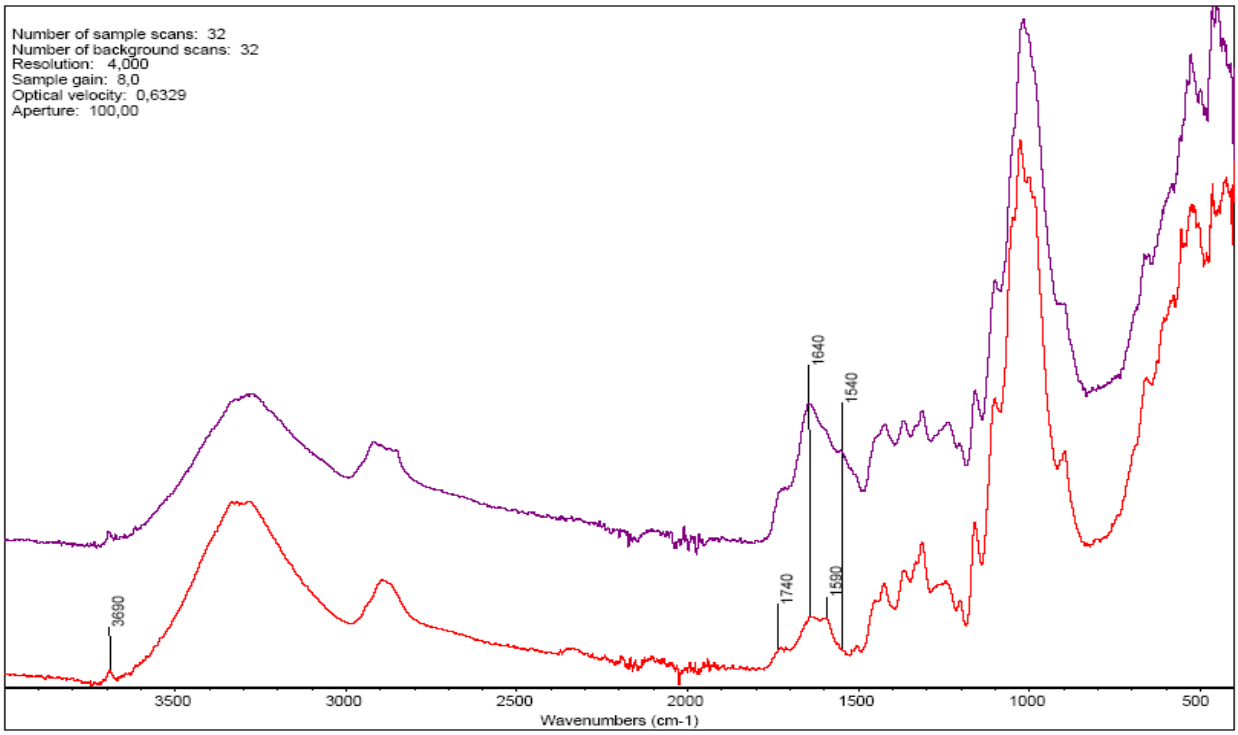

Fig. 56: FTIR spectra of book *J yr.1945*. Unstained surface (bottom curve) and brown yellowish stains (top curve)

The analyzed foxed area of the sample *K yr. 1859* is showed in fig 57. The unstained paper of book *K yr. 1859* (fig. 58 bottom curve) contains gypsum, as shown by the shoulders at 3519 and 3394 and bands at approximately 1110, 665, and 600 cm^{-1} (Zotti et al. 2008), while the increase of 1000 and 984 cm^{-1} bands in the fingerprints region suggests the presence of starch.

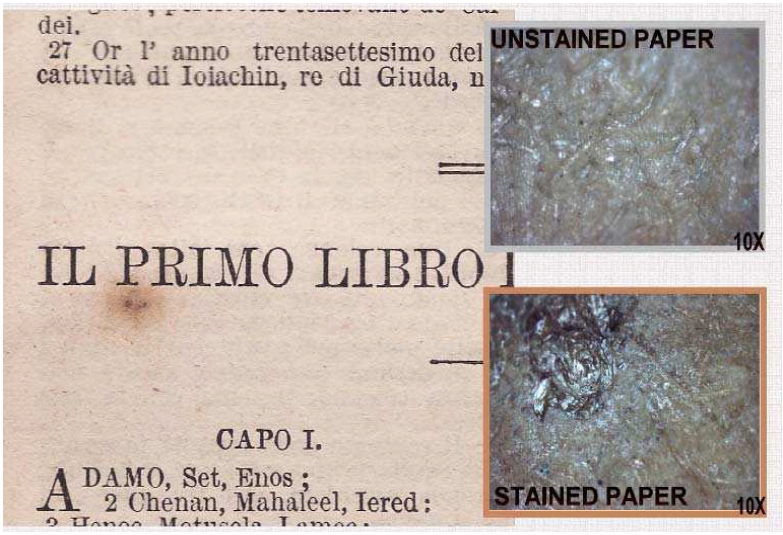

Fig. 57: Stained surface from book *K yr.1859* acquired by an optical scanner at 1200 dpi. The insets show a microscopic magnification (10X) of the unstained paper (top) and of the brown spot (bottom)

Figure 58 (top curve) shows the FTIR spectrum of the brown spots on book *K yr.1859*. The FTIR absorbance of biotic foxing is evident (amide bands at approximately 1635 and 1540 cm^{-1} and plateau between 1500 and 1200 cm^{-1}). However, the amide II band at about 1540 cm^{-1} is too high to be due only to infrared absorbance of live fungi and suggests the presence of other substances, probably deacetylated chitin and/or chitosan (Duarte et al. 2002; Szeghalmi et al. 2007) from dead fungal cell walls.

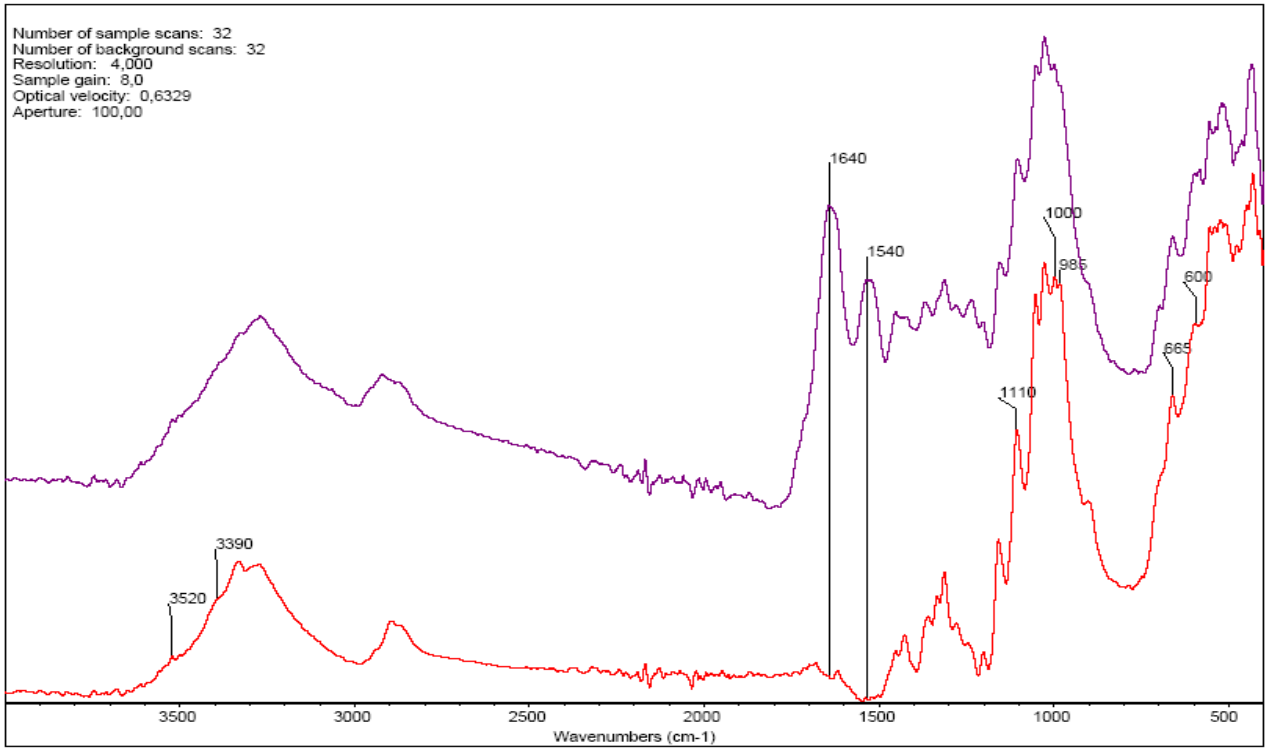

Fig. 58: FTIR spectra of book *K yr.1859*. Unstained surface (bottom curve) and brown spot (top curve)

The analyzed foxed area of the sample L is showed in fig 59.

Figure 60 (bottom curve) shows the spectra of an unstained area of book L which is composed by good-quality cellulose fibres without clay or other coating agents, with the only presence of some gypsum, bands at 1110, 665, and 600 cm^{-1}.

Figure 60 (top curve) shows the spectrum of a brown

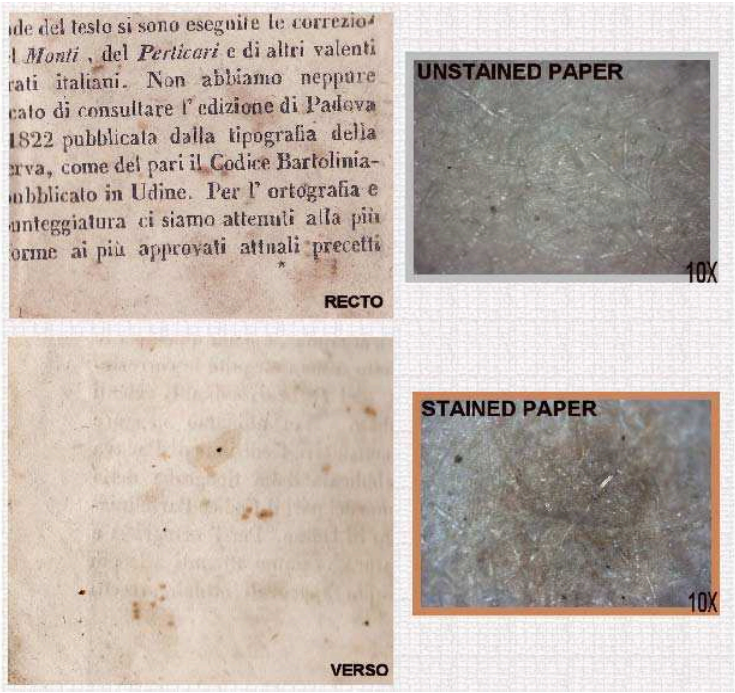

Fig. 59: Stained surface from book L acquired by an optical scanner at 1200 dpi. The insets show a microscopic magnification (10X) of the unstained paper (top) and of the brown stain (bottom)

stain of book L. As in the top part of figure 58, the amide II band at approximately 1540 cm^{-1} is too high to be due only to live fungi.

Another small band appears at 1600 cm^{-1}, probably due to deacetylated chitin and/or NH_2 groups of chitosan (Duarte et al. 2002; Szeghalmi et al. 2007) due to fungi degraded cell walls. These findings are enhanced in other regions of the foxed area, characterised by further sharp bands between 1800 and 550 cm^{-1} that give rise to a rugged profile, typical of low-molecular-weight organic compounds. The identification of these compounds is beyond the limits of this study, but the microscopic analysis revealed several mycelia filaments protruding from the fissures of some folding pages (fig. 61). The presence of these filaments suggests that a fungal attack is occurring on the book.

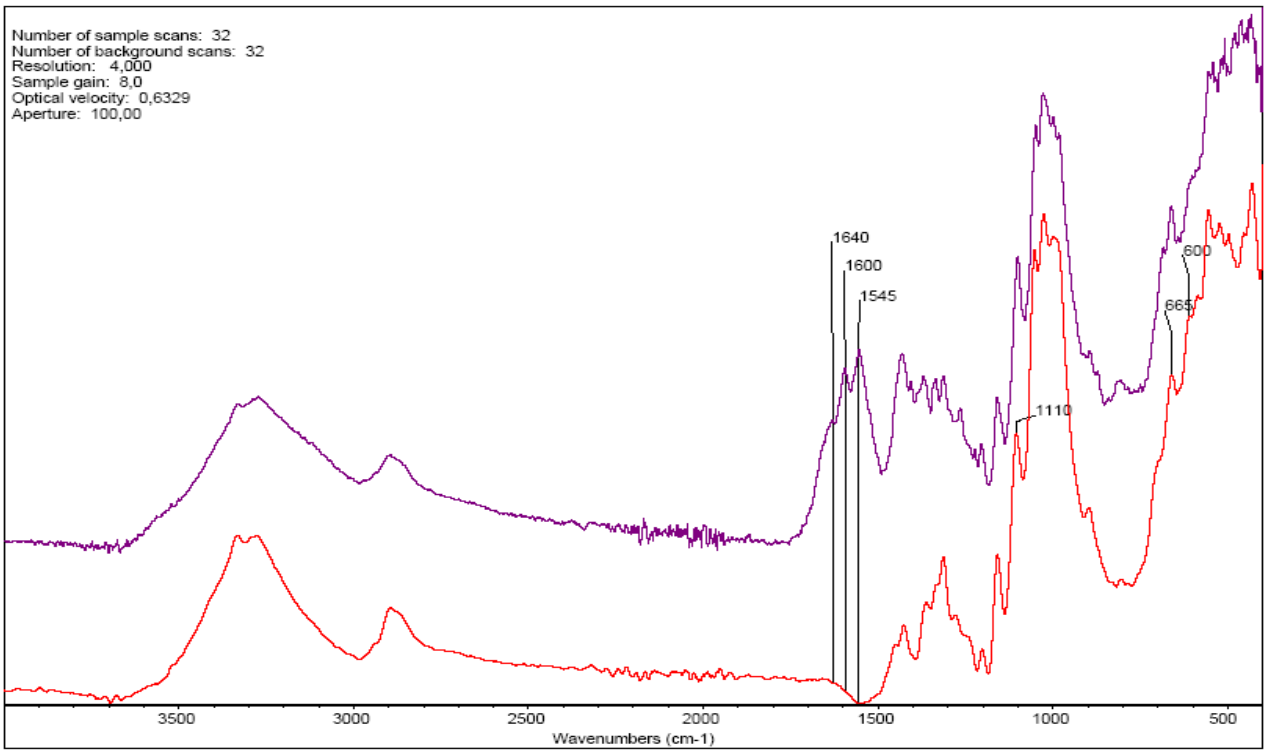

Fig. 60: FTIR spectra of book L. Unstained surface (bottom curve) and brown stain (top curve)

Fig. 61: Fungal filaments protruding from the fissures of folding pages of book L (images acquired by a Zeiss Stemi SV11 Microscope – 66X)

Sample preparation

During my work on particulate matter, a sample collection and preparation procedure has been set. It was chosen the best FTIR method to get the best signal to noise ratio and the most defined spectrum. In order to determine which filter medium was best fitted for analysis, different substrates commonly used for environmental PM collection were tested too.
All those steps will be explained in this section.

A key step was choosing the appropriate filter substrate that meets the requirements of both FTIR and Raman spectroscopic techniques. In order to determine which filter medium was best fitted for analysis, a spectra library of potential filter substrates was developed. Figure 62 shows the FTIR spectra of filter substrates commonly used for environmental PM collection: quartz fiber, glass fiber, tedlar foil, aluminium foil. FTIR spectra indicates that aluminium foil is a suitable material for its low absorbance in this spectral range. The other FTIR spectra showed very strong absorption bands that coincided with samples peaks, making the data interpretation difficult. The Raman spectra of the aluminium foil showed a low Raman response, so the aluminium foil was selected as the filter substrate for this work.

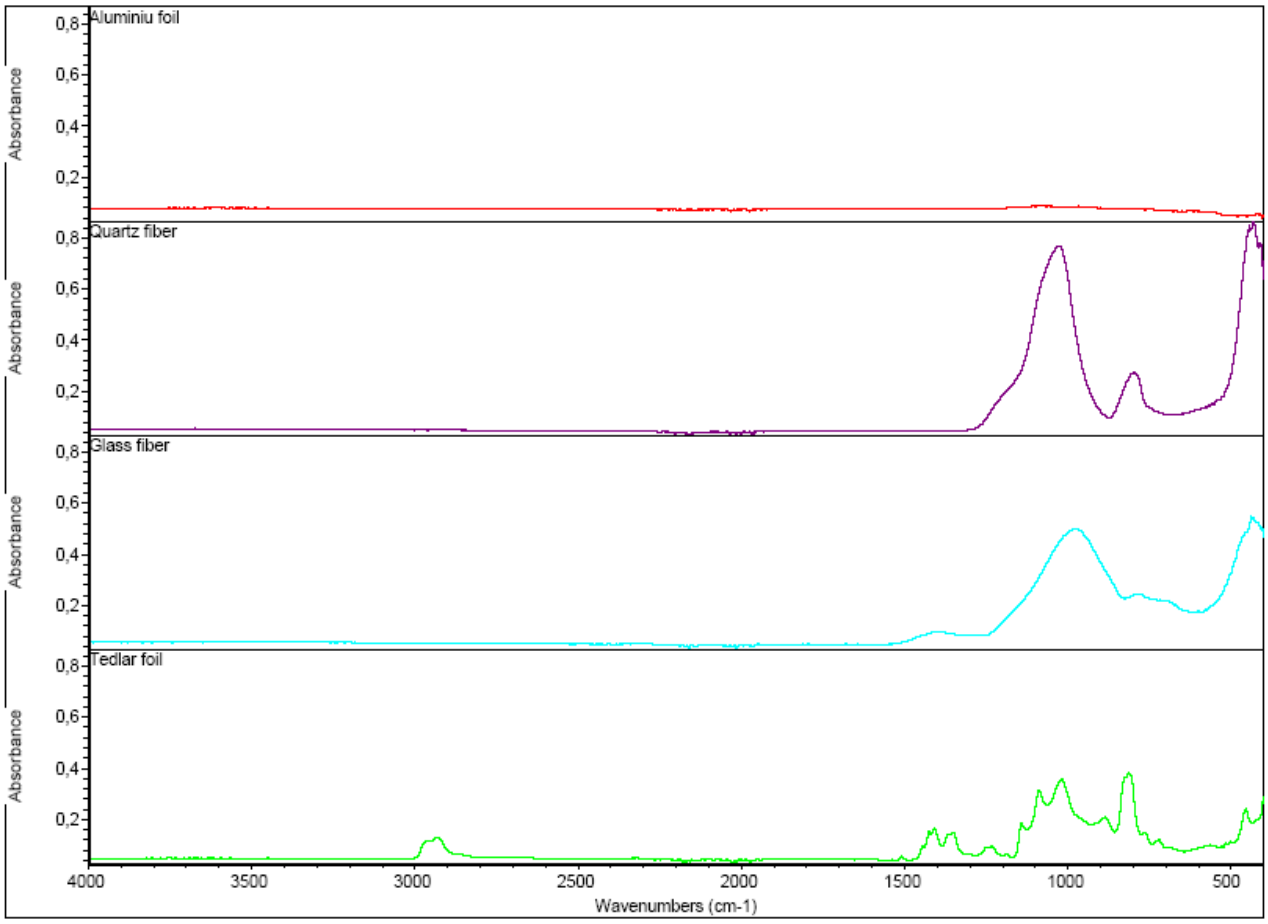

Fig. 62: FTIR spectra of potential filter substrates.

Particulate matter (PM) samples were collected in Catania using an high-volume five-stage cascade impactor air sampler, TE-230 Tisch Environmental (fig. 63). It was placed approximately at 50 m far from an high vehicular traffic road. The impactor sampler has been working for 8 hours (in order to collect enough material for the analysis) at flow rate of 1,18 m^3/min.

Fig. 63: Five stage cascade impactor

Aluminium foils *TE-230Al* were used to collect PM, table 7 lists the five stage cut-off aerodynamic diameter (*Da*) of particles collected, their mass concentration (*Mc*) and deposit mass (*Dm*) weight:

Tab. 7: PM cut-off and mass size distribution

Stage	Da [µm]	Mc [µg/m^3]	Dm [mg]
1	10 - 4.2	2.6164	1.9
2	4.2 - 2.1	4.5443	3.5
3	2.1 - 1.3	1.5148	1.1
4	1.3- 0.69	0.9639	0.7
5	<0.69	0.6885	0.5

Particulate matter from each stage was washed off from the aluminium foil, using Millipore water. After the evaporation of water in a room protected from light, the PM samples were analyzed using FTIR spectroscopy to get the distribution of functional groups in the particulate matter.

Infrared measurements were performed using a Continuum IR microscope coupled with a Nicolet 6700 FTIR.

Four different analytical methods were used:

- Reflection
- Transmission through NaCl disc
- Attenuated Total Reflection (ATR)
- Micro-ATR

The comparison was made between the average spectrum of the five spectra obtained for each impactor stage (without considering the differences of the five size fractions spectra) (fig. 63).

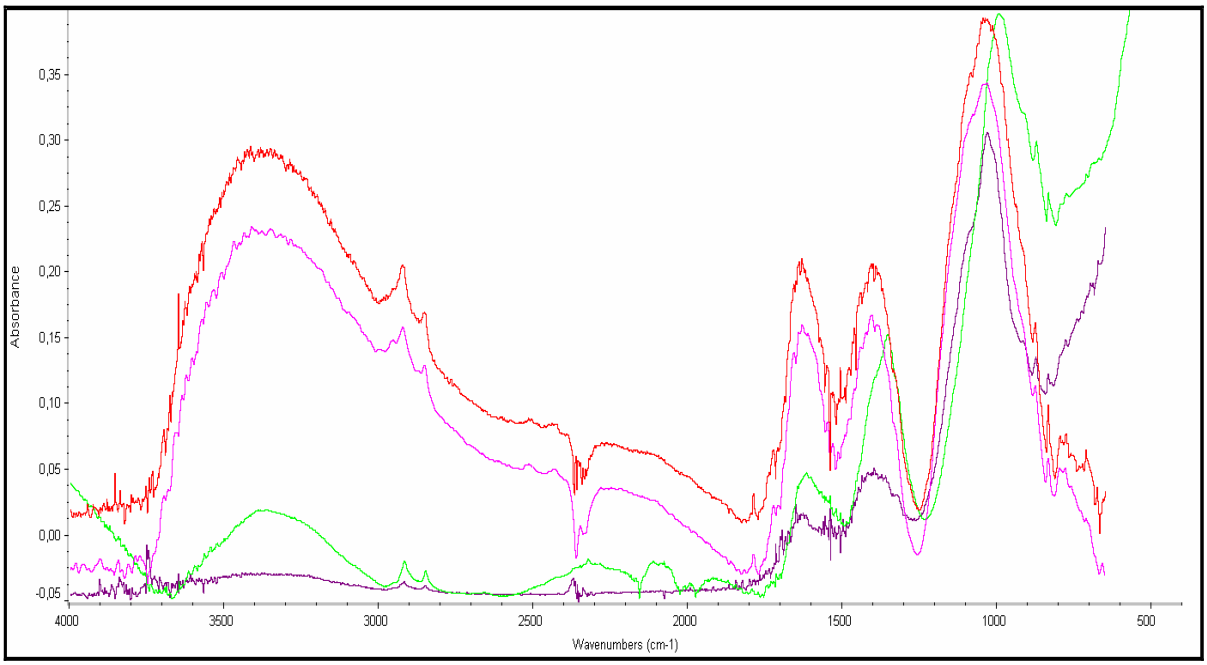

Fig. 63: FTIR spectra of PM obtained in Reflectance mode (red), Transmittance made (pink), μATR mode (violet) and ATR mode (green).

By comparing the different techniques, although they are excellent non-destructive methods, some differences can be observed: μATR methods show weak absorption bands; ATR methods gives a slight shift of the bands; Transmission and Reflection show very similar absorption bands, but Reflection gives more definite peaks. For these reason only the spectra obtained in reflection mode have been selected for the discussion about PM characteristic absorption bands.

The average FTIR spectrum of particulate matter in Reflection mode is shown on figure 64.

The spectrum shows a broad band in the 3700-3200 cm^{-1} region which may represent the OH stretching bands of Si-OH groups. The 2800–3000 cm^{-1} region (aliphatic stretching region) represents the combination of CH_2 and CH_3 functional groups vibration mode. The 1800-1100 region represents the

oxygen-containing structures i.e. C=O and C-O-R. The distribution of aromatic hydrogen is represented in the 900-700 cm^{-1} zone (out of plan aromatic CH bending). The most intense bands at 835 and 770 cm^{-1} are attributed to di- and tri-substituted aromatic rings and/or aromatic structures with 1-2 rings (Ibarra et al., 1996). Based on reported infrared band assignations for PAHs (Semmler *et al.,* 1991), the bands centred at 870 and 780 cm^{-1} could be attributed to aromatic ring sizes of 3-4 or more.

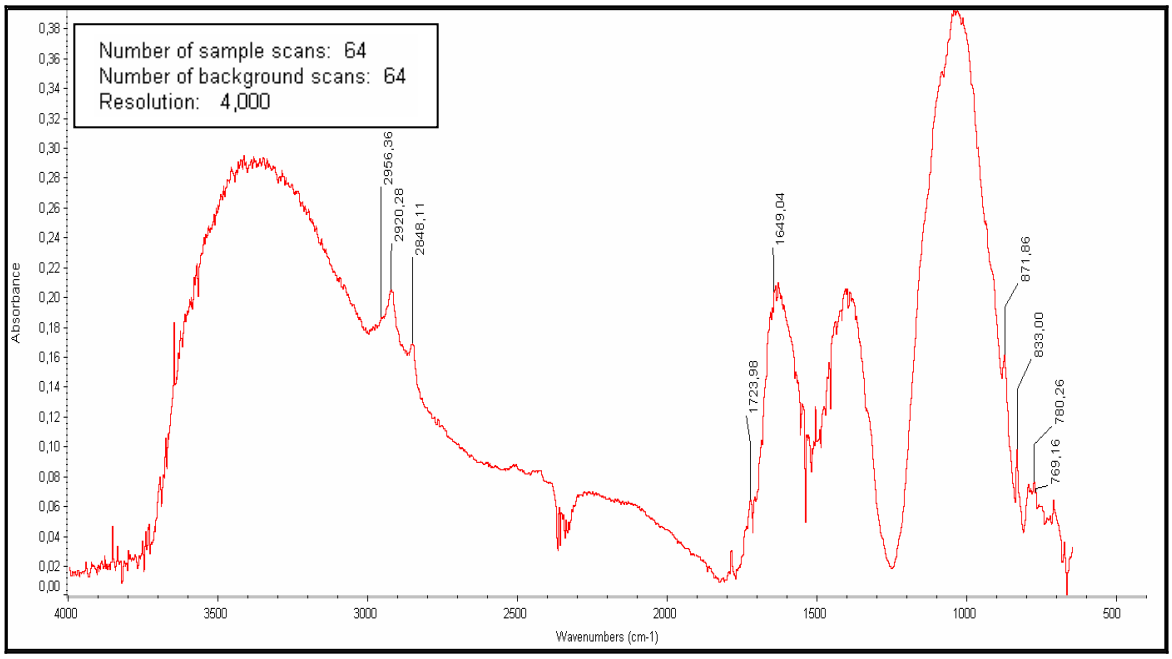

Fig. 64: FTIR average spectrum of the five spectra obtained from PM of each impactor stage.

The bands were assigned (tab. 8) by literature references: Baruak, 1986; Painter *et al.,* 1981, 1983; Starsinic *et al.,* 1984; Michaelian and Friesen, 1990; Ibarra and Juan, 1985; Ibarra *et al.,* 1994; Kister *et al.,* 1990; Van der Marel and Beutelspacher, 1976; Wang and Griffiths, 1985; Yen *et al.,* 1984; Supaluknari *et al.,* 1989, Stuart, 2003.

In the 900-1200 cm^{-1} region there is a strong band, whose interpretation is difficult because of the overlap of different functional groups and the possible contribution of mineral matter.

Tab. 8 : FTIR PM vibrational mode assignment

Wavenumber cm^{-1}	Vibrational mode
3700-3200	OH stretching
2955	CH_3 stretching asym.
2920	CH_2 stretching asym.
2850	CH_2 stretching sym.
1770	Phenolic esters
1720	Carboxyl acid
1650	Conjugated C=O
1275-1000	Aromatic CH bending
1300-1100	C-O stretching
1220-1020	Aliphatic C-N stretching
1130-1000	Si-O-Si stretching
900-700	Aromatic CH bending

Interpretation of spectra from fractionated PM

The data obtained from FTIR analysis reflect the bulk composition of the particulate matter. During my third year work the data obtained from each impactor stage were compared and discussed in order to figure out the correlation between the PM size fractions and the functional groups distribution. To simplify the procedure and avoid excessive manipulation of the samples, the spectra were recorded directly from the filters used to collect particulate samples, without solvent extraction.

Figure 65 shows a set of FTIR spectra representing the five stages PM fractions. By comparing the PM spectra with those ones present on published papers, it was possible to confirm the presence or absence of certain compounds o compounds classes in the atmospheric PM. Both inorganic and organic functional groups will be considered and discussed.

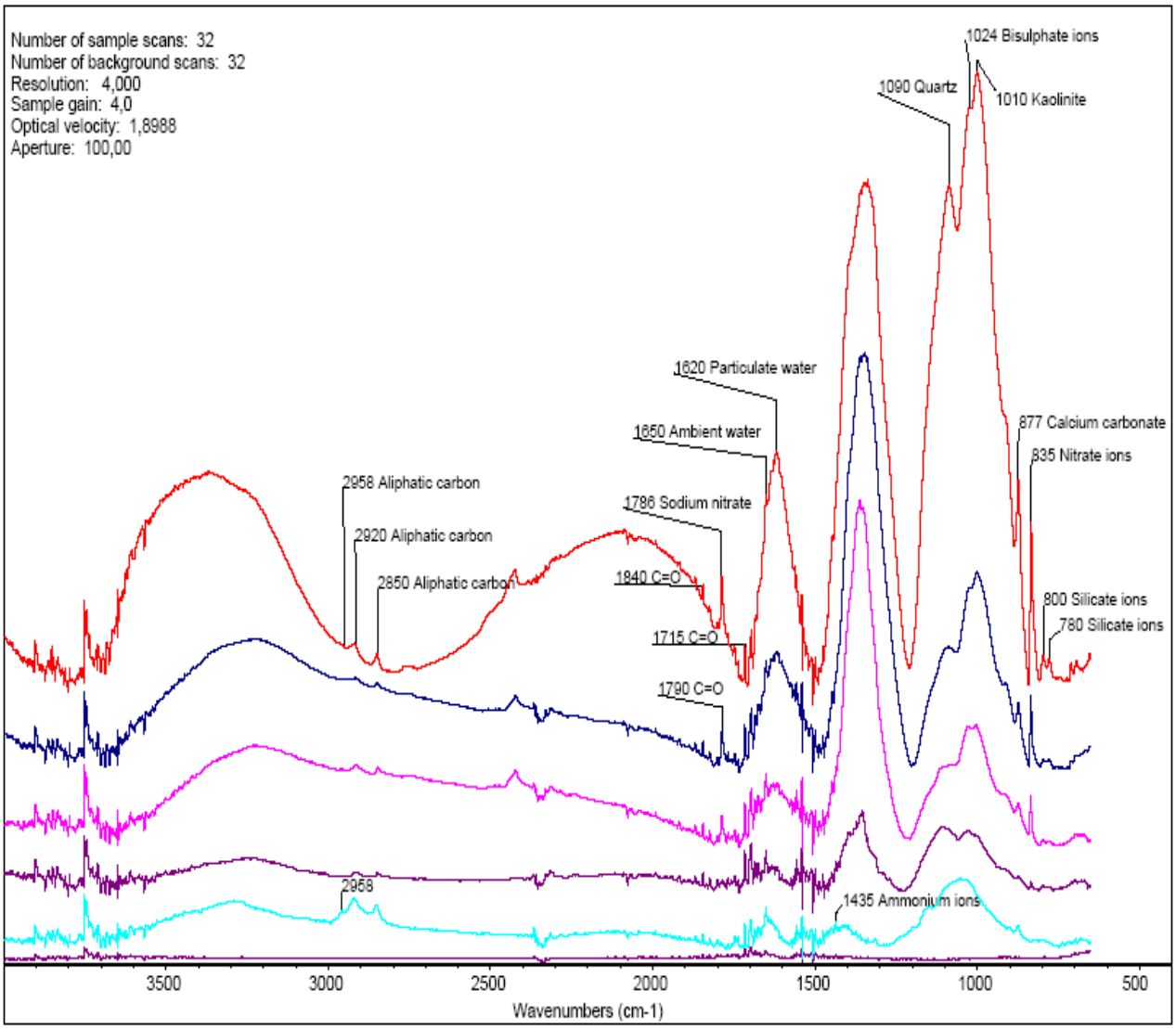

Fig. 65: FTIR spectra representing the five stages PM fractions; all spectra are plotted on the same absorbance scale

Inorganic absorption assignments

This section describes the functional groups that are responsible for the absorptions observed in the FTIR spectra of environmental particulate matter. A summary of the major inorganic absorbances observed in this work is given on table 9.

Sulphate and bisulphate absorptions

Absorption due to bisulphate ions of NH_4HSO_4 peaks at 1025 cm^{-1} , while the absorption due to sulphate ions in $(NH_4)_2SO_4$ has a strong absorbance in the 1103-1135 cm^{-1} region. Those absorbances are very strong in the spectra of stages 2, 3 and 4.

Nitrate absorptions

Nitrate ions in NH_4NO_3, absorb at 830-835 cm^{-1}, this band is strong in the spectra of stages 2, 3 and 4. Nitrate ions absorb also in the 1318-1335 region, but it is very difficult to distinguish this band because of the severe overlap with others absorption bands. The absorption band due to sodium nitrate salts (1786 cm^{-1}) was observed in the spectra of stages 2, 3 and 4.

Ammonium absorptions

Ammonium ions absorption is associated with $(NH_4)_2SO_4$ and NH_4HSO_4 peaking at 1410-1435 cm^{-1}, the precise frequency depends upon mixing ratio and anion type (Palen, 1991). In this case the ammonium absorption was observed as a weak peak at 1435 cm^{-1} in stages 1 and 5, but it is very difficult to distinguish this band because of the severe overlap with the other absorption bands.

Silicate absorptions

Silicate ion and silica absorption can be due to a number of minerals. Blanco and McIntyre (1975) identified quartz and kaolinite to be the major species in atmospheric PM. Quartz (SiO_2) absorbs most strongly around 1090 cm^{-1} and 730 cm^{-1}; the first band is very strong in the stage 2 spectrum, it is like a shoulder in spectra from stage 3 and 4 and a broad band in stage 1 and 5. Kaolinite ($Al_2(OH)_4(Si_2O_5)$) absorbs at around 1010 cm^{-1}, this band is strong in stage 2, weak in stage 3 and 4. Silicate ion library spectra exhibited strong absorptions peaking at 990-1140 cm^{-1}. Cunningham et al. (1974) assigned the strong absorptions at 1035 cm^{-1} and the weaker absorptions at 780 and 800 cm^{-1} to SiO_4^{4-}. The spectra obtained during this work exhibit silicate absorptions at 780 and 800 cm^{-1}. Higher frequency absorptions overlap to sulphate absorptions around 1024 cm^{-1}.

Particulate water absorptions

The water strongly bound to PM salts absorbs at 1600-1700 cm^{-1}, peaking at 1620-1655 cm^{-1}. Water absorptions at 1620 cm^{-1} were observed in all spectra, but were strongest in spectra from stage 2 and 3. The peak at 1650 cm^{-1} was present in all spectra stages and also in the blank one, so it was probably due to environmental humidity and not due to water in salt hydrates.

Sulphites and Nitrites absorptions

Sulphite absorption are at 925, 945 and 620 cm^{-1}, but none of these absorption were observed in the collected PM. Nitrite ions absorb strongly at 1220-1280 cm^{-1}. This nitrite absorption band is broad and would be easily recognized in the minimum absorption between the strong and broad sulphate absorption at 900-1200 cm^{-1}, and the nitrate ion or ammonium ion absorptions at 1150-

1450 cm^{-1} and at 1300-1470 cm^{-1}. This nitrite ion absorption was not observed in any of the PM fractions spectra analyzed in this work.

Carbonate ion and Phosphate ion absorptions

Calcium carbonate was the main carbonate species identified in coarse PM by Blanco and McIntyre (1975). Carbonate ions absorb strongly and broadly at 1433 cm^{-1}, and with a slightly weaker but sharper peak at 877 cm^{-1}. These absorption bands were observed in all samples, but the 1433 cm^{-1} absorption band appears as a little tick on the broad absorption between 1200-1470 cm^{-1}. Phosphate absorptions were not consistently identified in my spectra. The spectra showed weak sharp absorptions at 670 and 916 cm^{-1}, which could be due to calcium phosphate when strong absorptions at 950 and 1235 cm^{-1} had also been observed. Since these absorptions were not observed, it was concluded that phosphate ion loadings were negligible.

Ammonium Chloride Absorptions

Ammonium chloride can be distinguished through an absorption of moderate strength and width at 1760 cm^{-1}, and a strong absorption at 1400-1404 cm^{-1}. The former could be distinguishable on the high-frequency shoulder of carbonyl carbon absorptions which peak at about 1714 cm^{-1}, but it could not be distinguished in any of my PM spectra. No shifts of ammonium ion absorptions to 1400 cm^{-1}, indicative of NH_4Cl, were observed. It was concluded that ammonium chloride was not present in my samples in significant quantities.

Organic Absorption Assignments

Organic absorptions in environment PM are due to a complex hydrocarbon mixture of hundreds of different compounds (Schuetzle et al., 1975; Appel et al., 1979; Mazurek et al., 1989; Rogge et al., 1993). The variety of potential organic absorbances complicates considerably the data interpretation, and, as a result, the interpretation of the spectra will be limited to just a few absorbances. Aliphatic carbon, carbonyl carbon and organonitrate absorbances will be examined. Absorbances due to alkenes, aromatics and nitro groups are near or below current detection limits. A summary of the major organic absorbances observed in this work is given in table 10.

Aliphatic Carbon Absorptions

Aliphatic carbon absorptions are observed at 2800-3000 cm^{-1}, peaking at 2850, 2920, and 2958 cm^{-1}. The 2958 cm^{-1} absorption is due to CH_3 aliphatic carbon bond absorptions, these were present in stages 1 and 2 and the absorptions at 2920 and 2850 cm^{-1} are due to CH_2 bonds (Nakanishi, 1962) that were present in all stages.

Carbonyl Absorptions

Carbonyl carbon absorptions were the most difficult among the organic absorbances to figure out. The carbonyl complex absorbed over the broad range of 1640-1850 cm^{-1}, generally peaking at about 1714 cm^{-1}. This carbonyl absorption may have included contributions from ketones, aldehydes, and carboxylic acids. Sometimes the carbonyl absorbance appear as a single, smooth broad peak and no single, strong carbonyl absorptions due to single species were identified. In this study it was possible to distinguish three distinct bands at 1840 cm^{-1} and 1715 cm^{-1} (in all stages), 1790 cm^{-1} (in stages 2, 3 and 4).

Organonitrate Absorptions

Organonitrate absorptions peaked at 1631, 1278, and 856 cm^{-1}.

Water absorptions overlapped the 1631 cm^{-1} peak, and so the 1278 and 856 cm^{-1} peak could not be observed. Actually organonitrate absorptions are rarely detected in PMs larger than 1.0 μm in aerodynamic diameter.

Alcohol Absorptions

Weak, high frequency alcohol absorptions were observed in the 3500-3750 cm^{-1} region. This broad absorption is due to free OH stretching and hydrogen-bonding of alcohol groups (Nakanishi, 1962).

Alkenes, Aromatics, and Nitro Groups

Alkenes absorb strongly and sharply at 1640-1650 cm^{-1}, and aromatics absorb most strongly around 3030 cm^{-1}. These absorptions were not generally detected in fine environment PM spectra because of overlapping absorbances, low molar absorptivities and, in some cases, low concentrations. Aliphatic nitro groups absorb most strongly around 1540-1570 cm^{-1}, and aromatic nitro groups around 1530 cm^{-1}. No strong aromatic nitro groups absorptions were detected in my samples spectra. The spectra showed a very weak absorbance at 1540 and 1560 cm^{-1} and this may be due to aliphatic nitro groups present at low concentration levels.

Tab. 9: Inorganic absorption assignment

Functionality	Absorption frequency	Stage
Sulphate ions	1103-1135	2-3-4-5
Bisulphate ions	1025	2-3-4-5
Calcium sulphate	671	2-3-5
Nitrate ions	830-835, 1318-1335	2-3-4 2-3-4
Sodium nitrate	1786	2-3-4
Silicate ions	780; 800	All stages
Silica	1090	All stages
Kaolinite	1010	2-3-4
Ammonium ions	1410-1435	1-5
Particulate water	1620-1655	2-3
Carbonate ions	877; 1433	All stages
Phosphate ions	670; 916; 950; 1235	No absorption
Ammonium chloride	1760; 1400-1404	No absorption
Sulphite	925; 945; 620	No absorption
Nitrite	1220-1280	No absorption

Tab. 10 Organic absorption assignment

Functionality	Absorption frequency	Stage
Aliphatic carbons	2800-3000: 2958 2920; 2850	 1-2 All stages
Carbonyl carbons	1640-1850: 1840; 1715 1790	 All stages 2-3-4
Organonitrates	856, 1278, 1631	No absorption
Alcohols	3500-3750	All stages

Figure 66 shows a set of spectra from the five stages PM fractions. Raman spectra of air particulate matter exhibited fluorescence when illuminated by the excitation laser. This emission masks weaker Raman peaks so that it was possible to distinguish only the broad absorbance due to amorphous carbon at 1588 and 1334 cm^{-1}.

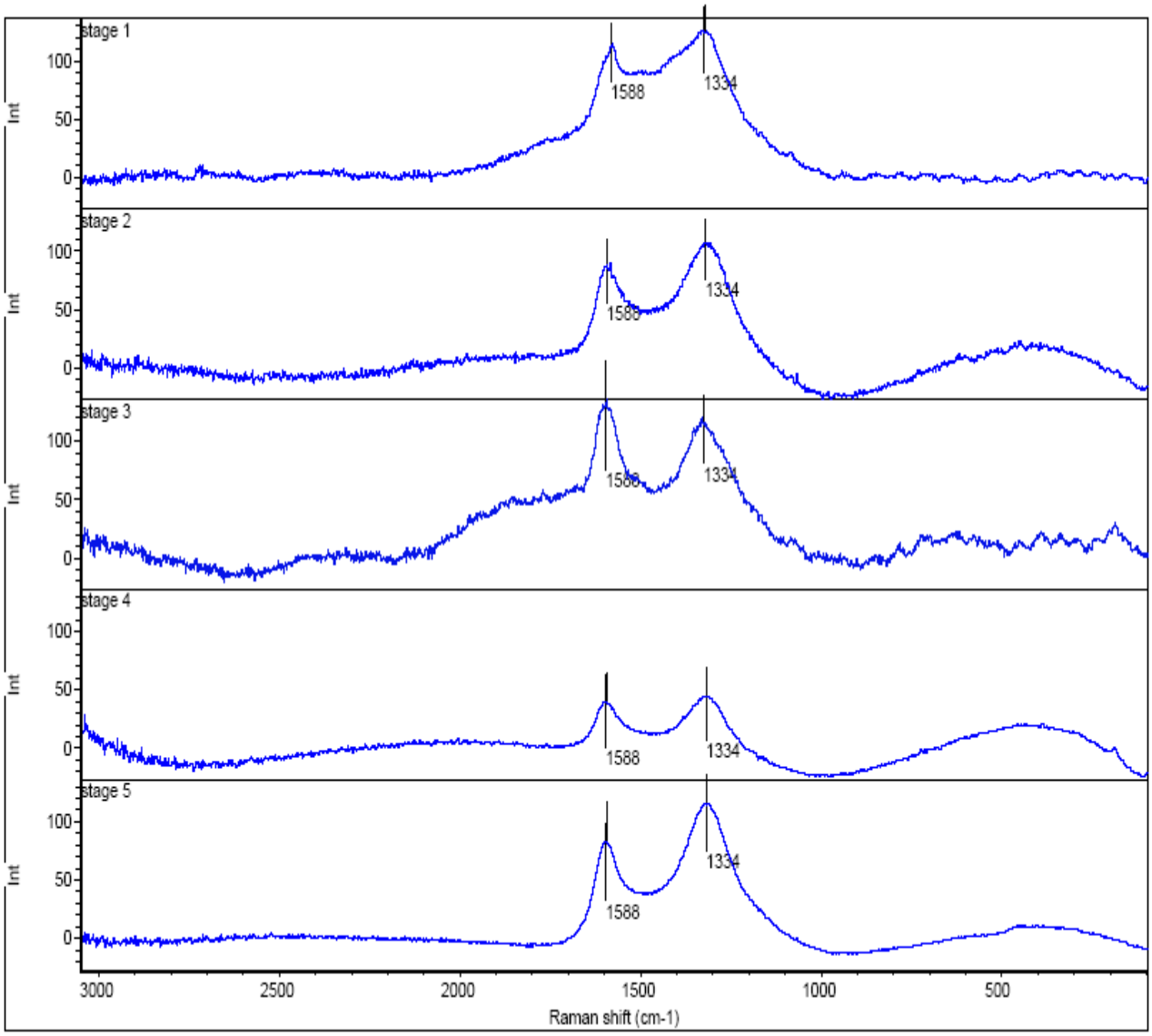

Fig. 66: Raman spectra representing the five stages PM fractions; all spectra are plotted on the same absorbance scale

FTIR Mapping

The FTIR micro-spectroscopic mapping system is a powerful technique that combines the image analysis of light microscopy, chemical analysis of FTIR spectroscopy and a mapping stage. A mapping stage can translate the sample along the X- and Y- axes thereby moving different areas of the sample into the microscope's beam path. The IR spectra can be directly related back to the sample's microstructure. This FTIR micro-spectroscopic mapping system was used to assess the homogeneity of PM distribution on the filter and the homogeneity of the distribution of loading functional groups along the filter.

A portion of the sampling filter was set on the stage of the FT-IR microscopic spectrometer, an appropriate sample area was selected and the reflectance IR spectra were collected from the actual analysis area by a mapping process.

In order to measure maps, spectra were collected along the sampling filter. The aperture was set at 100 μm x 100 μm, with a step size of 100 μm, so that 15 spectra per sample were collected. Spectra were collected in the range of 4000 -500 cm^{-1}, using 32 scans and 4 cm^{-1} resolution. Each line mapping took about 8–10 min. The IR data acquisition and microscope mapping were controlled by a PC using the software *Omnic* and *Atlus* respectively. The automatic atmospheric suppression function in the OMNIC™ software was used to minimise the infrared absorption by CO_2 and the water vapour in the ambient air.

Figures from 67 to 71 presents the FTIR spectral maps and frequency distribution plots of the PM on the sampling filters (one for each stage). The corresponding maps and plots represent a 3D and 2D distribution of the peak height of the IR bands. To the left is a false-colour display of the absorbance intensities at a particular IR frequency. The blue, or cool, colours show low

absorbance values, and the red, or hot, colours are high absorbance values. The colour bar below the spectrum shows the range of absorbance values for that frequency.

The FTIR mapping confirms the homogeneity distribution of the particles along the filter in all stages except for the stage 1 that shows only big sparse particles randomly distributed along the filter.

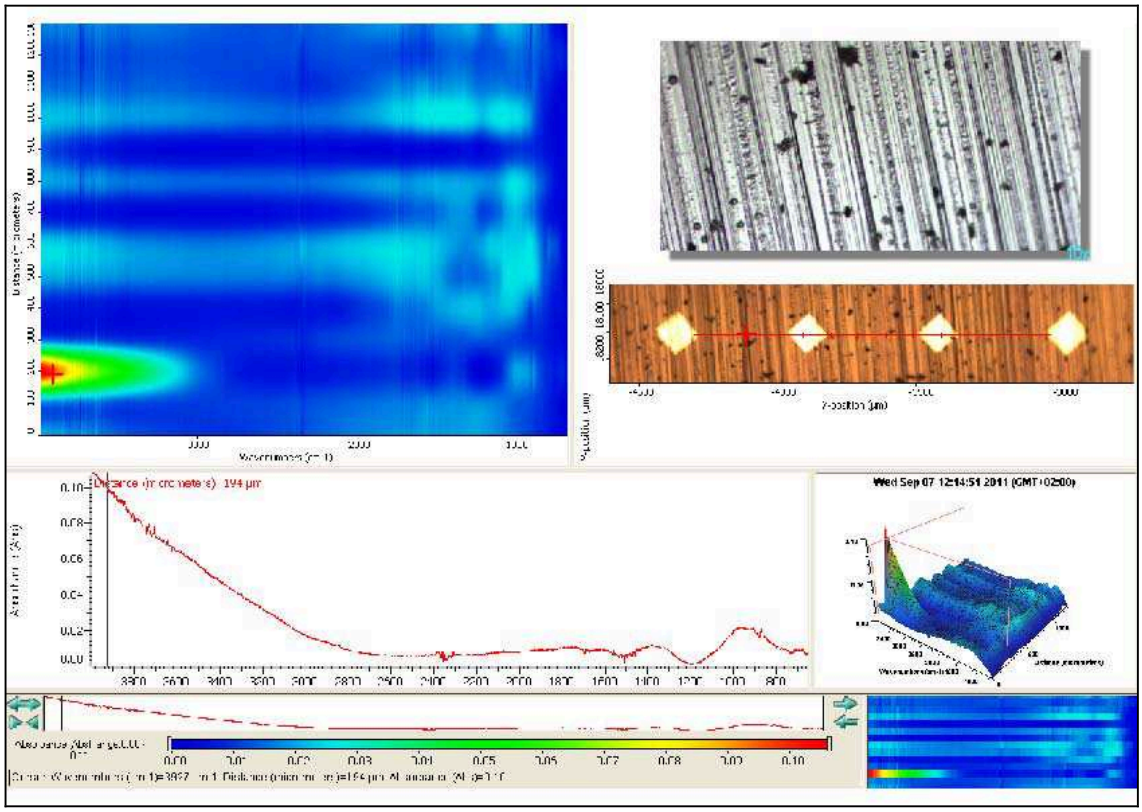

Fig. 32: FTIR spectral map and frequency distribution plots of the PM on the sampling stage 1

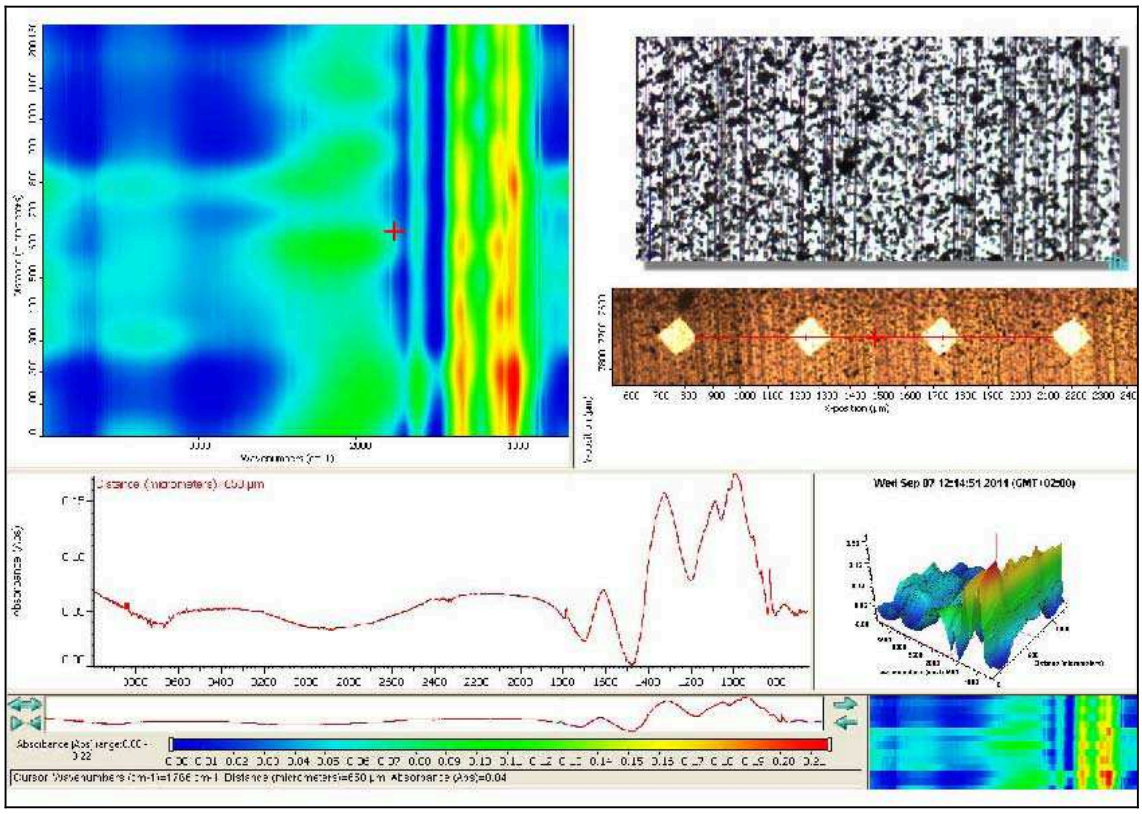

Fig. 33: FTIR spectral map and frequency distribution plots of the PM on the sampling stage 2

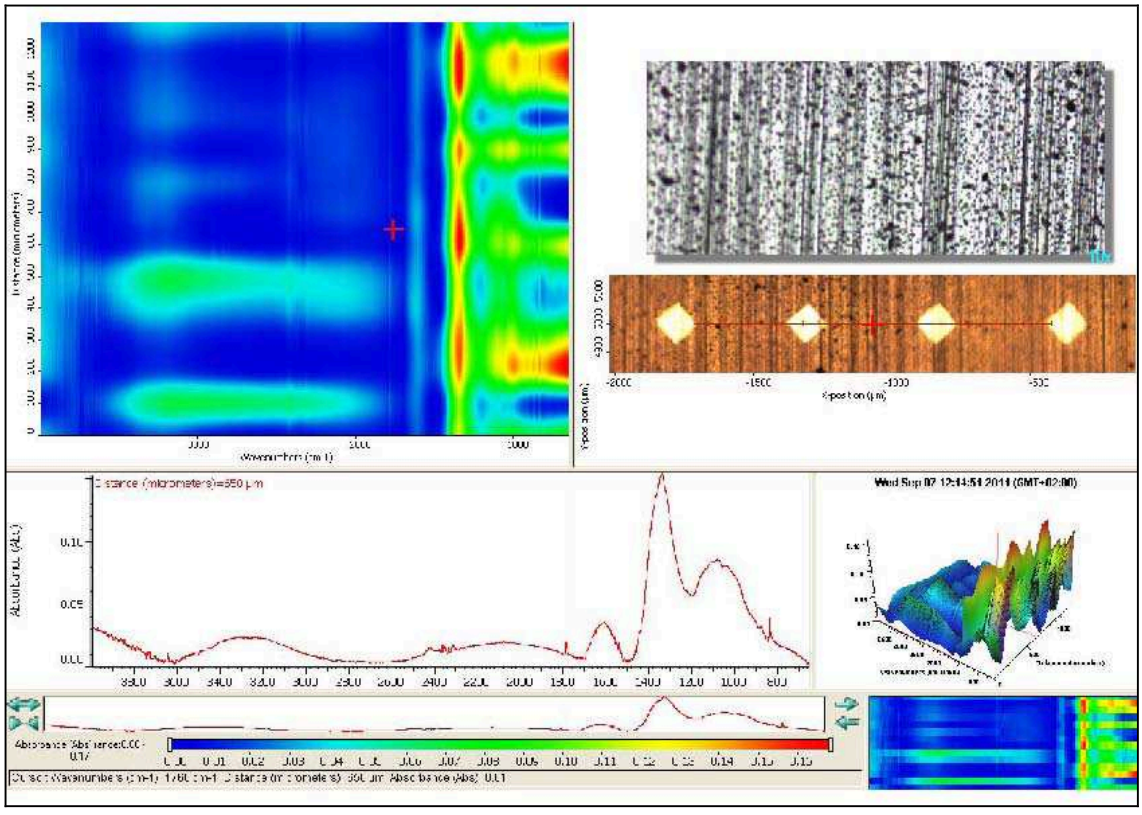

Fig. 34: FTIR spectral map and frequency distribution plots of the PM on the sampling stage 3

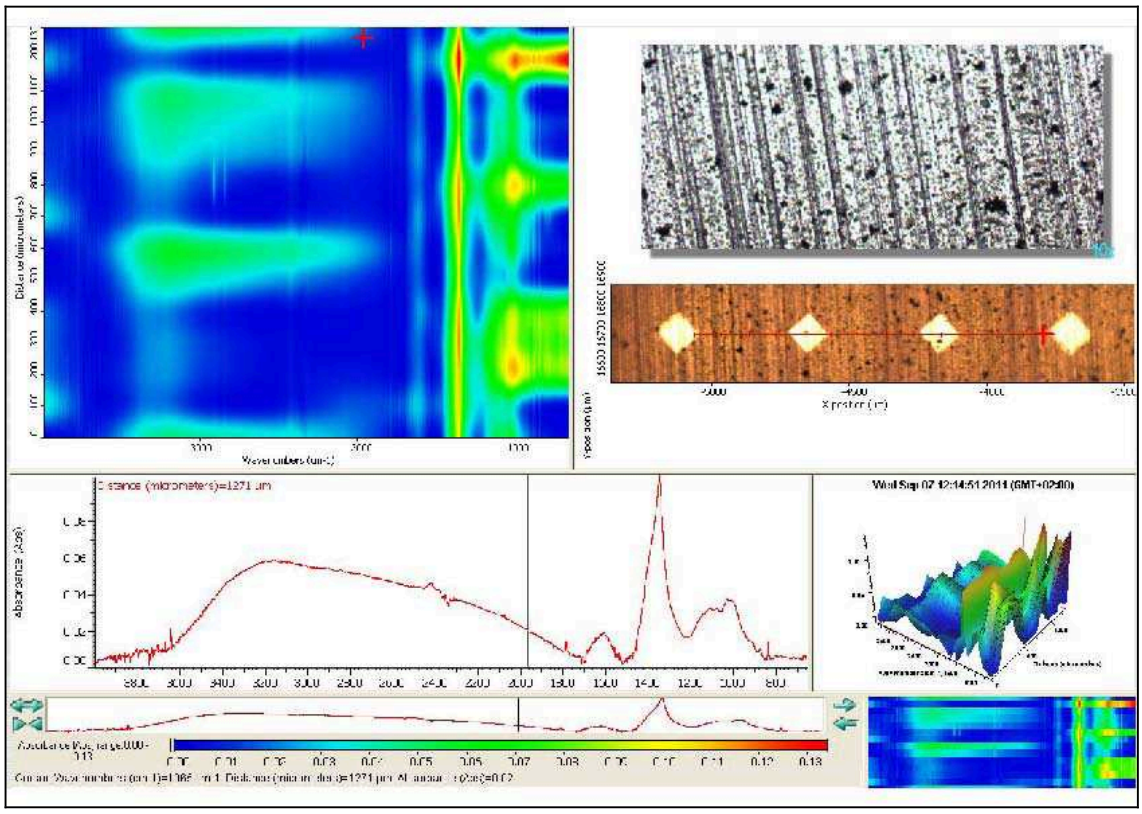

Fig. 35: FTIR spectral map and frequency distribution plots of the PM on the sampling stage 4

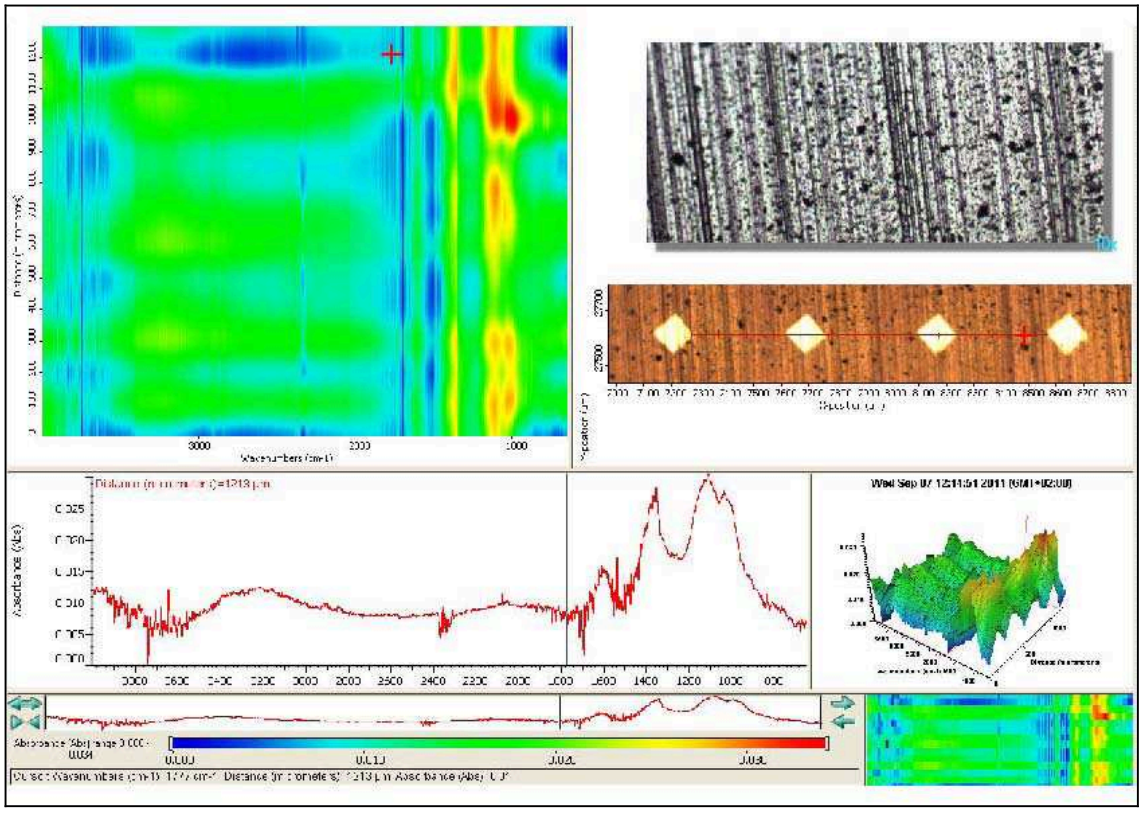

Fig. 36: FTIR spectral map and frequency distribution plots of the PM on the sampling stage 5

CONCLUSIONS

In this work it has been shown a study on old and damaged cellulose paper samples utilizing non-destructive spectroscopic techniques. This work was meant to investigate and better understand the degradation processes of cellulose paper samples. Aged paper showed a pattern of carbonyl groups, whose vibration modes were observed in FTIR and Raman spectra. The use of two complementary techniques made the spectra interpretation easier.

Different aged paper samples were compared to each other and to modern paper in order to point out the differences among the new and old samples and the increase of the degradation processes in older samples. Aging process is related to the presence of acid substances and oxidative agents that result in cellulose hydrolysis leading to the shortening of its chain along with changes in the amount of the crystalline form. This hydrolysis causes changes in hydrogen bonds that influences CCH, COH, OCH and HCH bending vibrations mode.

FTIR and Raman spectra of ancient paper and parchment samples were discussed too.

Those samples came from old books of high historical and artistic interest provided by the Public Library in Siracusa after authorization by the Superintendent BBCCAA of Siracusa, Italy.

Through non-destructive spectroscopic techniques both organic materials like paper and parchment and inks used on them were characterized.

The analysis of the ancient paper revealed a minor presence of additives compared to the analysis of modern samples and of the sample belonging to the twentieth century. In the ancient paper samples also the amount of

amorphous cellulose was lower than the amount measured in the contemporary samples. These results could be explained by the significantly higher quality of materials making up the oldest paper. Those, being composed essentially of long chain cellulose derived from cotton rags used in the old mills, have better withstood the attacks of external agents and are less affected by processes of hydrolysis and oxidation.

At last, some parchment fragments glued to the board of the back plate of an ancient book (yr.1794) were analyzed. These samples, although not accurately datable, gave noticeable information about the major parts of these writing supports and the inks used on them.

The FTIR analysis of different stains on paper of different composition confirmed the biotic nature of the stains due to the presence of fungal strains or traces of fungal activity. The presence of fungal activity was easily detected by FTIR analysis through their typical amide I and amide II bands at about 1640 and 1540 cm^{-1} and the plateau between 1500 and 1200 cm^{-1}. Sometimes the amide II band was too high to be only due to living fungi and a third band at about 1600 cm^{-1} appeared, probably due to degraded cell walls of dead fungi. In another sample the amide II band appeared as a shoulder, in this case the handling probably caused the partial removal of fungal agents. This helps to explain why most foxing stains generally do not show a large amount of fungal agents under microscope and it explains the reason why fungal species are not often visible on foxed spot of ancient paper samples. In some samples the presence of low-molecular-weight organic compounds due to fungal metabolism or to the decomposition of cell walls of dead fungi, yields a rugged spectra profile. This profile may support the Arai hypothesis of the Maillard reaction between low-molecular-weight oligosaccharides and amino acids produced by the grow of fungi on paper. In the examined sample the identification of these compounds is beyond the limits of this study, but

the microscopic analysis revealed several mycelia filaments protruding from the fissures of some folding pages. The presence of these filaments suggested that a fungal attack was occurring on the book.

In this study the data obtained from the analysis of PM collected in Catania, using an high-volume five-stage cascade impactor were also investigated. Different FTIR methods were applied to this samples and the spectra obtained in ATR, μATR, transmission and reflection mode were shown and discussed. Some characteristic bands were observed and identified utilizing spectra data obtained in reflection mode.

An FTIR spectra library of the most common sampling filter used for environmental PM collection was created. The FTIR spectra of different sampling filters showed very strong absorption bands that overlapped sample peaks, making the data interpretation difficult. The only filter that showed a low infrared absorption was the aluminium foil. The Raman spectra of the aluminium foil showed also a low Raman response, so the aluminium foil was selected as the filter substrate for this work.

Infrared spectroscopy was used to characterize the organic and inorganic species present in size segregated atmospheric PM. Organics, sulphates, nitrates, ammonium, and some trace species were detected using infrared methods.

For the organics, aliphatic carbon, carbonyl, and organonitrates can currently be detected, providing new chemical insights into the compound classes present in atmospheric PM.

The main sulphur and nitrogen species were SO_4^{--}, HSO_4^{-}, NO_3^{-}, NH_4^{+} probably due to ammonium nitrate and ammonium sulphate salts. Besides,

Ammonium chloride, Nitrite, Sulphite and Phosphate ions, implicated in the atmospheric pollution, were not detected in none of the five stages.

The qualitative comparison between the different stages spectra shows evident similarities in the distribution of absorption bands with only a decrease in bands intensity according with the lower amount of PM collected, except for the first stage where the bigger particles were collected. In the first stage because of the extremely scarce PM particle distribution, the spectroscopic analysis does not reflect the real composition of the sample

The FTIR mapping confirmed the homogeneity distribution of the particles along the filter in all stages except for the stage 1 that present only big sparse particles randomly distributed along the filter.

Raman spectroscopy did not allow any molecular analysis of environmental PM. Raman spectra showed only the broad absorbance due to amorphous carbon.

REFERENCES

Allen, D. T., and Palen, E. Recent advances in aerosol analysis by infrared spectroscopy. J. Aerosol Sci. 20, 441-455, 1989.

Appel, B. R., Hoffer, E. M., Kothny, E. L., Wall, S. M., and Haik, M. . Environ. Sci. Tech. 13, 98-104, 1979.

Arai, H. Foxing caused by fungi: twenty five years of study. Int. Biodeterior. Biodegrad. 46, 181-188, 2000.

Arney, J.S., Jacobs, A.J., A Study of the relative importance of oxidation by atmospheric oxygen in the aging chemistry of paper, in A.I.C. Preprints, 3-11, 1978.

Baruak, M. K., Assignment of the IR absorption band at 1050 cm^{-1} in lignite humic acid. Fuel 65, 1756-1759, 1986.

Bell, I.M., Clark, R.J.H., Gibbs, P.J., Raman spectroscopic library of natural and synthetic pigments (pre- 1850 AD), Spectrochimica Acta Part A 53, 2159-2179, 1997.

Bicchieri, M., Monti, M., Piantanida, G., Sodo, A., Tanasi, M. T., Inside the Parchment, 9th International Conference on NDT of Art, Jerusalem Israel, 25-30 May 2008.

Bicchieri, M., Sodo, A., Piantanida, G., Coluzza, C., Analysis of degraded papers by non-destructive spectroscopic techniques, J. Raman Spectrosc. 37, 1186–1192, 2006.

Bicchieri, M.; Brusa, P., The bleaching of paper by reduction with the borane tert-butylamine complex, Restaurator, 18(1), 1-11, 1997.

Bitossi, G., Giorgi, R., Mauro, M., Salvadori, B.and Dei, L., Spectroscopic techniques in cultural heritage conservation: A survey, Appl. Spectrosc. Rev. 40, 187–228, 2005.

Blanco, A. J. and McIntyre, R. G. Atmos. Environ. 65.57, 1975

Blumich, B., Anferova, S., Sharma, S.,Segre, A., and Federici, C., Degradation of historical paper: nondestructive analysis by the NMR-MOUSE, J. Magn. Res. 161, 204–209, 2003.

Bogard, J. S., Johnson, S. A., Kumar, R., and Cunningham, P. T. Environ. Sci. Tech. 16:136-140, 1982.

Brandt, N.N., Chikishev, A. Yu., Itoh, K., Rebrikova, N.L. ATR-FTIR and FT Raman spectroscopy and laser cleaning of old paper samples with foxings. Laser Physics, 19, 3, 483-492, 2009.

Browing, B.L., Analysis of Paper, Marcell-Dekker, New York, 1977.

Bugio, L., Ciomartan, Dan A., Clark, Robin J.H., Pigment identification on medieval manuscripts, paintings and other artefacts by Raman microscopy: applications to the study of three German manuscripts, Journal of Molecular Structure 405 , 1-11, 1997.

Burandt, J., An Investigation toward the identification of traditional drawing inks, The Book and Paper Group, 9-16, 1994.

Butz-Mann, H., Die Wolfenbuttel Fragmente der 'Historien' des Gregor von Tours, Scriptorium 20 , 31-40, 1966.

Buzio, R., Calvini, P., Ferroni, A., Valbusa, U. Surface analysis of paper documents damaged by foxing. App. Phys. A 79, 383-387, 2004

Cahill, T., Matsumura, R., Wakabayashi, P., and Surovik, M. Air & Waste Management Assoc. 1989 Annual General Meeting, Anaheim, California, paper 89-154.3, 1989.

Calvini, P., Gorassini, A. FTIR-deconvolution spectra of paper documents. Restaurator 23, 48-66, 2002.

Calvini, P., Gorassini, A., Chiggiato, R., Fourrier transform infrared analysis of some Japanese papers, Restaurator 27, 81–89, 2006.

Calvini, P., Vassallo, S. Computer-assisted infrared analysis of heterogeneous works of art. Preservation Science 4, 13-17, 2007.

Calvini, P., Gorassini, A., Albillos C., Ferroni A., FTIR analysis of historic documents degraded by iron-gall inks, Associazione Italiana di Archeometria (AIAr), IV Congresso Nazionale di Archeometria, Scienza e Beni Culturali, Pisa 1-3 Febbraio 2006.

Calvini, P., Organic chemistry: chemical processes which foster degrading agents, conservation of Paper Materials and Books in Central and Eastern Europe, TVM, Mestre, 2001.

Capitani, D., Proietti, N., Ziarelli, F. and Segre, A.L., NMR study of waterfilled pores in one of the most widely used polymeric material: the paper, Macromolecules 35, 5536–5543, 2002.

Castro, K., Pessanha, S., Proietti, N., Princi, E., Capitani, D., Carvalho, M.L., Madariaga, J.M., Noninvasive and nondestructive NMR, Raman and XRF analysis of a blaeu coloured map from the seventeenth century, Anal. Bioanal. Chem. 391, 433–441, 2008.

Choisy, P., De La Chapelle, A., Thomas, D., Legoy, M.D. Non invasive techniques for the investigation of foxing stains on graphic art material. Restaurator 18, 131e152, 1997.

Copedè M., La Carta e il suo Degrado, IV ed., Cardini Ed., Firenze, 2003.

Cunningham P. T., Johnson S. A. and Yang R. T. Variations in chemistry of airborne particulate material with particle size and time. Envir. Sci. Technol. 8, 131-135, 1974.

Dangler M., Burke S., Hering S. V. and Allen D. T. A direct FTIR method for identifying functional groups in size segregated atmospheric aerosols. Atmospheric Environment 21, 1001-1004, 1987.

Duarte, M.L., Ferreira, M.C., Marvão, M.R., Rocha, J. An optimised method to determine the degree of acetylation of chitin and chitosan by FTIR spectroscopy. International Journal of Biological Macromolecules 31, 1-8, 2002.

Edwards, H.G.M., Farwel, D.W., Newton, E.M., Rull Perez, F., Jorge Villar, S., Application of FT-Raman Spectroscopy to the characterisation of parchment and vellum, Spetrcochimica Acta Part A, 1223-1234, 2001.

Erhardt, D., Tumosa, C.S., Chemical degradation of cellulose in paper over 500 years, Restaurator 26, 151–158, 2005.

Erukhimovitch, V., Pavlov, V., Talyshinsky, M., Souprun, Y., Huleihel, M.,. FTIR microscopy as a method for identification of bacterial and fungal infections. Journal of Pharmaceutical and Biomedical Analysis 37, 1105-1108, 2005.

Fengel, D., Wegener, G., Wood, Chemistry, Ultrastructure, Reaction, Walter de Gruyter. Berlin, 1989.

Ferrer, N., Sistach, M.C., Characterisation by FTIR spectroscopy of ink components in ancient manuscripts. Restaurator 26, 105-117, 2005.

Fischer, G., Braun, S., Thissen, R., Dott, W. FT-IR spectroscopy as a tool for rapid identification and intra-species characterization of airborne filamentous fungi. Journal of Microbiological Methods 64, 63-77, 2006.

Florian, M.L.E., Manning, L.,. SEM analysis of irregular fungal fox spots in an 1854 book: population dynamics and species identification. Int. Biodeterior. Biodegrad. 46, 205-220, 2000.

Fuchs, R.; "The history and biology of parchment" Karger Gazette 67, 13-16, 2004.

Gallo, F. and Pasquariello, G. Foxing: ipotesi sull'origine biologica. Bollettino dell'Istituto Centrale di Patologia del Libro, 43, 139-176, 1989.

Gambaro, A., Ganzerla, R., Fantin, M., Cappelletto, E., Piazza, R., Cairns, W.R.L., Study of 19th century inks from archives in the Palazzo Ducale (Venice, Italy) using various analytical techniques., Microchemical Journal, 91, 202–208, 2009.

Gilbert, C., Kokot, S., Meyer, U., Application of DRIFT spectroscopy and chemometrics for the comparison of cotton fabrics. Applied Spectroscopy, 47, 741-748, 1993.

Gilbert, M., Sutherland, I., Guest, A., Characterization of coated particulate fillers. Journal of Materials Science 35, 391–397, 2000.

Gilli, E., Horvath, A.E., Horvath, A.T., Hirn, U., Schennach, R.,. Analysis of CMC attachment onto cellulosic fibers by infrared spectroscopy. Cellulose 16, 825-832, 2009.

Gordon, R. J., Trivedi, N. J., Singh, B. P., and Ellis, E. C. Characterization of aerosol organics by diffuse reflectance Fourier transform infrared spectroscopy. Emiron. Sci. Tech. 22, 672-677, 1988.

Gordon, S.H., Schudy, R.B., Wheeler, B.C., Wicklow, D.T., Greene, R.V. Identification of Fourier transform photoacustic spectral features for detection of Aspergillus flavus infection in corn. International Journal of Food Microbiology 35, 179e186, 1997.

Griffiths, P.R. and de Haseth, J.A., Fourier Transform Infrared Spectrometry, Wiley, New York, 1986.

Groblicki, P. J., Wolff, G. T., and Countess, R., Visibility-reducing species in the Denver "Brown Cloud"--I: Relationships between extinction and chemical composition. J. Atmos. Environ. 15, 2473-2484, 1981.

Gunzler, H. and Gremlich, H.-U., IR Spectroscopy: an introduction, Wiley-WCH. Weinheim, Germany, 2002.

Hon, D., Fourier-transform IR spectroscopy and electron-spectroscopy for chemical-analysis — use in the study of paper documents, Adv. Chem. Ser. 212, 349–361, 1986.

Humecki, H.J. (Ed), Practical Guide to Infrared Microspectroscopy, Marcel Dekker, New York, 1999.

Ibarra, J. V. and Juan, R., Structural changes in humic acids during the coaliflcation process. Fuel 64, 650-656, 1985.

Ibarra, J. V., Moliner, R. and Bonet, A. J., FTIR investigation on char formation during the early stages of coal pyrolysis. Fuel 73, 918-924, 1994.

Ibarra, J.V., Munoz E. and Moliner, R., FTIR study of the evolution of coal structure during the coalification process, Org. Geochem., 24, 6-7, 725-735, 1996.

Innocenti, P., *Maculatura*, in «Biblioteche oggi» 12, 11-12, novembre-dicembre, 74-76, 1994.

Irudayaraj, J., Yang, H., Sakhamuri, S. Differentiation and detection of microorganisms using Fourier transform infrared photoacustic spectroscopy. Journal of Molecular Structure 606, 181-188, 2002.

John, W., Wall, S., Ondo, J., and Winklmayr, W. (1989a). Proceedings from the 1989 annual general meeting of the Air and Waste Management Assoc., Anaheim, California, paper 89, 141.3, 1989.

John, W., Wall, S., Ondo, J., and Winklmayr, W. (1989b). Report prepared for the California Air Resources Board, June 1989.

Kellner R. and Malissa H. FTIR microscopy: a tool for speciation of impactor sampled single particles on In Proceedings of the Third International Conference on Carbonaceous Particles in the Atmosphere, 1987.

Kellner R. Identification and determination of particulate compounds: infrared spectroscopy, extraction and chromatography. In Analysis of Airborne Particles by Physical Methods (edited by H. Malissa and J. W. Robinson). CRC Press, Boca Raton, 1978.

Kellner, R., and Malissa, H. FTIR microscopy: a tool for speciation of impactor sampled single particles on particle clusters. Aerosol Sci. Tech. 10, 397-407, 1989.

Kidder, L.H., Haka, A.S. and Lewis, E.N., Instrumentation for FTIR Imaging, in Handbook ao Vibrational Spectroscopy, Vol.2 Chalmers, J.M. and Griffiths, P.R. (Eds), Wiley, Chichester, UK, 2002.

Kister, J., Giuliano, M., Largeau, C., Derenne, S. and Casadevall, E., Characterization of chemical structure, degree of maturation and oil potential of Torbanites (type I Kerogens) by quantitative FTIR spectroscopy. *Fuel* 69, 1356-1361, 1990.

Lin-Vien, D., Colthup, N.B., Fately, W.G., Graselli, J.G., The Handbook of Infrared and Raman Characteristic Frequencies of Organic Molecules, academic Press, San Diego, CA, 1991.

Liu, Y. Kokot, S. Sambi, T.J., Vibrational spectroscopy investigation of australian cotton cellulose fibres. Part 2. A Fourier transform near-infrared preliminary study, Analyst 123, 1725-1728, 1998.

Lojewska, J., Missori, M., Lubanska, A., Grimaldi, P., Zieba, K., Proniewicz, L.M., Congiu Castellano, A., Carbonyl groups development on degraded cellulose. Correlation between spectroscopic and chemical results, Appl. Phys. A 89, 883–887, 2007.

Manso, M., Pessanha, S., Figueira, F., Valadas, S., Guilherme, A., Afonso, M., Rocha, A.C., Oliveira, M.J., Ribeiro, I., Carvalho, M.L. Characterisation of foxing stains in eighteenth to nineteenth century drawings using nondestructive techniques. Analytical and Bioanalytical Chemistry 395, 2029-2036, 2009.

Maraval, M., Flieder, F., The stability of printing inks, Restaurator 14, 141–150, 1993.

Mastalerza, M., Gliksonb M. and Simpsonc R.W., Analysis of atmospheric particulate matter; application of optical and selected geochemical techniques, International Journal of Coal Geology, 37, 1-2, 143-153, 1998.

Mazurek, M. A., Cass, G. R., and Simoneit, B. R. T., Interpretation of high-resolution gas chromatography and high-resolution gas chromatography/mass spectrometry data acquired from atmospheric organic aerosol samples. Aerosol Sci. Technol. 10, 408-420, 1989.

McMurry, P. H., and Zhang, X. Q., Size Distributions of Ambient Organic and Elemental Carbon. Aerosol Sci. Technol. 10, 430-437, 1989.

Monn, C., Fuchs, A., Hogger, D., Junker, M. Particulate matter less than 10 mm (PM10) and fine particles less than 2.5 mm (PM2.5): relationships between indoor, outdoor and personal concentrations. Science of the Total Environment 208, 15-21, 1997.

Mossini, V., Calvini, P., Mattogno, G., Righini, G., Derivative infrared spectroscopy and electron spectroscopy for chemical analysis of ancient paper documents, Cellul. Chem. Technol. 24, 263–272, 1990.

Nakanishi, T. Infrared absorption spectroscopy: Practical, Holden-Day Inc. and Nakodo Company Limited, 1962.

Neukirch, F., Segala, C., Le Moullec, Y., Korobael, M. Short-term elects of low-level winter pollution on respiratory health of asthmatic adults. Archives of Environmental Health 53, 320-328, 1998.

Ondov, J. M., Dodd, J. A,, and Tuncel, G., Nuclear Analysis of Trace Elements in Size-Classified Submicrometer Aerosol Particles from a Rural Airshed. Aerosol Sci. Technol. 13, 249-263, 1990.

Ouimette, J. R., and Flagan, R. C. The extinction coefficient of multicomponent aerosols. Atmos. Environ. 16, 2405-2419, 1982.

Painter, P. C., Snyder, R. W., Starsinic, M., Coleman, M., M., Kuehn, D. W. and Davis, A., Concerning the application of FTIR to the study of coal: a critical assessment of band assignments and the application of spectral analysis programs. Appl. Spectrosc. 35, 475-485, 1981.

Palen, E. J. Ph.D. thesis, University of California, Los Angeles, 1991.

Reißland, B., Hofenk de Graaff, J., Conditioning rating for paper objects with iron–gall ink, ICN-Information 1, 1–4, 2001.

Ripley Ker, N., Fragments of medieval manuscripts used as pastedowns in Oxford binding with a severy of Oxford bindings, c. 1515-1620, The Oxford Bibliographical Society, 1954.

Rogge, W. F., Mazurek, M. A., Hildemann, L. M., Cass, G. R., and Simoneit, B. R. T. Atmos. Environ. 27A, 1309-1330, 1993.

Schuetzle D., Cronn D., Crittenden A. L. and Charlson R. J. Molecular composition of secondary aerosol and its possible origin. Envir. Sci. Technol. 9, 838-845, 1975.

Semmler J., Yang P. W. and Craford G. E., Gas chromatography/Fourier transform infrared studies of gas-phase polynuclear aromatic hydrocarbons. *Vibrational Spectrosc.* 2, 189-203, 1991.

Senvaitienė, J., Beganskienė, A., Salickaitė-Bunikienė, L., Kareiva, A., Analytical Identification of Historical Writing Inks – A new methodological Approach, Lithuanian Journal of Physics, 46, 1, 109-115, 2006.

Starsinic, M., Otake, Y., Walker, P. and Painter, P. C., Application of FTIR spectroscopy to the determination of COOH groups in coal. Fuel 63, 1002-1007, 1984.

Stuart, B.H., Infrared Spectroscopy: Fundamentals and Application, University of Technology, Sydney, Australia. John Wiley & Sons, Ltd, 2004.

Supaluknari, S., Larkins, F. P., Redlich, P. and Jackson, W. R., Determination of aromaticities and other structural features of Australian coals using solid state 13C NMR and FTIR spectroscopies. Fuel Proc. Tech. 23, 47-61, 1989.

Szeghalmi, A., Kaminskyj, S., Gough, K.M.,. A synchrotron FTIR microspectroscopy investigation of fungal hyphae grown under optimal and stressed conditions. Analytical and Bioanalytical Chemistry 387, 1779-1789, 2007.

Thermo Electron, Molecular Spectroscopy: Introduction to Raman Spectroscopy, 2008.

Tu, A.T., Lee, J., Milanovich, F.P., Laser-Raman spectroscopic study of cyclohexaamylose and related compounds; spectral analysis and structural implications. Carbohydr, Res. 76, 239-244, 1979.

Turpin, B. J., Cary, R. A,, and Huntzicker, J. J. (1989b). Aerosol Sci. Technol. 12, 161-171, 1989.

Turpin, B., and Huntzicker, J. (1989a). Proceedings from the 1989 annual general meeting of the Air and Waste Management Assoc., Anaheim, California, paper 89-153.3, 1989.

Van der Marel, H. W. and Beutelspacher, H., Atlas of Infrared Spectroscopy of Clay Minerals and their Admixtures. Elsevier, Amsterdam 1976.

Vasco, P.D., Blackwell, J., Koenig, J.L., Infrared and Raman spectroscopy of carbohydrates. Part II: normal coordinate analysis of glucose, Carbohydr. Res., 23, 407-416, 1972.

Viola, I., Bubici, S., Casieri, C. and Luca, F.D., The codex major of the collection altaempsiana: a non-invasive NMR study of paper, J. Cult. Herit. 5, 257–261, 2004.

Wang, S. H. and Griffiths, P. R., Resolution enhancement of diffuse reflectance IR spectra of coal by Fourier self-deconvolution. 1. C H stretching and bending modes.. Fuel 64, 229-236, 1985.

Wiley, J.H., Atalla, R.H., Carbohydr. Res. 76, 339, 1979.

Wilson, K.W., Parks, E.J., An analysis of the aging of paper: possible reactions and their effects on measurable properties, Restaurator 3 , 1-2, 1979.

Wilson, W.E., Suh, H.H. Fine particles and coarse particles: concentration relationships relevant to epidemiologic studies. Journal of the Air and Waste Management Association 47, 1238-1249,1997.

Winter, J., East Asian Paintings, Archetype Publications Ltd., 2008

Workman, J.J., Infrared and Raman spectroscopy in paper and pulp analysis, Appl. Spectrosc. Rev. 36, 139–169, 2001.

Yen, T. F., Wu, W. H. and Chilingar, G. V., A study of the structure of petroleum asphaltenes and related substances by infrared spectroscopy. Energy Sources 7, 203-235, 1984.

Zhbankov, R.G., Adrianow, W.M., Ratajczak. H., Marchewka, Vibrational Spectra and Stereochemistry of Mono- and Polysaccharides. Anomers of D-Glucose. Zh. Strukt. Khim., 36 (1995) 322-329 (in Russian); J. Struct. Chem., 36, 287-294, 1995.

Zhbankov, R.G., Adrianow, W.M., Ratajczak. H., Marchewka, M., Vibrational Spectra (IR and Raman) and Stereoisomers of Carbohydrates. Zh. Fiz. Khim., 69 (1995) 553-558 (in Russian); Russ. J. Phys. Chem., 68, 1995.

Zotti, M., Ferroni, A. and Calvini, P. Mycological and FTIR analysis of biotic foxing on paper substrates. International Biodeterioration & Biodegradation 65 569-578, 2011.

Zotti, M., Ferroni, A., Calvini, P. Foxing biologico: diagnostica multidisciplinare. V National Congress IGIIC. Cremona, 11-13 October. Nardini Ed, Firenze, 267-272, 2007.

Zotti, M., Ferroni, A., Calvini, P. Microfungal biodeterioration of historic paper: preliminary FTIR and microbiological analyses. Int. Biodeterior. Biodegrad. 62, 186-194, 2008.